8-2015

Development and Improvement of Cerium Activated Gadolinium Gallium Aluminum Garnets Scintillators for Radiation Detectors by Codoping

Fang Meng
University of Tennessee - Knoxville, fmeng2@vols.utk.edu

To the Graduate Council:

I am submitting herewith a dissertation written by Fang Meng entitled "Development and Improvement of Cerium Activated Gadolinium Gallium Aluminum Garnets Scintillators for Radiation Detectors by Codoping." I have examined the final electronic copy of this dissertation for form and content and recommend that it be accepted in partial fulfillment of the requirements for the degree of Doctor of Philosophy, with a major in Materials Science and Engineering.

Charles L. Melcher, Major Professor

We have read this dissertation and recommend its acceptance:

Mariya Zhuravleva, Claudia J. Rawn, Jason Hayward

Accepted for the Council:
Dixie L. Thompson

Vice Provost and Dean of the Graduate School

(Original signatures are on file with official student records.)

Development and Improvement of Cerium Activated Gadolinium Gallium Aluminum Garnets Scintillators for Radiation Detectors by Codoping

A Dissertation Presented for the
Doctor of Philosophy
Degree
The University of Tennessee, Knoxville

Fang Meng
August 2015

ACKNOWLEDGEMENTS

I would like to express my deepest gratitude to my advisor, my mentor Dr. Charles Melcher, for guiding me through the adventurous journey into the field of scintillation materials. Thanks to his expert insight and inspiring ideas on scientific researches, along with his amiable and considerate personality, I have spent four productive and enjoyable years working under his supervision. Today, I still remember how he encouraged me with his personal experience and the story about the “apple tree”, when I was puzzled in the maze of my research. His impact on me will benefit for my life.

This work would have not been possible without the valuable training from Ms. Merry Koschan. Everything I know about Czochralski crystal growth comes from her. Beyond the technical area, she also helped greatly in improving my language and presentation skills with huge patience. I am also indebted to Dr. Mariya Zhuravleva for her critical suggestions which always movitated me to dig for better solutions.

I am grateful to my dissertation committee, comprised of Dr. Charles Melcher, Dr. Mariya Zhuravleva, Dr. Jason Hayward and Dr. Claudia Rawn, for their valuable time and constructive advices on this work.

I was fortunate enough to have two brilliant post-doctoral fellows, Dr. Mohit Taygi and Dr. Yuntao Wu, working closely on the same project. Our pleasant collatoration has resulted in six papers so far. I can never learn enough

from Mohit on the characterization skills, and Yuntao on the theoretical understanding.

I wish to thank especially my colleague Dr. Hua Wei, for generously sharing ideas on experiments and equipment. I am also thankful to all other colleagues in the Scintillation Materials Research Center who helped directly or indirectly on this work, including Adam Lindsey, Bonnie Blalock, Dr. Sam Donnald, Luis Stand, Will McAlexander, Victoria Caroline, Christ Hobbs, Matt Loyd, Jesse Johnson, and Dr. Sasmit Gokhale.

A special thank goes to our collaborators in Siemens. Thanks to Dr. Peter Cohen's advice from the industrial perspective, this work gained tremendous potential in application. Dr. Harold Ruthfuss and Dr. Lars Eriksson provided solid hardware support with their rich experience and brilliant solutions on instrumentation.

I must also acknowledge the machine shop staff, Doug Fielden and Danny Hackworth for cleaning our crucibles, the facilities staff, Frank Holiway and Randy Stooksbury for managing various orders, and the office staff, Carla Lawrence, Martha Gale and Tracy Lee for taking care of all kinds of administrative issues and travel arrangements.

Last but not least, I would like to thank my family for their constant love and understanding. I owe my success to their faith in me.

ABSTRACT

Ce doped Gd3Ga3Al2O12 [gadolinium gallium aluminium oxides] is considered as a promising candidate for the next generation Positron Emission Tomography material due to its high light yield in theory. This dissertation is focused on studying the Gd3Ga3Al2O12:Ce crystals by codoping, aiming to improve the light yield and decay time experimentally and understand the underlying mechanism.

The work starts from prescreening appropriate codopants for Gd3Ga3Al2O12:Ce crystals. A cost-effective method is developed to predict the performance of the single crystals by characterizing the radioluminescence intensity and photoluminescence decay of the small polycrystalline pellets. This method is demonstrated by showing that the results from pellets and crystals are sufficiently similar. Based on the prescreening, crystals codoped with B, Ba and Ca are selected for growth and further study on the scintillation properties, optical properties, and charge traps. B and Ba codoping increase the light yield from 47,000 to ~ 53,000 photons per megaelectron volt, whereas Ca codoping reduces the scintillation decay time from 51 to 43 nanoseconds, and suppresses the shallow traps hence improves the afterglow.

The properties of Ca codoped crystals show strong dependence on the concentration of Ca. The relationship between Ca concentration and the optical/scintillation properties is explored. The Ce valence state and F+ [F plus] center are first studied by annealing in the Ca codoped crystals. As Ca

concentration increases, both light yield and decay time decrease, which can be understood by considering a Ce4+ [tetravalent cerium] emission model. Ca promotes the transition of Ce valence state from Ce3+ [trivalent cerium] to Ce4+ and introduces an F+ center, both of which can be affected by annealing. A redox mechanism and a charge compensation process are proposed to explain the change in Ce valence state and F+ center.

An innovative method was invented to create an intrinsic self-reflective layer serving as an alternative to the traditional external reflector used in radiation detectors. The intrinsic self-reflector is a white layer formed on Gd3Ga3Al2O12 crystals after annealing in a reducing atmosphere, and shows excellent performance in terms of maximizing photon collection thanks to its high reflectivity (92%).

TABLE OF CONTENTS

LIST OF TABLES

LIST OF FIGURES

Chapter 1 INTRODUCTION

Scintillator

A scintillator is a material that exhibits luminescence after absorbing ionizing radiation. It transforms incident ionizing radiation into visible light with high efficiency [1]. The resulting visible light can be detected by a photomultiplier tube or photodiode that ultimately results in an electrical signal that is representative of the incident quanta absorbed in the scintillator [2], as shown in Figure 1.1. Scintillator was first used by Sir William Crooks in the device screen in 1903 [3, 4]. The scintillations produced by a ZnS screen were visible to the naked eye if viewed by a microscope in a darkened room; the device was known as a spinthariscope. This technique led to a number of important discoveries but was obviously impractical. Scintillators started to gain additional attention in 1944, when Curran and Baker replaced the naked eye measurement with a newly developed photomultiplier (PMT). This was the birth of the modern scintillation detector [5].

Scintillation detectors are widely used in neutron and high energy particle physics experiments, new energy resource exploration, X-ray security, nuclear cameras, computed tomography and gas exploration. Additional applications of scintillators include computer tomography (CT) scanners and positron emission tomography (PET) in medical diagnostics, and screens in older style cathode ray tube (CRT) computer monitors and television sets [1]. Scintillators can be categorized into organic and inorganic scintillators. Among the inorganic scintillators, they can be further divided into oxide, metal halides, ceramic, glass

and gas scintillators [1].

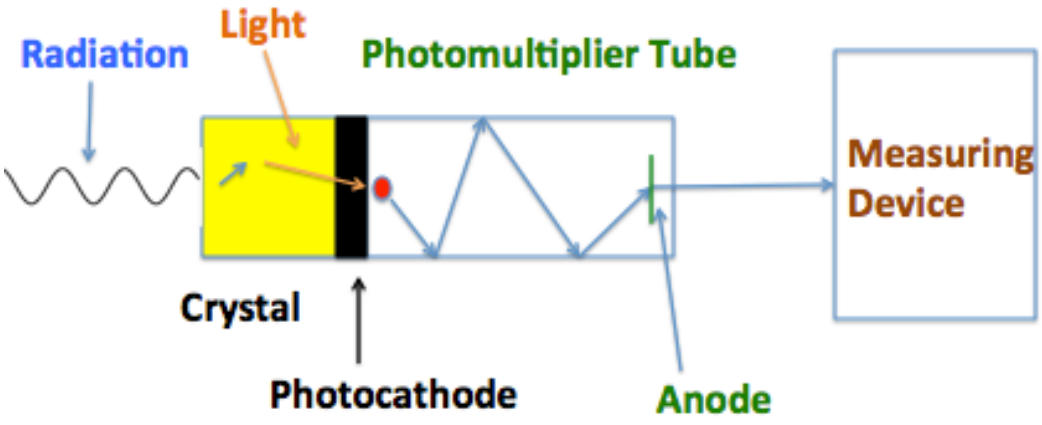

Figure 1.1. Basic configuration of a scintillator-based radiation detector.

An ideal scintillator should possess many desired properties, such as high density, fast operation speed, low cost, radiation hardness, production capability and durability of operational parameters. Additional properties are also desired for a good detector scintillator are [1]: 1) a high gamma output (i.e., a high efficiency for converting the energy of incident radiation into scintillation photons); 2) transparency to its own scintillation light (for good light collection); 3) a high stopping power; 4) good linearity over a wide range of energy; 5) a short rise time for fast timing applications (e.g., coincidence measurements); 6) a short decay time to reduce detector dead-time and accommodate high event rates, 7) appropriate emission range matching the spectral sensitivity of existing PMTs; 8) an index of refraction near that of glass (≈1.5) (to allow optimum coupling to the PMT window); 9) capability to operate at room temperature without quenching.

However, the practical choice of a scintillator material is usually a compromise among those properties to best fit a given application. Generally, organic scintillators have fast decay time but low light yield. The inorganic scintillator could have high light yield but sometimes slow response time. The inorganic scintillators with high atomic number and high density are widely used for gamma-ray spectroscopy, whereas the organics are preferred for beta spectroscopy and fast neutron detection because of their large cross-section area for neutron [1].

Scintillation process in inorganic scintillator

A scintillator can be described as an insulator material with band gaps in the order of few electron volts (eV). The scintillation mechanism starts with the initial ionizing radiation interacting with the crystal and emitting a primary electron via photoelectric absorption, Compton scattering and pair production [1]. In the following stage, the electron-electron relaxation produces numerous secondary electrons, photons and plasma; subsequently electron-hole pairs form due to the thermalization of secondary electrons; then the energy transition occurs from electron-hole pairs to luminescence center [1]. Finally, the emission of detective photons is produced by the relaxation of luminescence centers, which is the result of electron-hole recombination in an activator site [1, 6]. Figure 1.2 shows the scintillation processes in the inorganic crystals [7].

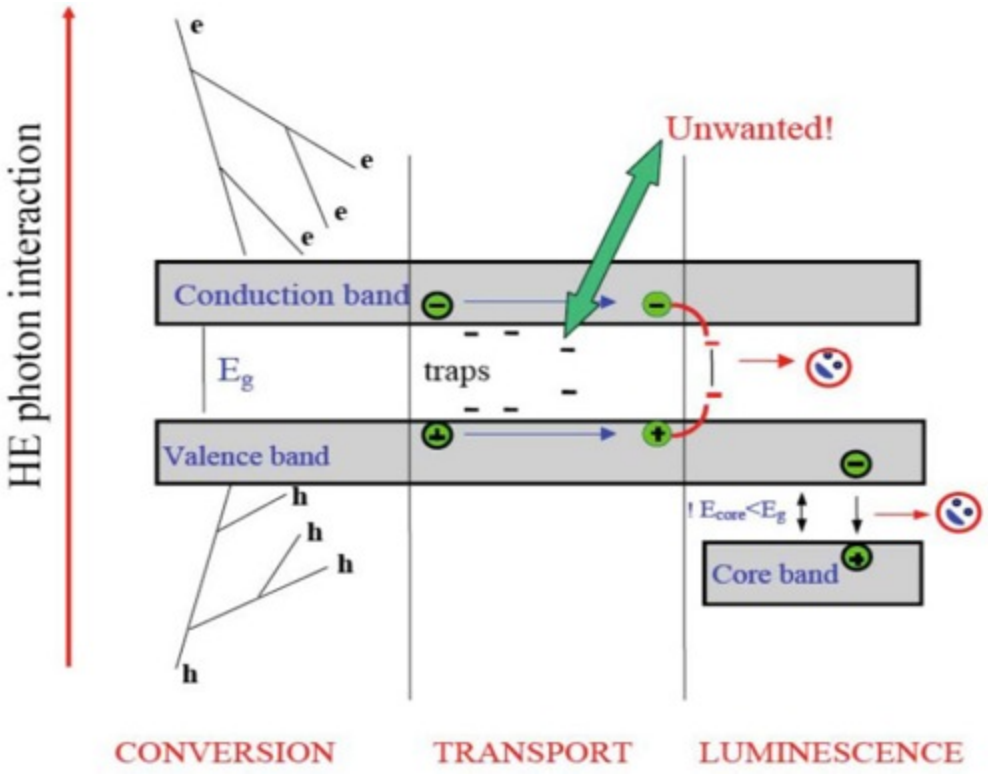

Figure 1.2. Scintillation processed in inorganic crystals [7].

Most inorganic scintillators are grown using well-known single crystal growth techniques such as the Bridgman or Czochralski methods. They can be divided into two categories: intrinsic scintillator and activated scintillator.

The intrinsic scintillators emit light from a constituent related defect. They are divided into four types [1, 6, 8]: 1) self-trapped: hole and electron combine to form a self-trapped exciton that radiates (e.g., NaI, CsI, BaF_2); 2) self-activated: luminescence ion is a major constituent of the crystal (e.g., $Bi_4Ge_3O_{12}$, $CeBr_3$); 3) charge exchange: ionization electron on the cation combines with a hole on the anion (e.g., $CaWO_4$, $PbWO_4$); 4) core-valence: valence electron drops into hole in upper core band (e.g., BaF_2).

Activated scintillators emit light from an introduced luminescence center, usually a rare earth dopant. Such process includes 1) luminescent ion promptly captures electron/hole, hole/electron diffuses to form an excited state (e.g., CsI:Tl, Lu_2SiO_5:Ce); 2) hole and electron combine to form a self-trapped exciton that transfers its energy to a luminescent ion (e.g., $LaBr_3$:Ce) [1, 6, 8].

The work here focuses on the garnet type ($A_3B_5O_{12}$) of scintillators, which utilizes the highly efficient 4f-5d transitions in Ce^{3+} luminescence center, in the single crystal inorganic family.

Ce^{3+} luminescence center

Generally, Ce^{3+}, Eu^{2+} and Pr^{3+} are used as activators in the inorganic scintillators, based on the specific application of scintillators. The luminescence transition in Ce^{3+} is 5d (^{2}D)-4f (^{2}F). Its transition energy is the lowest among the lanthanide ions, but the energy gap from the $5d_1$ states to the nearest 4f state is so large that the 5d level serves as an efficient light-emitting state [9]. It is well known that the 4f ground state of Ce^{3+} is split into two energy levels, $^2F_{5/2}$ and $^2F_{7/2}$, due to spin–orbit coupling, and lead to a double-peak structure due to the two terminating levels of the 4f configuration of Ce^{3+} [9]. The decay time of the Ce^{3+} emission is ~ 10-50 ns [10], the shortest one observed in lanthanide ions. Figure 1.3 shows a typical energy level of the Ce^{3+} luminescence center [9].

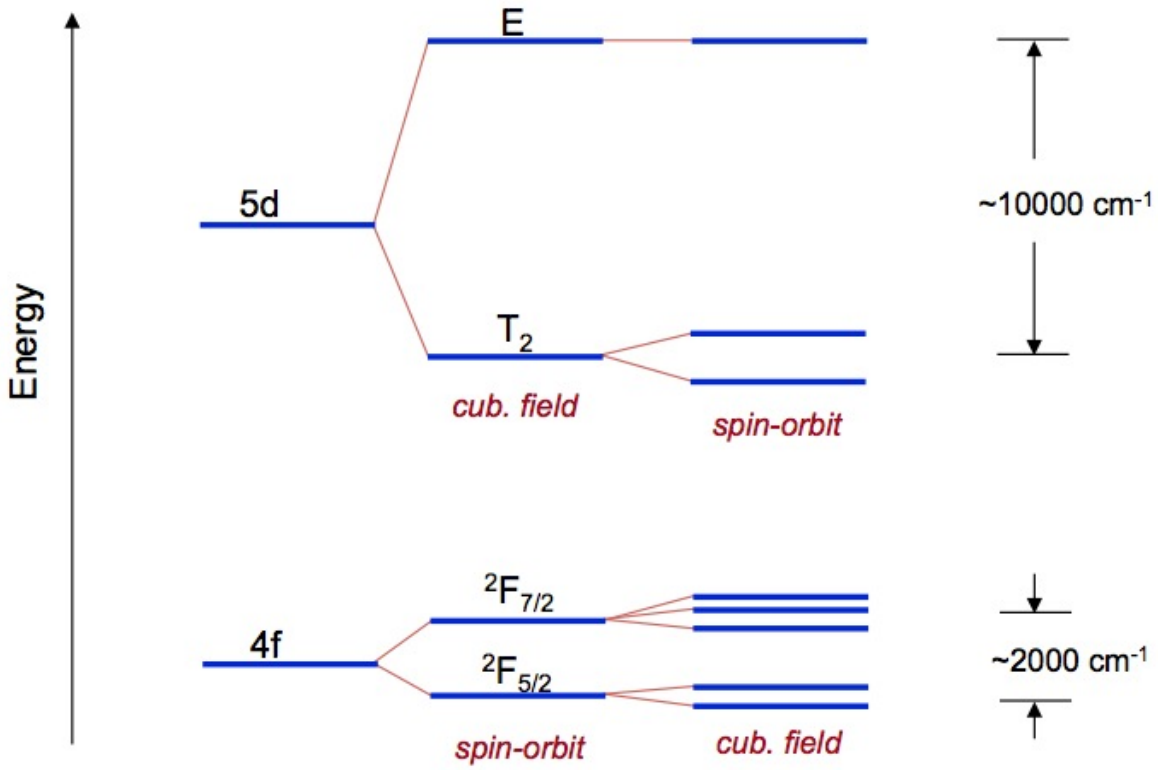

Figure 1.3. Energy level of Ce^{3+} luminescence center [9].

Properties of common inorganic oxides scintillators

Table 1.1 [11,12] shows the properties of some common inorganic oxides scintillators. Their density and effective atomic number are relative high. Light yield and decay time are in the order of several thousand and nanoseconds respectively. The emission light is in the visible light range. Those properties result in the wide applications as sicintillation detectors.

Table 1.1 Properties of common inorganic oxides scintillators [11, 12]

Name	Formula	Density (g/mm^3)	Zeff	Light yield (ph/MeV)	Primary Decay time (ns)	Emission (nm)
LSO:Ce	Lu_2SiO_5:Ce	7.40	66	35,000	32	420
GSO:Ce	Gd_2SiO_5:Ce	6.71	59	20,000	60	440
LPS:Ce	$Lu_2Si_2O_7$:Ce	6.2	64	23,000	30	380
GPS:Ce	$Gd_2Si_2O_7$:Ce	5.5	58	30,000	46	380
BGO	$Bi_4Ge_3O_{12}$	7.13	74	8,000	300	480
YAP:Ce	$YAlO_3$:Ce	5.35	34	20,000	24	365
LuYAG:Pr	$Lu_{2.25}Y_{.75}Al_5O_{12}$:Ce	6.20	60	33,000	20	310
GGAG:Ce	$Gd_3Ga_3Al_2O_{12}$: Ce	6.5	54	47,000	51	540

$A_3B_5O_{12}$ garnets structure

The garnet crystal structure has been extensively studied after the first determination of it in 1926. In General, garnet crystals have a cubic structure and the space group is *Ia3d*. In a unit cell, there are eight molecules with the stoichiometric formula $\{A_3\}[B_2](C_3)O_{12,}$ where {}, [] and () denote dodecahedral, octahedral and tetrahedral coordination respectively, as shown in Figure 1.4 [13,14].

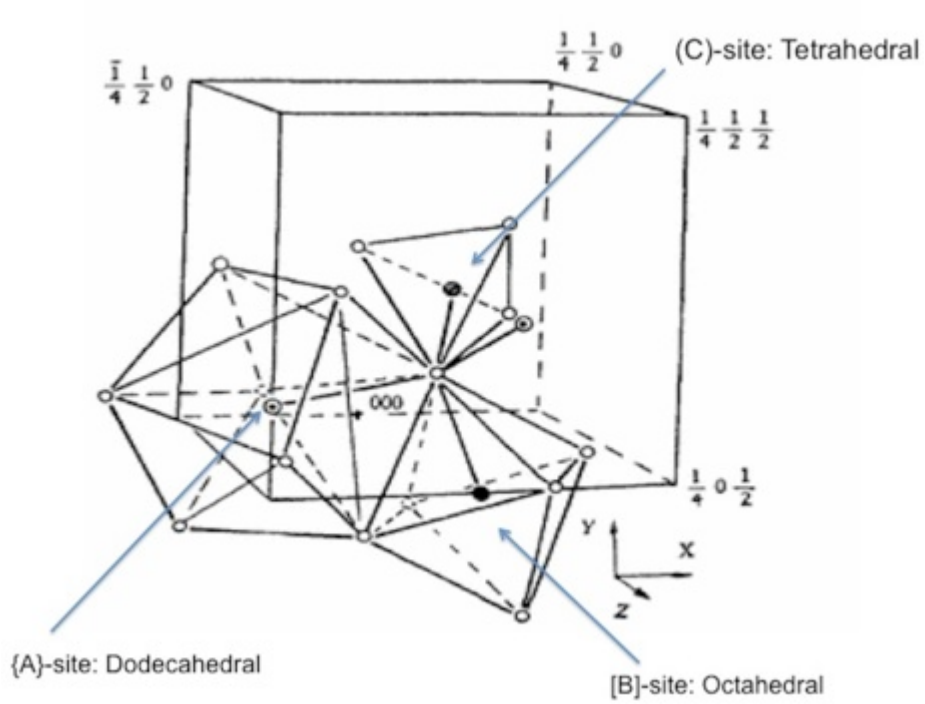

Figure 1.4. Structure of $A_3B_5O_{12}$ garnets in *Ia3d* space group [13,14].

Ce doped $Y_3Al_5O_{12}$ (YAG:Ce) is a widely used phosphor. It emits yellow light when subjected to ultraviolet light, gamma ray or X-ray [15]. So it can be used in white light-emitting diodes, PET scanners, high-energy gamma radiation charged particle detectors, and high-resolution imaging screens for gamma, X-ray, and ultraviolet radiation [15]. YAG is a synthetic crystalline material of the garnet group. It is also one of the three phases of the yttrium-aluminum composite, the other two being yttrium aluminum monoclinic (YAM, $Y_4Al_2O_9$) and yttrium aluminum perovskite (YAP, $YAlO_3$) [16]. The phase diagram of the Y_2O_3-Al_2O_3 garnet is shown in Figure 1.5 [17]. Other garnets with the same structure show the similar phase diagram.

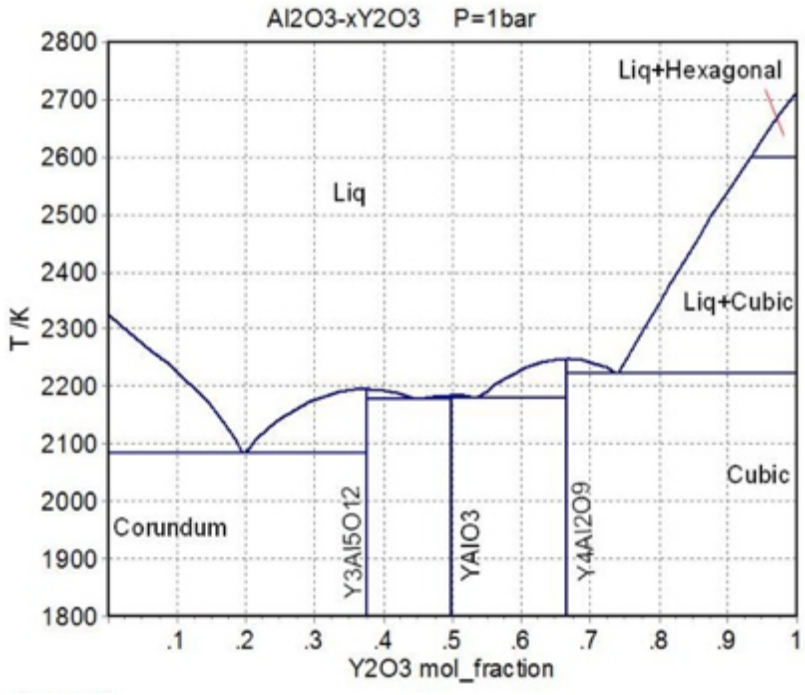

Figure 1.5. The garnet phase diagram of the Y_2O_3-Al_2O_3 system [16].

The current progress of $R_3(Ga,Al)_5O_{12}$ (R = Gd, Lu, Y or mix of them) single crystals

Ce activated garnets are excellent scintillation detectors due to their achievement of combining stopping power, decay time, light yield and non-hygroscopicity [18]. Ce doped yttrium/lutetium aluminum garnets are particularly interesting in view of its maximum theoretical light yield (LY) in the order of 60,000 phs/MeV based on Bartram-Lempicki theory [19], a relatively high density of 6.7 g/cm^3, and a fast scintillation response of about 60-80 ns. However, the measured LY values are much lower (12,000-25,000 phs/MeV) due to the intrinsic defects such as Lu_{Al} antisite defects and vacancies [20, 21]. Many

approaches were undertaken to improve the LY. It has been reported that the energy trapping effects were diminished and hence the LY was increased by adding 20 at% Ga into the $Lu_3(AlGa)_5O_{12}$:Ce crystals [22]. However, higher Ga concentration in these crystals will rapidly decreased the LY due to the proximity of the $5d_1$ excited state of Ce^{3+} to the bottom of the conduction band [22, 23]. Based on a 'band gap engineering' strategy (Figure 1.6) for favorable low 5d Ce^{3+} level positioning, the most remarkable improvements were achieved by Kamada et al. [24] via substituting Y/Lu with Gd and admixing Ga with Al in $(Lu,Y)_3Al_5O_{12}$ single crystals. They reported the highest LY value (~ 45,000 ph/MeV) in the $Gd_3Al_3Ga_2O_{12}$:Ce crystal and the shortest decay time (~ 53 ns) in the $Gd_3Al_2Ga_3O_{12}$:Ce crystal grown by the micro pulling down method [24].

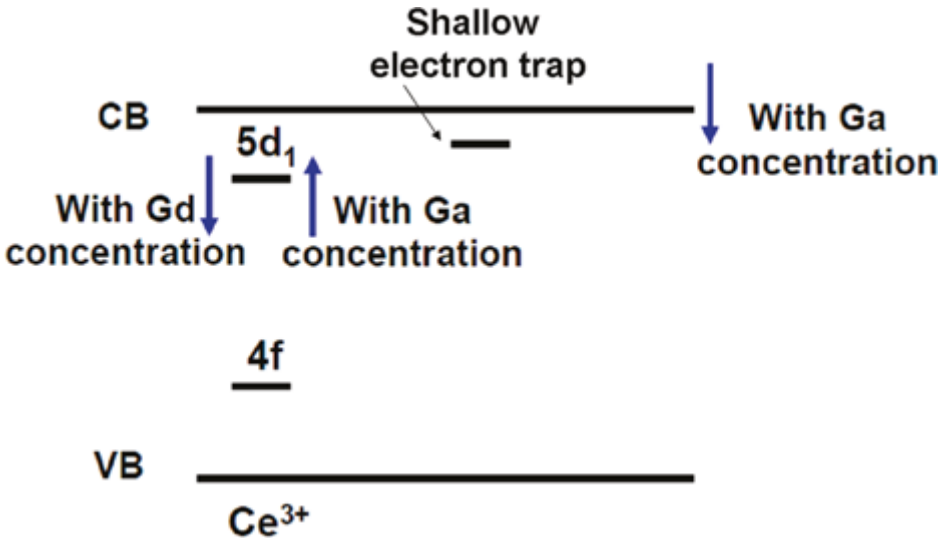

Figure 1.6. Energy level scheme related to the $(RE_{1-y}Gd_y)_3(Ga_xAl_{5-x})_5O_{12}$ material design [24]. VB and CB are abbreviations of valence and conduction bands, respectively.

Purposes and organization of this dissertation

The medical imaging equipment in the last few decades requires inorganic scintillators with outstanding scintillation performance. In particular, a high light yield allows a reduced irradiation dose received by the patients during medical application but a more accurate diagnostic. A fast decay time allows a good coincidence resolving time, which improves the events statistics [1]. The scintillator used in PET has seen transition in the early 2000s from BGO to LSO:Ce and LYSO:Ce single crystals, due to their good LY (~ 35,000 ph/MeV), fast scintillation decay time (~ 32 ns) and high stopping power resulting from their high density (7.4 g/cm^3) and effective atomic number (66) [26]. As mentioned above, Ce doped GGAG single crystal has emerged as a strong candidate for the next generation PET scintillator due to its advantageous LY (~ 46,000 ph/MeV) over LSO, despite the longer decay time (~ 92 ns) [24, 25, 27]. Given that, improving the decay time and LY of GGAG is clearly of interest.

Prior work by our group has demonstrated that it is possible to modify the scintillation properties of LSO:Ce, YSO:Ce, GSO:Ce by codoping with other dopants [25, 28, 29]. Therefore, the work presented in this dissertation is focused on studying the GGAG:Ce crystals by codoping, aiming to improve the LY and decay time and understand the underlying mechanism.

The work starts from prescreening the appropriate codopants for GGAG:Ce. However, it is not practical to test every possible codopant candidate by growing single crystals, given the cost and time investment required for CZ

growth. A cost-effective method was developed to predict the performance of the single crystals by characterizing the radioluminescence (RL) intensity and photoluminescence (PL) decay of the small polycrystalline pellets. Chapter 2 demonstrates that the performance of the crystals is as predicted by presenting the scintillation properties (LY, decay time, etc.) of the crystals, using the example of Ca, B and Ba codoping, which all results in modified properties of the pellets.

Besides the scintillation properties studied in Chapter 2, there are several other important properties. The optical properties (absorbance, PL, RL, etc.) give information about dopant energy level in the scintillator material host. Good thermal stability is required for scintillators used in the high temperature atmosphere. Weak afterglow is desired for medical imaging applications, such as CT and high-speed imaging in which the existence of afterglow causes the pulse pileup problem. Afterglow is caused by impurities or defects which create traps or metastable states with long lifetime. Therefore the traps structure is also necessary to be investigated in the form of thermoluminescence. All the aforementioned properties were characterized and discussed in Chapter 3 for Ca, B and Ba codoped crystals.

The properties of Ca codoped crystals show strong dependence on the concentration of Ca. Therefore the scintillation properties, optical properties, afterglow and traps were further investigated as a function of Ca concentration, which comprises the main subject of Chapter 4.

During studying the effect of Ca concentration in Chapter 4, there are two noticeably interesting phenomenon: a) GGAG crystal with the highest Ca concentration shows different color (rust) from the other samples (yellow), and b) an additional luminescence center shows up in the Ca codoped sample. Motivated by a), the change of Ce valence state was investigated as a function of Ca concentration. The origin of this new center was also fully understood with the help of a series of annealing experiments. The discoveries for this part are presented in Chapter 5.

As a byproduct of the codoping work, a technique was invented to create an intrinsic self-reflective layer serving as an alternative to the traditional external reflector used in radiation detectors. The intrinsic self-reflector is a white layer formed after annealing in a reducing atmosphere. In Chapter 6, the detailed process to form this reflector is introduced, and the composition, reflectivity and reflector performance are characterized.

References for Chapter 1

[1] G. F. Knoll, (2010). “In Radiation Detection and Measurement”. Wiley: New York, fourth edition.

[2] F. Grum, and R. J. Becherer, (1979). “Optical radiation measurements.” Volumn (1), Radiometry (Book). New York, Academic Press, Inc.,

[3] W. R. Leo, (1994). “Techniques for Nuclear and Particle Physical Experiments.” second edition, Springer, ISBN 354057280.

[4] S. A. Dyer, (2011). “Survey of Instrumentation and Measurement.” Wiley-IEEE. pp. 920. ISBN 0-471-39484-X,.

[5] L. Micheal, (2003). “Handbook of Radioactivity Analysis.” Chemical reviews, pp. 404,

[6] P.A. Rodnyi, (1997). “Physical Processes in Inorganic Scintillators” CRC Press.

[7] https://crystalclear.web.cern.ch/crystalclear/scintmechanisms.html.

[8] P. Lecoq, et al., (2006). “Inorganic scintillators for detector systems.” Springer, Heidelberg.

[9] T. Hoshina (1980). “5d-4f radiative transition probabilities of Ce^{3+} and Eu^{2+} in crystals”, J. Phys. Soc. Jpn. pp. 1261-1268.

[10] P. Dorenbos, (2000). “The 5d level positions of the trivalent lanthanides in inorganic compounds.” J. Lumin. 91:155-176.

[11] J. L. Lefaucheur and C. D. Brandle, “Single crystal scintillators.” patent no: EP1466955 B1.

[12] http://scintillator.lbl.gov/

[13] J. L. Wu, et al., (2007). “Structure-property correlations in Ce doped garnet phosphors for use in solid state lighting.” Chem. Phys. Lett. 441: 250-254,

[14] Z. Wu, et al., (1991). “EXAFS studies of the coordination structure of (ErxY1-x)3Al5O12 garnet solid solutions.” J. Phys.: Condens. Matter 82: 15-21.

[15] G. Blasse and A. Bril, (1967). “A new phosphor for lying-spot cathode ray

tubes for color televisions.” Appl. Phys. Lett. 11:53-54.

[16] I. Warshaw and R. Roy, (1959). “Stable and Metastable Stable and Metastable Equilibrium in the Systems Y2O3-Al2O3, and Gd2O3.” J. Am. Ceram. Soc. 42: 434-438.

[17] A. F. Giamei and E. R. Thompson, “Directionally solidified eutectic reinforcing fibers.” patent no: EP0712382 B1.

[18] M. Balcerzyk, et al., (2000). “Future hosts for fast and high light output cerium-doped scintillator.” J. Lumin. 87: 963-966.

[19] C. R. Ronda, (2007). “Luminescence: from theory to applications.” John Wiley & Sons.

[20] M. Nikl, et al., (2005). “The antisite LuAl defect-related trap in Lu3Al5O12:Ce single crystal.” Phys. Status Solidi 242: 119-121.

[21] J. A. Mares, et al., (2004). “Scintillation response of Ce-doped or intrinsic scintillating crystals in the range up to 1MeV.” Radiat. Meas. 38: 353-3572004.

[22] H. Ogino, et al., (2009). “Growth and optical properties of Lu3(Ga, Al)5O12 single crystals for scintillator application.” J. Cryst. Growth 311: 916-911.

[23] M. Nikl, et al.. (2006). “Antisite defect-free Lu3 (Gax Al1-x)5O12:Pr scintillator.” Appl. Phys. Lett. 88:141916-141918.

[24] K. Kamada, et al., (2011). “Composition engineering in cerium-doped (Lu, Gd)3(Ga, Al)5O12 single-crystal scintillators.” Cryst. Growth Des. 11: 4484-4490.

[25] K. Kamada, et al., (2011). “Scintillator-oriented combinatorial search in Ce-doped (Y, Gd)3(Ga, Al)5O12 multicomponent garnet compounds.” J. Phys. D: Appl. Phys. 44: 505104.

[26] M. A. Spurrier, et al., (2008). "Effects of co-doping on the scintillation properties of LSO: Ce." IEEE Trans. Nucl. Sci. 55(3): 1178-1182

[27] K. Kamada, K., et al., (2012). "Crystal growth and scintillation properties of Ce doped single crystals." IEEE Trans. Nucl. Sci. 59(5): 2112-2115.

[28] M. Koschan, et al., (2012). "A comparison of the effect of Ca 2+ codoping in cerium doped GSO with that of LSO and YSO." J. Cryst. Growth, 352(1):133-136.

[29] H. E. Rothfuss, et al., (2009). "The effect of codoping on shallow traps in YSO: Ce scintillators." IEEE Trans. Nucl. Sci. 2009, 56(3): 958-961.

Chapter 2 SINTERED PELLETS: A SIMPLE AND COST EFFECTIVE METHOD TO PREDICT THE PERFORMANCE OF GGAG:CE SINGLE CRYSTALS

A version of this chapter by Fang Meng was accepted and published by a peer-reviewed journal. The full citation is as following: F. Meng, M. Koschan, C. L. Melcher and P. Cohen, "*Sintered pellets: a simple and cost effective method to predict the performance of GGAG:Ce single crystals", Materials Science and Enginerring B 193 (2015): 20-26.*

This chapter is the reformatted version of the original work submitted to the referenced journal. No additional changes to the content of the original article were done other than formatting to conform to the dissertation format.

Abstract

Polycrystalline $Gd_3Ga_3Al_2O_{12}$:Ce (GGAG:Ce) pellets with various codopants were prepared via solid- state synthesis and characterized by X-ray diffraction, radioluminescence (RL), photoluminescence (PL), reflectivity and PL decay measurements. GGAG:Ce pellets codoped with B and Ba were found to have higher RL intensity than pellets with other codopants, while Ca codoping improved the decay time but reduced the RL intensity. These results were strongly correlated with the performance of these codopants in GGAG:Ce single crystals. The light yield of the single crystals codoped with B or Ba was ~ 15% higher than the light yield of the GGAG:Ce crystal without codoping, while Ca codoping in single crystals resulted in lower light yield but shorter scintillation decay time (43 ns vs. 56 ns). The consistent performance of these codopants in

both matrix forms indicates that sintering pellets may be used as a simple cost effective technique to evaluate compositions for likely single crystal scintillator performance.

Introduction

Inorganic oxide single crystals activated as Ce^{3+} are promising scintillator candidates which can be used to detect high energy photons and particles in medical imaging equipment, high-energy and nuclear physics detectors, and X-ray security systems [1]. For example, Ce doped lutetium oxyorthosilicate (LSO) has been widely used in medical imaging detectors since the late 1990s due to its relatively high light yield (~ 30,000 ph/MeV) and fast decay time (~ 40 ns) [2]. Ce3+ doped gadolinium–gallium–aluminum garnet crystals have recently attracted much attention due to their good mechanical and chemical stability, high density (6.67 g/cm^3), high light yield and short decay time [3,4]. It is well known that the luminescence properties of Ce^{3+} doped garnet materials originate from the 4f-5d radiative transition [5,6]. At present, $Gd_3Ga_3Al_2O_{12}$:Ce (GGAG:Ce) scintillation crystals for research have been mainly grown by the Czochralski (CZ) and micro-pulling down methods. Kamada [7,8] and his co-workers focused on the growth of $RE_{3-y}Gd_yGa_xAl_{5-x}O_{12}$:Ce crystals with higher light yield by adjusting the ratio of Ga/Al, Gd/RE and the concentration of Ce. They reported light yield as high as ~ 45,000 ph/MeV and decay time as short as ~ 53 ns in a series of GGAG crystals grown by the micro- pulling down method when the ratio of Ga/Al is equal to 2 or 3 [8]. The GGAG crystals grown by the CZ method and

doped with 1 at% Ce had higher light yield (~ 46,000 ph/MeV) than that of the crystals doped with 2 at% or 3 at% Ce, while the decay time becomes longer (~ 92 ns) [9]. Kang [10] reported the luminescence intensity could be markedly increased by adding B3+ as the codopant in GGAG:Ce phosphors. Prior work by our group has demonstrated that it is possible to modify the scintillation properties of LSO:Ce, YSO:Ce, GSO:Ce and GGAG:Ce by codoping with other dopants [11–14]. However, it is not practical to test every possible dopant candidate by growing single crystals, given the cost and time investment required for CZ growth, and therefore a cost-effective method to select the most promising dopant candidates based on the radioluminescence (RL) intensity and photoluminescence (PL) decay of small polycrystalline GGAG:Ce pellets is presented here.

Materials and methods

GGAG:Ce pellets codoped with B, Ca, Ba Mg, Sr, Zr, Fe, Bi, Zn, Ag, Nb, Cu, K and Na were prepared by solid-state synthesis and characterized by PL, RL, reflectivity and PL decay measurements. PL and RL measurements provide the information regarding the dopant energy level position. Due to the opacity of the pellets, transmission measurements were not available, and therefore reflectivity measurements were used to determine the wavelength of the absorbance bands. RL intensity and PL decay of the pellets were used to predict the light yield and scintillation decay of single crystals. The codopants B^{3+} and Ba^{2+} were selected for crystal growth experiments due to their higher RL intensity

and Ca^{2+} was selected due to its faster PL decay.

Pellets preparation

The raw material used including Gd_2O_3 (99.9995%), Ga_2O_3 (99.999%), Al_2O_3 (99.997%) and CeO_2 (99.99%) powders, with codopants provided by H_3BO_3, CaO, $BaCO_3$, MgO, SrO, ZrO_2, Fe_2O_3, Bi_2O_3, ZnO, Ag_2O, Nb_2O_5, CuO, K_2CO_3, and Na_2CO_3. The cerium dopant and various codopants were mixed stoichiometrically according to the formula $(Gd_{1-y-z}Ce_yR_z)_3\ Ga_3Al_2O_{12}$ (y=z= 0.5%) where R designates the codopants. Thus, the concentration of the dopant and all codopants is 0.5 at% with respect to gadolinium. In cases where the codopant starting material was a carbonate, it was assumed that the carbon was removed as gaseous CO or CO_2. The powders were ball milled for 5 min in a SPEX 8000M mixer before being pressed into pellets in a Carver 4350.L press. The pellets were then sintered twice in an air atmosphere in a tube furnace at 1500 ˚C for 10 h each time in an air atmosphere. The color of the pellets changed from white to yellow after sintering, as shown in Figure 2.1, indicating that a reaction has occurred.

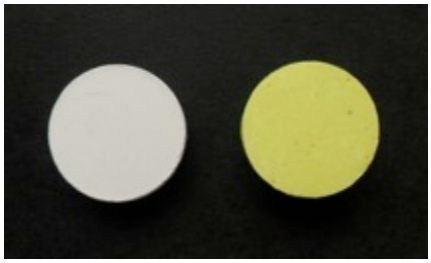

Figure 2.1. GGAG pellets before (a) and after (b) sintering at 1500 ^{o}C for 10 hours.

Crystal growth procedure

All GGAG crystals in this study were grown via the CZ method in the iridium crucible in a Cyberstar Oxypuller 05-03 growth station. All were doped with 0.2 atomic percent Ce. One set was grown with 0.2 at % of the codopants B, Ca, Ba; another set was grown with 0.4 at % B and Ba. In all cases the concentrations given are those of the initial starting melt; the concentration in the finished crystal will differ due to segregation at the solid-liquid interface during growth. The Gd_2O_3, Ga_2O_3, Al_2O_3 and CeO_2 used as the starting materials were at least 99.99% pure. In each crystal, an excess of 3% Ga_2O_3 was added to the melt to account for the loss of Ga due to the vaporization caused by instability of this element at the melt temperature [15]. The growth atmosphere was flowing nitrogen with a small fraction of a percent oxygen. One mm thick polished wafers and 5 × 5 × 5 mm^3 cubes were cut from the boules for measurements; these samples were taken from similar positions in each boule to ensure consistent cerium concentrations. A representative GGAG:Ce crystal boule and wafer are shown in Figure 2.2.

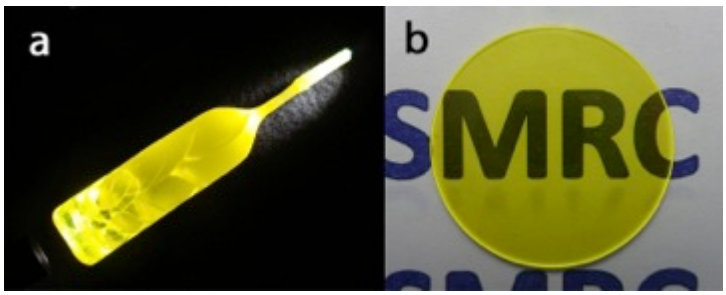

Figure 2.2. (a) Photographs of GGAG:Ce crystals grown by CZ method and (b) ~1mm thick polished wafer.

Characterizations

The X-ray diffraction measurements were performed on finely powdered single crystal and sintered pellet samples using a Bruker Axs D2 Phaser instrument. The reflectivity and transmittance (absorbance) spectra were measured with a Varian Cary 5000 spectrophotometer. The RL spectra were obtained at room temperature under X-ray radiation at 35 kV and 0.1 mA using an ACTON SP-2155 monochromator. The PL spectra were acquired with a Hitachi F-4500 fluorescence spectrophotometer equipped with Xe lamp. The PL decay time was measured with a HORIBA Jobin Yvon Fluorolog-3 spectrofluorometer using a time-correlated single photon counting module, where Nano LEDs (pulsed light-emitting diodes) were used as the excitation source. The scintillation decay time profile was measured using the Bollinger-Thomas time-correlated single photon technique with a ^{137}Cs gamma-ray source. The absolute light output was measured using a 10 μCi ^{137}Cs gamma-ray source, a Hamamatsu R2059 PMT with known quantum efficiency, a 3 μs shaping time, and a hemispherical Spectralon reflector to enhance the light collection.

Results and discussion

The effect of codoping on PL, RL, reflectivity and PL decay of GGAG pellets

PL, RL, reflectivity spectra and PL decay of GGAG:Ce pellets with different codopants are shown in Figure 2.3, Figure 2.4, Figure 2.5 and Figure

2.6 respectively. The excitation peaks around 345 nm and 445 nm shown in Figure 2.3 are due to the Ce 4f-$5d_2$ and 4f-$5d_1$ transitions and the emission peak around 540 nm shown in Figure 2.4 is due to the Ce 5d-4f transition [16]. For all codopants, the excitation peak intensity at 445 nm is much stronger than that of the peak at 345 nm. Similarly, the reflectivity spectra indicate absorption bands between 300 and 400 nm and between 400 and 500 nm as shown in Figure 2.5; the 300 - 400 nm band is less pronounced than the 400 - 500 nm band. Furthermore, the 300 - 400 nm absorption band for Ca codoping is stronger than the other codopants, as shown in the inset in Figure 2.5, suggesting that the Ce 4f-$5d_2$ transition is suppressed by Ca, which is consistant with the fact that the lowest intensity of the excitation peak at 345 nm is observed in the pellets with Ca codoping (Figure 2.3). In Figure 2.4, the highest RL intensity is given by B and Ba codoping while the lowest RL intensity is found with Ca codoping. This is consistent with the previous finding that the trivalent B assists the synthesis of GGAG:Ce powder phosphor, as evidenced by the increased luminescence intensity for the sample with additional B doping compared to the counterpart doped with Ce only, under the excitation of 470 nm photons [10]. The increased RL intensity in GGAG:Ce pellets may be due to the enhancement of crystallinity of phosphor with more B addition, suggested by XRD spectra [10]. Additionally, the increased RL intensity by Ba addition are possibly due to the reduced defects and/or the modified lattice parameters, as suggested by Kang [17] in the Ba codoped Zn_2SiO_4:Mn ceramic particles and by Liao [18] in Ba codoped YVO_4:Eu

phosphor. Among all codopants tested, the fastest PL decay was achieved in the pellets with Ca codoping, as shown in Figure 2.6. The PL decay was measured under 345 nm excitation and emission at 540 nm.

The effect of concentration of codopants B and Ca in PL, RL, Reflectivity and PL decay of GGAG pellets

The concentration dependence of the PL, RL, reflectivity spectra and PL decay of Ca and B codoped GGAG pellets are shown in Figure 2.7, Figure 2.8, Figure 2.9 and Figure 2.10 respectively. The concentration of codopants B and Ca varies from 0 to 2.5 at % with respect to the Gd rare earth. The PL results shown in Figure 2.7 demonstrate that the Ce 4f-5d_2 transition in terms of the excitation peak at 345 nm can be further suppressed as the concentration of Ca increases while it is not affected by the concentration of B. In Figure 2.8b, the RL intensity increases as the concentration of B increases. In contrast, the trend is reversed for Ca (Figure 2.8a). The concentration of the codopants has no significant influence on the reflectivity spectra of both Ca and B codoped pellets, as shown in Figure 2.9. However, in comparison to B codoped pellets, all of the Ca codoped pellets show obscure absorption band in the reflectivity spectra between 300 and 400 nm. The PL decay time (Figure 2.10) is reduced as the concentration of Ca increases, while no significant dependence on the concentration of B was observed. Furthermore, the concentration of the codopants does not affect the reflectivity, excitation or emission peak positions.

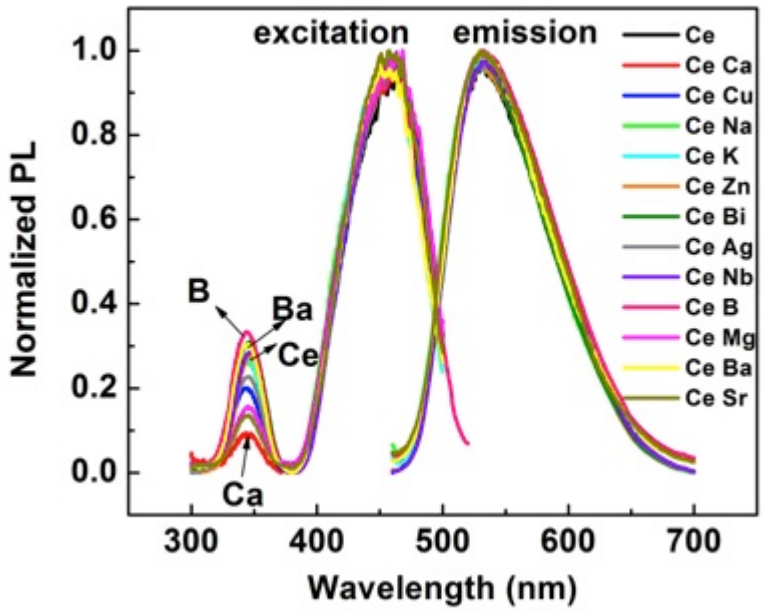

Figure 2.3. PL spectra of GGAG: Ce pellets with different codopants.

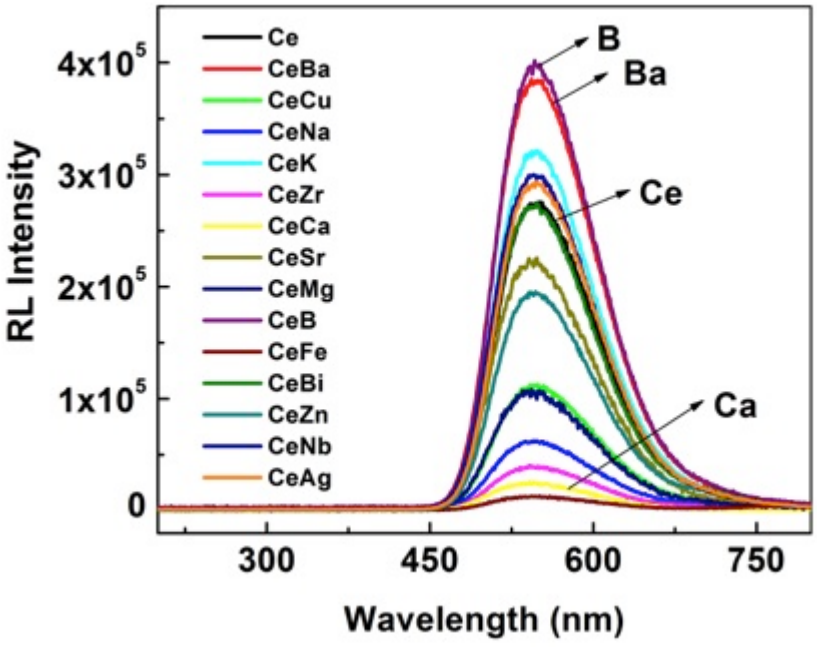

Figure 2.4. RL spectra of GGAG: Ce pellets with different codopants.

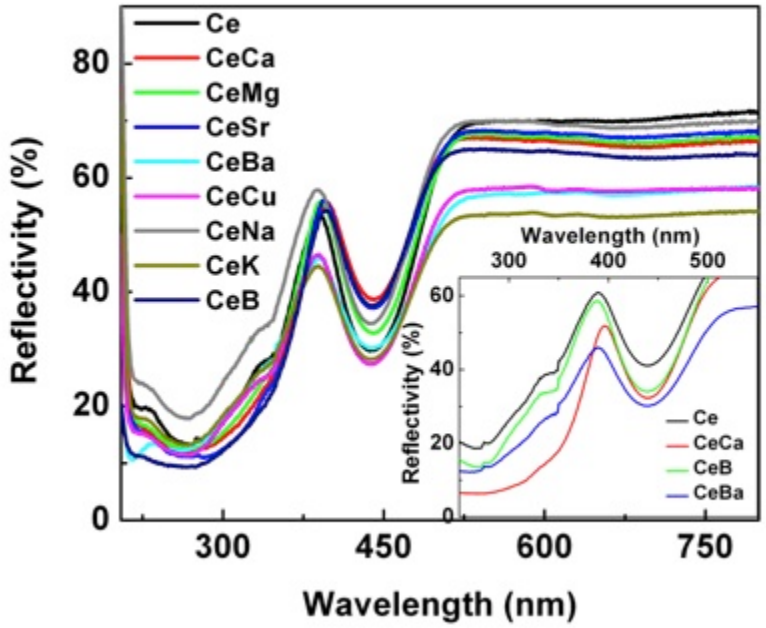

Figure 2.5. Reflectivity spectra of GGAG: Ce pellets with different codopants. The insert is an enlargement of the 250 - 550 nm wavelength range.

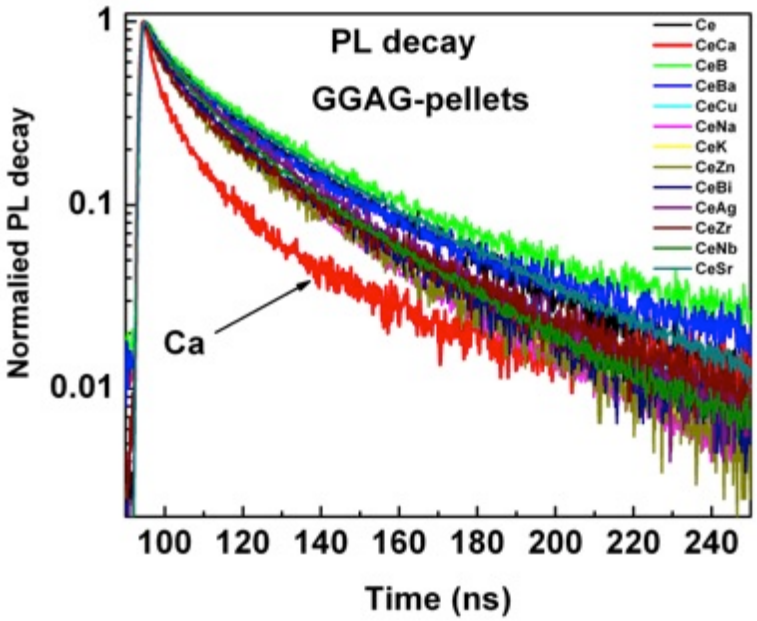

Figure 2.6. PL decay of GGAG: Ce pellets with different codopants.

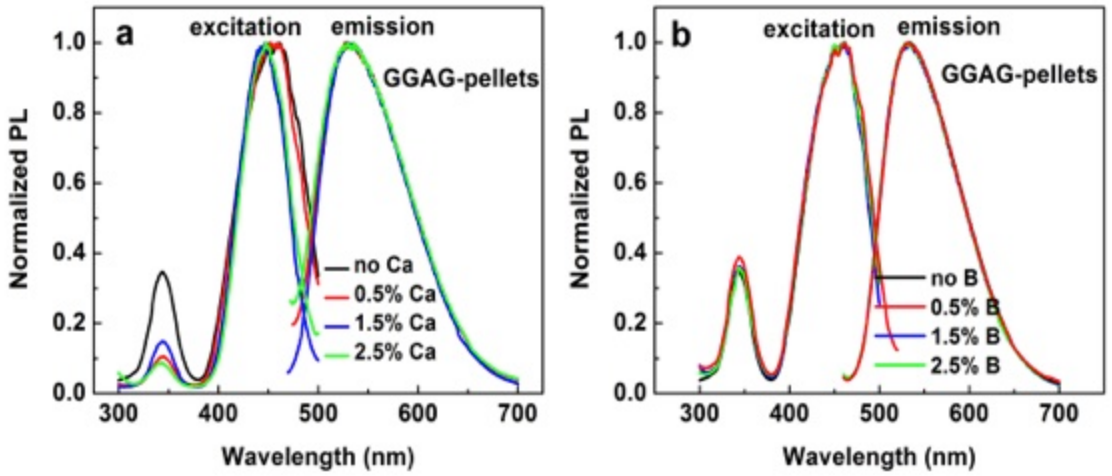

Figure 2.7. Concentration dependence of the PL spectra of Ca and B codoped GGAG pellets.

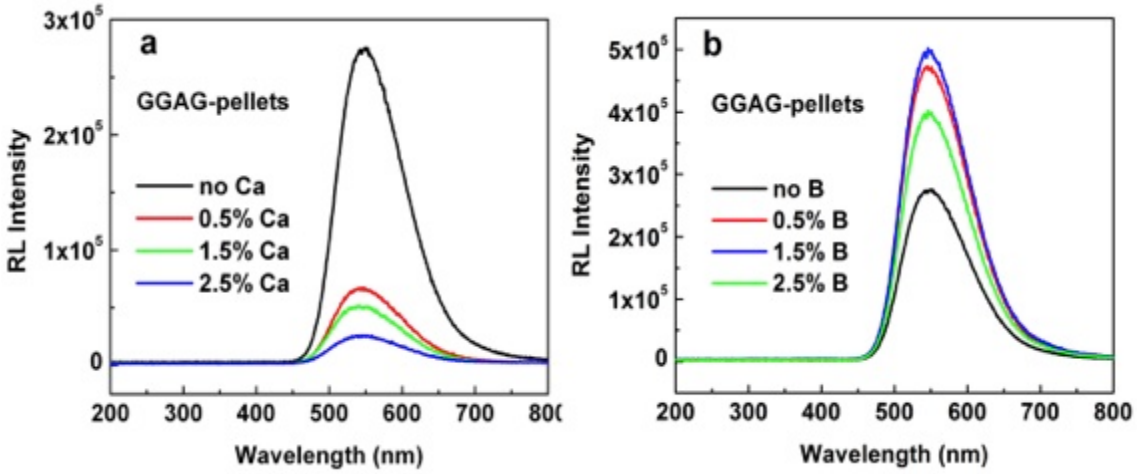

Figure 2.8. Concentration dependence of the RL spectra of Ca and B codoped GGAG pellets.

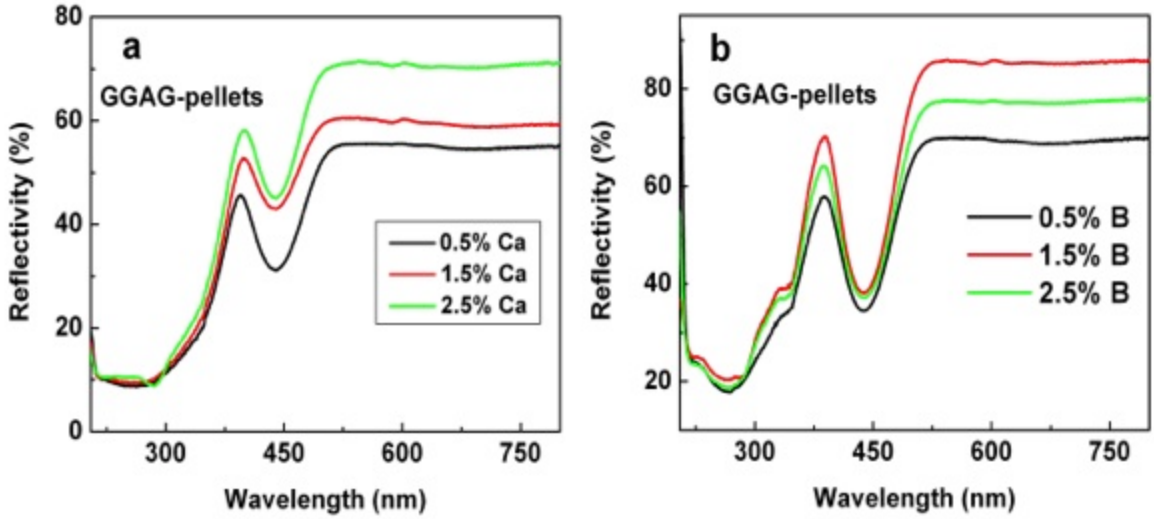

Figure 2.9. Concentration dependence of the reflectivity spectra of Ca and B codoped GGAG pellets.

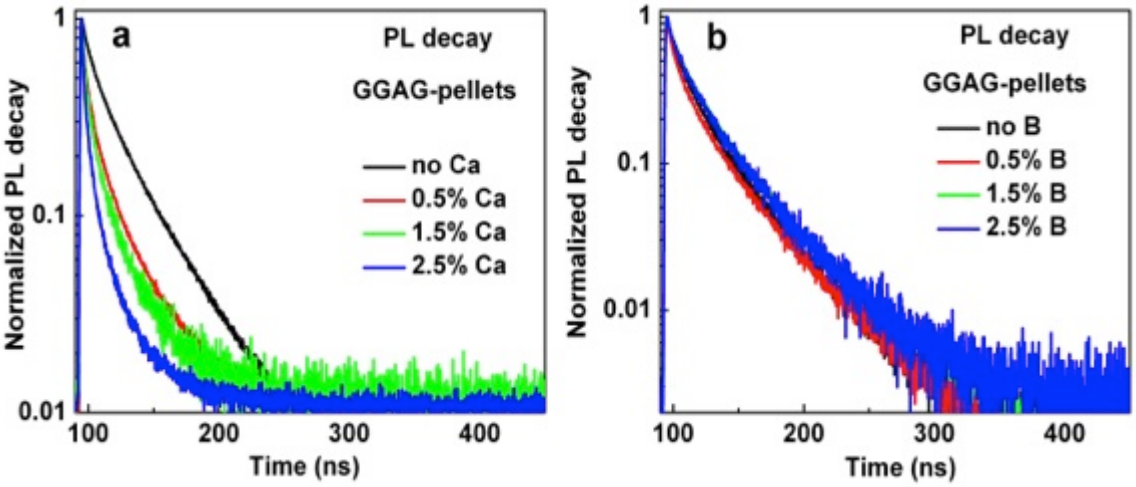

Figure 2.10. Concentration dependence of the PL decay of Ca and B codoped GGAG pellets.

Scintillation properties of GGAG crystals

The pulse height spectra and scintillation decay of the single crystals grown by the CZ method with different dopants under ^{137}Cs exposure are shown in Figure 2.11. Absolute light yield values based on the pulse height spectra of all samples are calculated and shown in Table 2.1. Compared to Ce only doped GGAG crystal, 0.2 at % B and Ba codoping increases the light yield by approximately 14.6% and 13.5%. However, doubling the concentration of B and Ba (from 0.2 at % to 0.4 at %) only further increases the light yield by 0.2% and 0.5%, respectively. In contrast, 0.2 at % Ca codoping reduces the light yield by 20.4%. The decay time value was also shown in Table 2.1. They were extracted by fitting Figure 2.11b with a double exponential decay model. The first component comes from de-excitation of the 5d state to the 4f state of Ce^{3+} center, while the slower second component can be attributed to energy transfer from Gd^{3+} to Ce^{3+} as reported in other Gd based scintillators [14, 19]. The ratios for the fast decay and the slow decay are also presented. Ca codoping shortens the scintillation decay time in the single crystal GGAG, while the light yield is reduced. The above scintillation properties of the crystals are consistent with the high RL intensity in the pellets with B and Ba codoping and the fast PL decay and low RL intensity in the pellets with Ca codoping. The highest light yield (~ 53,300 and 52,800 ph/MeV) is achieved in B and Ba codoped crystals. On the other hand, the Ca codoped crystal has the shortest scintillation decay time (~ 43 ns) as a major component in the double exponential decay. Compared to other

approaches to improve the scintillation properties of GGAG:Ce single crystals, such as varying Ce concentration [9] and the ratio of Ga/Al [8], we have achieved the highest light yield and shortest decay time by codoping.

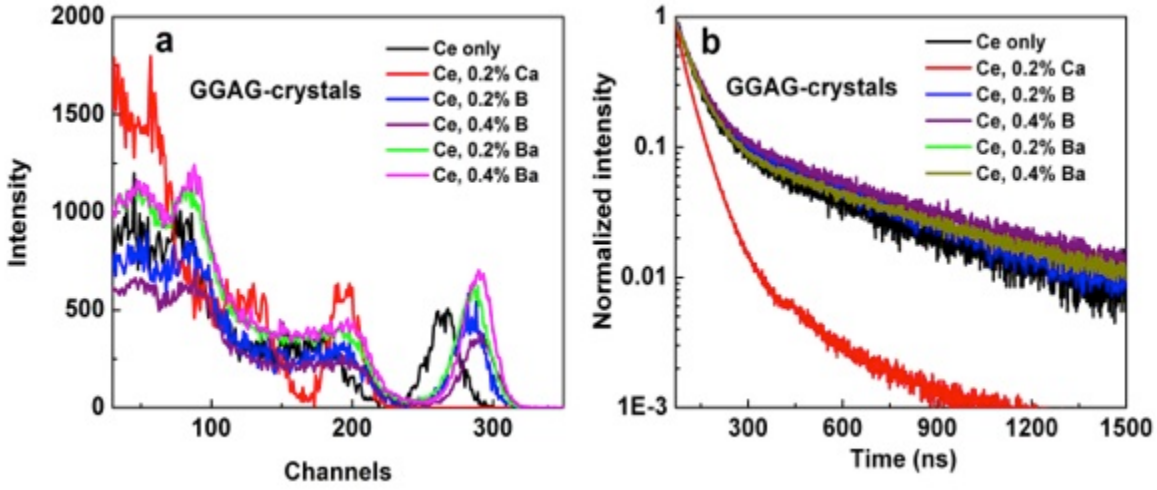

Figure 2.11. Relative light yield, scintillation decay time of GGAG crystals with different dopants.

Table 2.1 Light yield and scintillation decay time of GGAG crystals with different codopants.

Composition	LY (ph/MeV)	Fast decay time (ns)	Slow decay time (ns)
GGAG: 0.2% Ce	46,500	51 (73 %)	381 (27 %)
GGAG: 0.2% Ce, 0.2% Ca	37, 000	43 (75 %)	144 (25 %)
GGAG: 0.2% Ce, 0.2% B	53,300	51 (69 %)	388 (31 %)
GGAG: 0.2% Ce, 0.4% B	53,400	56 (66 %)	464 (34 %)
GGAG:0.2% Ce, 0.2% Ba	52,800	57 (59 %)	468 (41 %)
GGAG: 0.2% Ce, 0.4% Ba	53,000	56 (59 %)	438 (41 %)

Comparison between GGAG crystals and corresponding pellets

It was found that the pellets and crystals share several similar structural and optical properties. In Figure 2.12, a comparison of the GGAG single crystal and pellet XRD spectra show that both the synthesized pellet and the single crystal have a single cubic garnet phase, which agrees well with the GGAG reference pattern in Pearson's Crystal Data (No 1627563) and Kamada's results [8]. The XRD data did not show any evidence of any phase other than the major GGAG garnet phase, and there was no noticeable change in the XRD peak intensity or position for the pellets and crystals with different codopants. This is expected since the codopant concentration is very small (0.5 at % in pellets and 0.2 at % in crystals). Similarly, Kang [10] observed no evidence of other phase in the XRD and only minor peak intensity changes in the GGAG:Ce codoped with much higher concentration of B. The comparison of the normalized RL and PL spectra between the single crystals and the pellets with the same dopants are shown in Figure 2.13 and Figure 2.14 respectively. The peaks in both spectra appear at nearly the same positions. While it is not possible to measure the absorbance or transmittance of the opaque pellets, our results demonstrate that the reflectivity of the pellets is strongly correlated with the absorbance or transmittance of the single crystals, as seen in Figure 2.15. The peak that appears at 445 nm in the transmittance spectra of the crystal is consistent with that in the reflectivity spectra of the pellets. The suppression of the Ce 4f-5d_2 transition is also observed in the crystal codoped with Ca as evidenced by the

less pronounced peak around 345 nm in transmittance spectra (Figure 2.15b).

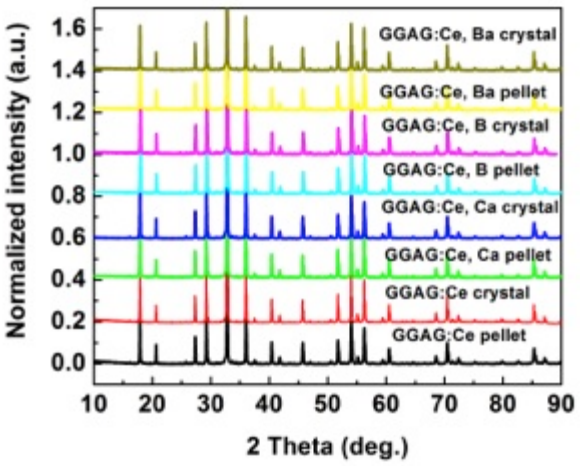

Figure 2.12. Powder X-ray diffraction comparison between GGAG pellets and crystals.

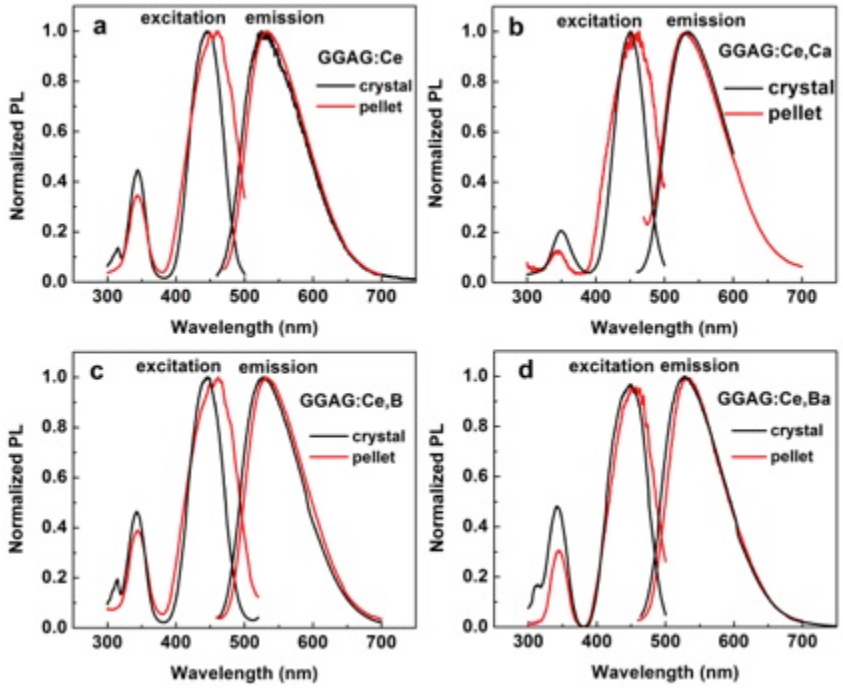

Figure 2.13. Normalized PL spectra comparison between GGAG crystals and pellets.

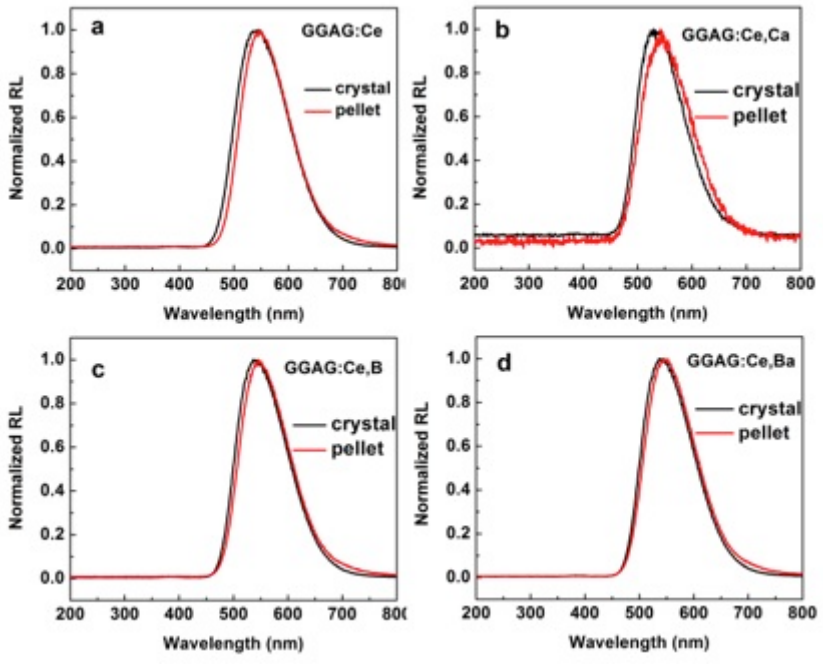

Figure 2.14. Normalized RL spectra comparison between GGAG crystals and pellets.

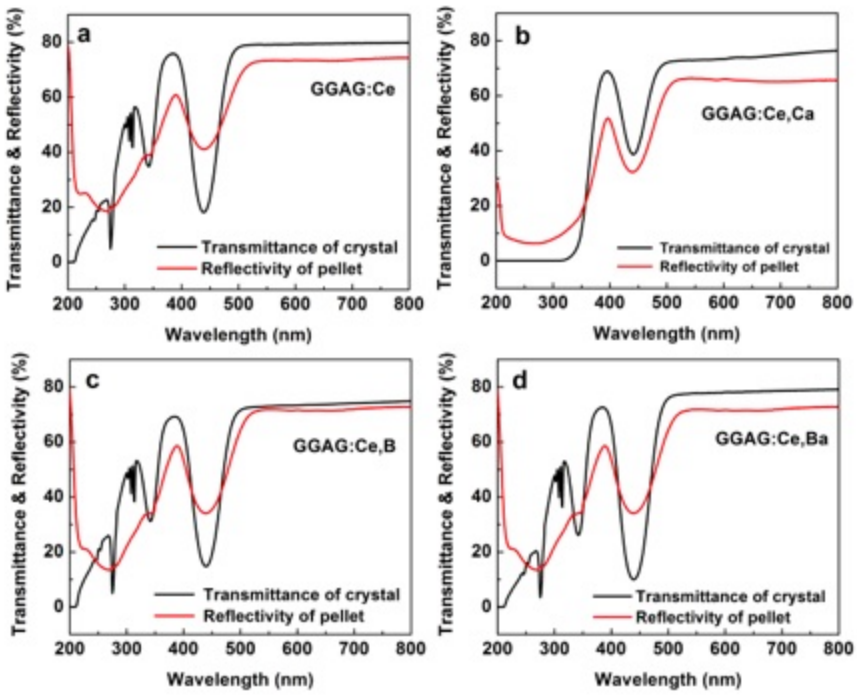

Figure 2.15. The comparison between the transmittance spectra of GGAG crystals and the reflectivity spectra of pellets.

The RL intensity and PL decay time of the pellets are strongly correlated with the light yield and scintillation decay time of the crystals. B and Ba codoping increase the RL intensity in the GGAG:Ce pellets (Figure 2.4), which is consistent with the higher light yield in B and Ba codoped GGAG:Ce crystals, while Ca codoping shortens the PL decay time (Figure 2.6) in the pellets and reduces the scintillation decay time in the corresponding crystals (Table 2.1). Based on the above similarities between the pellets and the crystals, which are summarized in Table 2.2, one can use the pellets to assess the probable optical and scintillation properties of single crystals of the same composition.

Conclusion

We have found that 0.5 at % B and Ba codoping help to increase the RL intensity in the GGAG:Ce pellets, which is consistent with the improved light yield (~ 53,000 ph/MeV) in 0.2 at % B and Ba codoped GGAG:Ce crystals, higher than the ~ 46,500 ph/MeV in Ce-only doped GGAG crystals. On the other hand, 0.2 at % Ca codoping reduces the scintillation decay time from 51 ns (Ce-only doped GGAG crystal) to 43 ns, which is in agreement with the shortened PL decay time in 0.5 at % Ca codoped GGAG:Ce pellets. The results from pellets and crystals are sufficiently similar for one to use pellets as an inexpensive and quick way to evaluate compositions prior to undertaking the time and expense involved in single crystal growth. This idea has been demonstrated in GGAG in this paper, and may also be extended to other scintillator materials whose scintillation properties could be improved by codoping.

Table 2.2 The comparison of the correlated properties between the pellets and the corresponding crystals. I0 and t0 are taken as the RL intensity and the PL decay time of the Ce-only doped GGAG pellet.

Pellets (0.5 at % for all dopant and codopants)					Crystals (0.2 at % for all dopant and codopants)				
Properties	Ce	Ce, B	Ce, Ba	Ce, Ca	Properties	Ce	Ce, B	Ce, Ba	Ce, Ca
XRD	garnet phase				XRD	garnet phase			
PL peak position (nm)	excitation: 345, 445 emission: 540				PL peak position (nm)	excitation: 345, 445 emission: 540			
RL peak position (nm)	540				RL peak position (nm)	540			
Reflectivity peak position (nm)	345, 445	345, 445	345, 445	445	Transmittance peak position (nm)	345, 445	345, 445	345, 445	445
RL intensity	I_0	> I_0	> I_0	< I_0	Light yield (ph/MeV)	46,500	53,300	52,800	37,000
PL decay time	t_0	~ t_0	~ t_0	< t_0	Scintillation decay time (ns)	51	51	57	43

References for Chapter 2

[1] M. Nikl, (2006). "Scintillation detectors for x-rays." Meas. Sci. Technol., 17(4): R37.

[2] F. Daghighian, et al., (1993). "Evaluation of cerium doped lutetium oxyorthosilicate (LSO) scintillation crystals for PET." IEEE Trans. Nucl. Sci. 40(4): 1045-1047.

[3] J. Iwanowska, et al., (2013). "Performance of cerium-doped $Gd_3Al_2Ga_3O_{12}$ (GAGG:Ce) scintillator in gamma-ray spectrometry." Nucl. Instrum. Methods Phys. Res. Sect. A., 712: 34-40.

[4] M. Nikl, et al., (2008). "Scintillator materials-achievements, opportunities, and puzzles." IEEE Trans. Nucl. Sci. 55(3):1035-1041.

[5] R.R. Jacobs, et al., (1978). "Measurement of excited-state-absorption loss for Ce3+ in $Y_3Al_5O_{12}$ and implications for tunable 5d→ 4f rare-earth lasers." Appl. Phys. Lett. 33(5): 410-412.

[6] T. Yanagida, et al., (2007). "Improvement of ceramic YAG (Ce) scintillators to $(YGd)_3Al_5O_{12}$ (Ce) for gamma-ray detectors." Nucl. Instrum. Methods Phys. Res. Sect. A., 579(1): 23-26.

[7] K. Kamada, et al., (2011). "Scintillator-oriented combinatorial search in Ce-doped $(Y,Gd)_3(Ga,Al)_5O_{12}$ multicomponent garnet compounds." J. Phys. D: Appl. Phys. 44(50): 505104..

[8] K. Kamada, et. al., (2011). "Composition engineering in cerium-doped $(Lu, Gd)_3(Ga,Al)_5O_{12}$ single-crystal scintillators." Cryst. Growth Des. 11(10): 4484-4490.

[9] K. Kamada, K., et al., (2012). "Crystal growth and scintillation properties of Ce doped single crystals." IEEE Trans. Nucl. Sci. 59(5): 2112-2115.

[10] J. G. Kang, et al., (2008). "Preparation and luminescence characterization of GGAG:Ce^{3+},B^{3+} for a white light-emitting diode." Mater. Res. Bull. 43(8): 1982-1988.

[11] M. Koschan, et al., (2012). "A comparison of the effect of Ca^{2+} codoping in cerium doped GSO with that of LSO and YSO." J. Cryst. Growth, 352(1): 133-136.

[12] H. E. Rothfuss, et al., (2009). "The effect of codoping on shallow traps in

YSO:Ce scintillators." IEEE Trans. Nucl. Sci. 2009, 56(3): 958-961.

[13] M. A. Spurrier, et al., (2008). "Effects of co-doping on the scintillation properties of LSO:Ce." IEEE Trans. Nucl. Sci. 55(3): 1178-1182.

[14] M. Tyagi, et al., (2013). "Effect of codoping on scintillation and optical properties of a Ce-doped $Gd_3Ga_3Al_2O_{12}$ scintillator." J. Phys. D, Appl. Phys. 46(47): 475302.

[15] C. D. Brandle, et al., (1972). “The Elimination of Defects in Czochralski Grown Rare-Earth Gallium Garnets.” J. Cryst. Growth 12: 195-200.

[16] J. M. Ogiegło, et al., (2013). "Luminescence and Luminescence Quenching in $Gd_3(Ga,Al)_5O_{12}$ Scintillators Doped with Ce^{3+}." J. Phys. Chem. A. 117(12): 2479-2484.

[17] Y. C. Kang, et al., (2003). “Ba^{2+} Co-doped Zn_2SiO_4: Mn phosphor particles prepared by spray pyrolysis process." J. Electrochem. Soc.150(1): H7-H11.

[18] Y. Liao, et al., (2013). “Strong luminescence enhancement of YVO_4:Eu^{3+}, Ba^{2+} phosphors prepared by a solvothermal method." J. Alloys Compd. 561: 214-219.

[19] H. Suzuki, et al., (1994). "Energy transfer mechanism in $Gd_2(SiO_4)O$:Ce scintillators." IEEE Trans. Nucl. Sci. 41(4): 681-688.

Chapter 3 EFFECT OF CODOPING ON THE LUMINESCENCE CENTERS AND CHARGE TRAPS IN GGAG:CE CRYSTALS

A version of this chapter by Fang Meng will be submitted to *Journal of Luminescence*. Copyright to this paper is assumed to belong to this journal.

This chapter is the reformatted version of the original work submitted to the referenced journal. No additional changes to the content of the original article were done other than formatting to conform to the dissertation format.

Abstract

Single crystals of $Gd_3Ga_3Al_2O_{12}$ (GGAG) doped with 0.2 at % Ce and codoped with Ca, B, or Ba (in all cases 0.2 at % with respect to the rare earth in the melt) were grown by the Czochralski technique. The effect of codoping on Ce luminescence centers was investigated via photoluminescence (PL), radioluminescence (RL), and temperature dependent PL decay measurements in the range of 40K-550K. Excitation bands were observed in PL spectra at 345 and 445 nm due to the 4f-5d transition of Ce^{3+} ions. An emission band in PL spectra was observed at 550 nm, which was consistent with the RL spectra. Ca codoped scintillator introduced an additional F^+ luminescence center with the excitation at 345 nm and emission at 400 nm. In addition, Ca codoping significantly suppressed the higher energy excitation band at 345 nm, while B and Ba codoping slightly increased this band relative to the 445 nm band. The RL spectra were similar for all codopants. The temperature dependence of the PL decay spectra showed that codopants affected the thermal quenching behavior;

For the studied codopants, the starting temperature for thermal quenching ranged from ~300 to 350 K and their thermal activation energy ranged from ~ 370 to 580 meV. On the other hand, the effect of codoping on charge traps was investigated with thermoluminescence (TL) and afterglow measurements. TL spectra showed that Ca codoping significantly reduced the trapped charge population around room temperature, which was correlated with the reduced afterglow.

Introduction

Recently, inorganic scintillation material with high density and high gamma-ray absorption coefficient combined with photodetectors are attracting a great deal of attention in the application for medical imaging, homeland security, high energy and nuclear physics detectors [1-2]. Oxides materials having garnet structure are promising candidates as scintillator, because of their well-mastered technology for many applications and easy doping with rare earth elements [3-4]. Cerium (Ce) activated garnets are excellent scintillation detectors due to their achievement of combining stopping power, decay time, light yield and non-hygroscopicity [5-6]. Ce doped yttrium/lutetium aluminum garnets are particularly interesting in view of its maximum theoretical light yield (LY) in the order of 60,000 photons/MeV based on Bartram-Lempicki theory [7]. However, the measured LY values are much smaller due to the intrinsic defects such as antisites and vacancies [8]. Many approaches were undertaken to improve its performance. The most remarkable improvement was achieved by Kamada [9-

10] via substituting yttrium/lutetium with gadolinium (Gd) and admixing gallium (Ga) with aluminum in $(Lu,Y)_3Al_5O_{12}$ single crystal. They have successfully grown $Gd_3Al_2Ga_3O_{12}$:Ce (GGAG) scintillator with higher LY (~ 45, 000 photons/MeV) and low decay time (~ 55 ns), thanks to the combination of band gap engineering for favorable low 5d Ce^{3+} level positioning. In addition, they optimized the concentration of Ce to improve the energy resolution and LY in the GGAG single crystals with 2 inches diameter [11-12].

Codoping has been proved to be an effective way to alter various properties of many scintillators. Koschan [13], Rothfuss [14] and Yang [15] demonstrated that Ca^{2+} codoping in LSO and YSO significantly shortens the scintillation decay time and improves the LY. B^{3+} codoping of GGAG:Ce phosphors has been shown to result in higher luminescence intensity [16]. These results motivated our investigations into the effect of codoping in GGAG:Ce single crystals, aiming to further improve the LY and decay time.

We previously reported on the effect of Ca, B, and Ba co-doping on energy resolution, scintillation kinetics and optical properties of GGAG:Ce scintillators [17-18]. Ca codoping shortens the scintillation decay time, while B and Ba codoping increase the light yield. Here we investigate the effect of codoping on luminescence center and charge traps in GGAG:Ce crystals. The former was studied via analyses of emission and excitation spectra, PL decay and thermal response over a range of temperatures. The latter was investigated by TL and afterglow spectra. Detailed traps parameters based on TL glow peak

analysis and the fast component of afterglow decay are presented.

Experimental procedure

The GGAG:Ce boules were grown from the melt via the Czochralski technique in inductively heated iridium crucibles. The Gd_2O_3, Ga_2O_3, Al_2O_3, CeO_2 and CaO, H_3BO_3, $BaCO_3$ used as the starting materials were at least 99.99% pure. Crystal growth was initialized on seed crystals and was controlled via an automated system, which used the derivative of the crystal weight as the process variable. All melts were doped with 0.2 at% Ce and co-doped with 0.2 at% Ca, B, or Ba respectively with respect to rare earth. All concentrations given are those of the initial starting melt; the concentration in the finished crystal will differ due to the segregation at the solid-liquid interface during growth. The flowing atmosphere was nitrogen mixed with a small amount of oxygen. The boule size was ~ 80 mm tall and ~ 32 mm in diameter. Table 3.1 lists the compositions of the crystals that were grown and characterized. The samples for the measurements were unpolished 5 mm cubes that cut from same point in the boule in order to get consistent Ce concentration.

The low temperature emission/excitation spectra and the X-ray excited luminescence were measured with a HORIBA Jobin Yvon Fluorolog-3 Spectrofluorometer. An Advanced Research Systems (ARS) (model DE202AE) closed cycle helium cryostat system was used to cool the samples down to 40 K. In the case of emission and excitation spectra, a 450 W continuous Xenon lamp was used as the excitation source. For X-ray excited luminescence

measurements, an X-ray tube operated at 35 kV and 0.1 mA was used as the excitation source.

Table 3.1 List of Samples

Sample	Composition	At% of Ce (in the melt)	At% of codopants (in the melt)
1	GGAG:Ce	0.2	0
2	GGAG:Ce, Ca	0.2	0.2
3	GGAG:Ce, B	0.2	0.2
4	GGAG:Ce, Ba	0.2	0.2

Photoluminescence decay was measured on the same Spectrofluorometer using a Time-Correlated-Single-Photon-Counting module where Nano LEDs (pulsed light emitting diodes) were used as the excitation source. All data were fit by a single exponential decay model.

The Scintillation decay time profile was measured using the Bollinger-Thomas time-correlated single photon technique and a ^{137}Cs gamma-ray source. The relative light output was measured using a 10 μCi ^{137}Cs gamma-ray source. 5 mm cubes were placed on the Hamamatsu R2059 photomultiplier tube (PMT) window, and a hemispherical Spectralon reflector was used to enhance the light collection. BGO as a reference WAS set to 100 channels.

For thermoluminescence glow curve measurements, the sample was mounted within the same ARS cryostat. The pressure was reduced to 20 m Torr and the sample was then heated to 600 K to empty traps. The sample was cooled down to 9K and irradiated with X-rays (35 kV, 0.1 mA) through a beryllium

window for approximately 15 min. Subsequently, the sample was brought back to 600 K at a rate of 0.15 K/s. A Hamamatsu H3177 PMT was used to measure the luminescence emitted by the sample as a function of temperature.

For afterglow measurements, crystals were first annealed for 10 min at 600 K. After cooled to room temperature, the crystals were coupled to a Hamamatsu R3177 PMT with a Dow Corning Q2-3067 optical couplant, and covered with a Tetratex TX3104 PTFE membrane. The crystals were then irradiated with X-rays at room temperature for 15 min. A Uniblitz XRS6S2P1-040 shutter was used to cut off the X-ray beam within 3 ms. The luminescence emitted was then measured as a function of time. All measurements were done at room temperature.

Results and discussion

Photoluminescence and radioluminescence

Figure 3.1a shows the a comparison of the excitation spectra for the GGAG:Ce crystals with different codopants. The excitation bands were observed at 445 and 345 nm due to the 4f-5d_1 and 4f-5d_2 transitions of Ce^{3+} ions. Sharp bands at 310 nm are assigned to the transitions of Gd^{3+} ion. Ca codoping significantly suppress the excitation band of Ce at 345 nm compared to that of Ce band at 445 nm. The same phenomena was observed in other Ca codoped silicate scintillators. Figure 3.1b and Figure 3.1c show the comparison of the emission spectra for the crystals with different codopants when exciting at 345 nm and 445 nm respectively. The transitions from excited 5d_1 and 5d_2 state to

ground 4f state of Ce^{3+} give rise to the emission bands at 550 nm, which is typical for the GGAG garnet structure. The intensity of these emission peaks was slightly increased in both B and Ba codoping, whereas they were reduced in Ca codping, comparing to the non-codoped GGAG cystals. The same trend was observed in RL spectra of GGAG crystals with different codopants as shown in Figure 3.1d. Apparently, when exciting at 345 nm, Ca codoping introduced an additional emission band around 400 nm (see Figure 3.1b), corresponding to the emission energy of 3.1 eV. The intensity of this additional emission peak was higher than that of Ce emission at 550 nm. The complete excitation/emission spectra of Ca codoping are shown in Figure 3.2a. The excitation band around 345 nm for the additional emission band around 400 nm appeared at the similar wavelength as the Ce 4f-$5d_2$ excitation band. The PL decay time of this new luminescence center (excitation/emission: 345 nm/400 nm) and the Ce luminescence center (excitation/emission: 345 nm/550nm) in Ca codoping was measured and shown in Figure 3.2b. Based on a single exponential decay model, the calculated PL decay time of the additional luminescence center was about 3.5 ns, in contrast to 45 ns for the Ce luminescence center. This emission energy (3.1 eV) and fast PL decay of the additional luminescence center were possibly due to the F^+ center, considering the similar emission energy and the PL decay time in YAG crystal reported by Zorenko [19]. A possible explanation is that the F^+ center luminescence may derive from an oxygen vacancy occurring with the introduction of divalent calcium into a trivalent site.

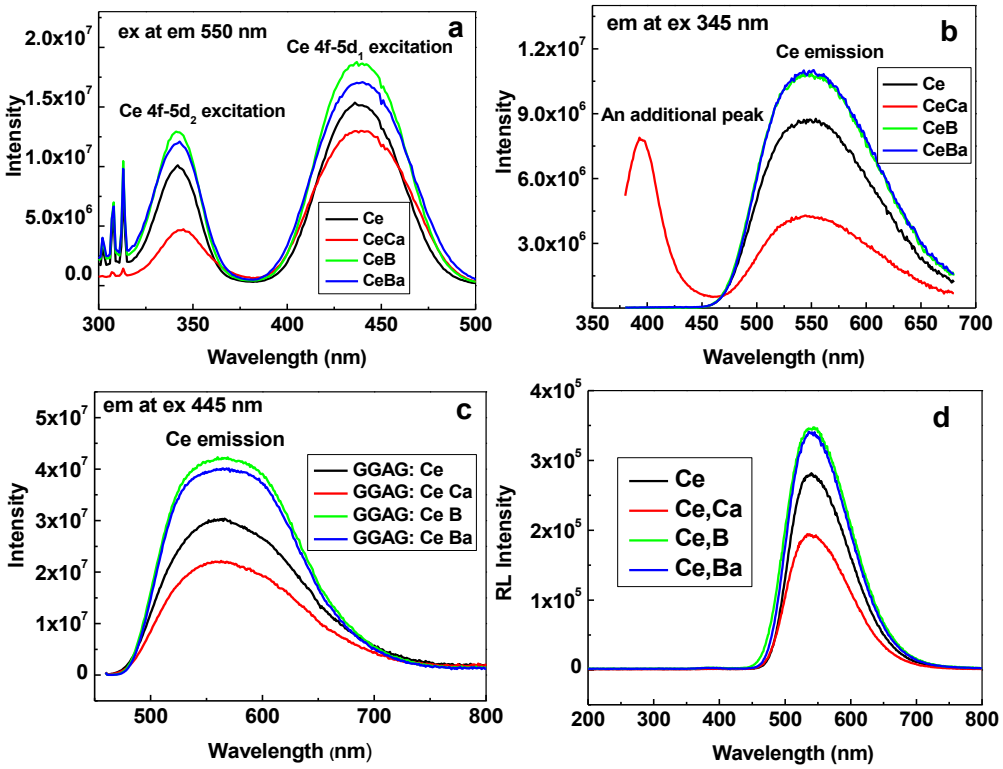

Figure 3.1. The effect of different codopants on the excitation & emission and RL spectra of GGAG:Ce crystals.

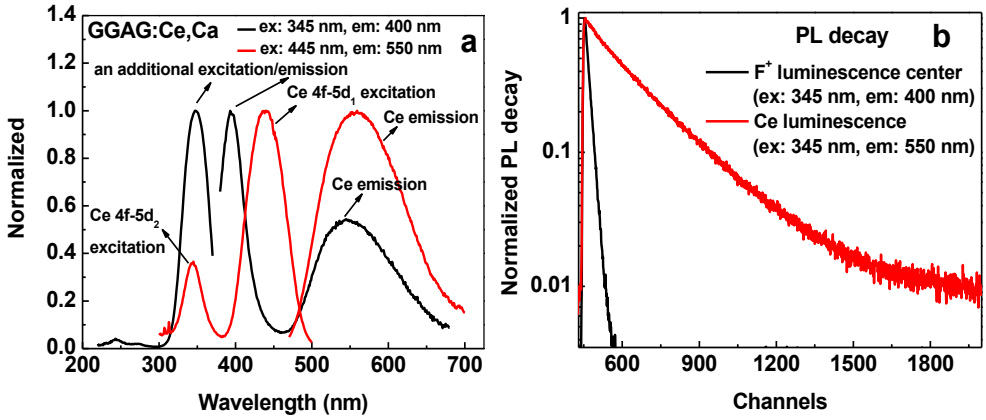

Figure 3.2. (a) The complete excitation and emission spectra of Ca codoped scintillator and (b) PL decay time of the extra luminescence center (Ex: 345 nm, Em: 400 nm) and Ce luminescence energy levels (Ex: 345 nm, Em: 550 nm).

Thermal quenching

Here we designate F^+ emission as the emission peak at 400 nm when exciting at 345 nm, and F^+ excitation as the excitation peak at 345 nm when exciting at 400 nm. The temperature dependence of PL spectra of Ca codoping scintillator is shown in Figure 3.3, including the Ce 4f-5d_1 and Ce 4f-5d_2 excitation (Figure 3. 3a), Ce emission when excited at 445 nm (Figure 3.3b), Ce emission when excited at 345 nm and F^+ emission (Figure 3.3c), and F^+ excitation (Figure 3.3d) in the range of 40-550 K. In general, the intensities of all excitation and emission peaks decreased as the temperature increased. However, the Ce luminescence centers and F^+ luminescence centers exhibited distinct thermal response profiles, as indicated by the evolution of the normalized intensity of Ce and F^+ excitation/emission upon raising the temperature in Figure 3.4. There is a thermal quenching for the Ce luminescence centers, beginning around room temperature. In contrast, decrease of the peak intensity for F^+ luminescence center was nearly linear. In addition, red shift (~ 10 nm) was observed for F^+ excitation band in the temperature region of 40-550 K (see Figure 3.3d).

Due to the non-availability of 445 nm LED, the decay time was only measured when exciting at 345 nm. The temperature dependence of the PL decay time is plotted for different codopants in Figure 3.5. At room temperature, the PL decay time of Ca codoping (~ 45 ns) was shorter than those of Ce-only, B and Ba codoping (~ 50-55 ns). Above the room temperature, a strong thermal

quenching in the PL decay time occurred. For different codopants, the thermal quenching in the PL decay time started at different temperatures i.e. ~ 300 K, 300 K, 325 K, and 350 K for Ce-only doping, Ca, B, and Ba codoping GAGG scintillators respectively. On the other hand, the F^+ luminescence center in Ca codoped crystal showed no quenching and the PL decay time remained constantly at ~ 3.5 ns.

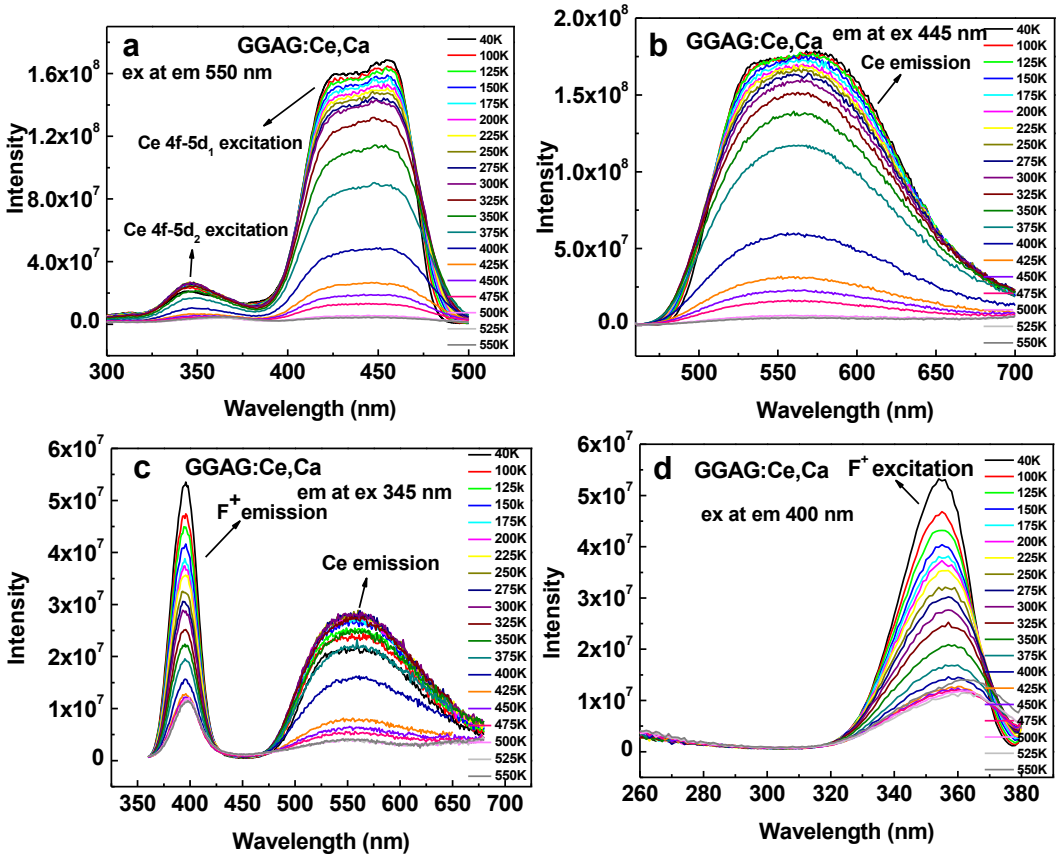

Figure 3.3. The temperature dependence of PL spectra of Ca codoped scintillator, showing (a) Ce excitation when emitted at 550 nm, (b) Ce emission when excited at 445 nm, (c) Ce emission when excited at 345 nm and F^+ emission, and (d) F^+ excitation.

The thermal quenching energy was obtained via fitting the thermal response profiles using Mott–Seitz equation [20]

$$\tau(K) = \frac{\tau_0}{1 + A \exp\left(-\frac{\Delta E}{kT}\right)} \quad (1)$$

where τ(K) is the decay time at temperature T(K), τ_0 is the decay time extrapolated to 0 K, A is a constant, k is the Boltzmann constant (8.6173 x 10-5 eV/K) and ΔE is the thermal activation energy for quenching. The solid lines in Figure 3.5 are the fitted curves using the above equation. Different activation energy values were obtained for the Ce-only doping, Ca, B, and Ba codoping GAGG scintillators, being ~ 470±20, 370±10, 490±10 and 580±20 meV respectively. Ogiegło [21] reported the activation energy of the similar range (~ 400-600 meV) in the Ce doped $Gd_3(Ga,Al)_5O_{12}$ scintillators.

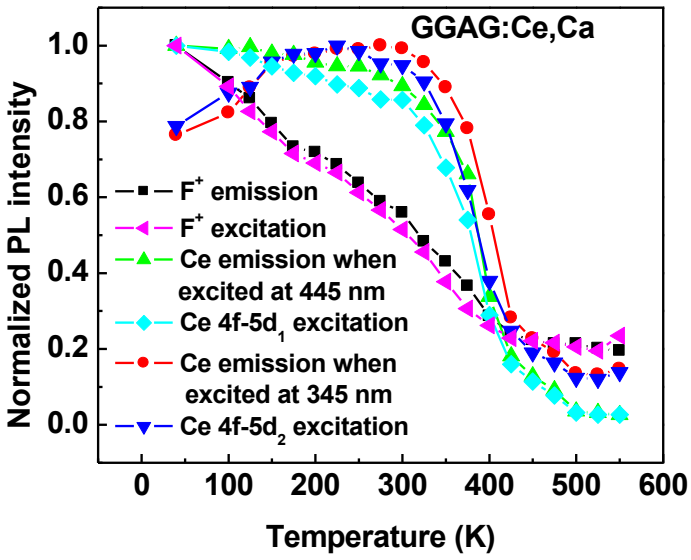

Figure 3.4. The temperature dependence of the normalized integrated intensity of Ce and F^+ excitation/emission in the Ca codoped scintillator.

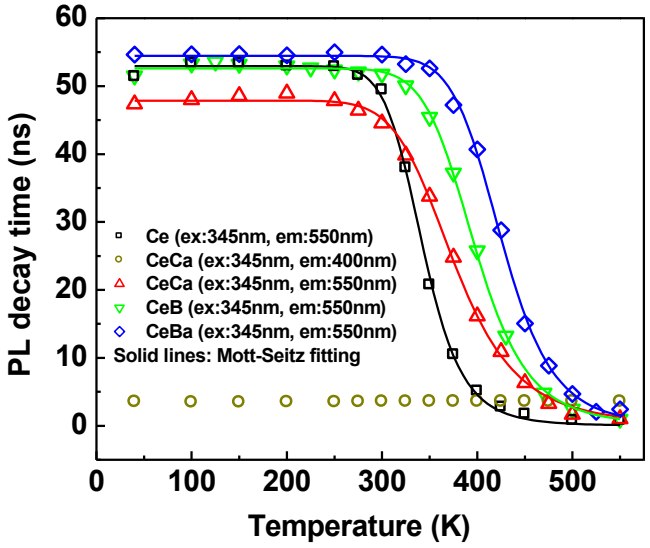

Figure 3.5. The temperature dependence of the PL decay time for different codopants. The solid lines are the fitted curves using Mott-Seitz equation.

Thermoluminescence

Our previous study stated Ca codoped GGAG crystal greatly reduced the charge traps but introduced a new deeper trap dominated at 390 K. On the other hand, B codoping eliminated the 200 K trap and the deeper traps above room temperature [18]. In this part, we further extracted the detailed traps parameters of the GGAG crystals in the temperature range from 100 to 500 K by fitting. The measured TL spectra with different codopants are shown in Figure 3.6. The TL curves were fitted by the first-order kinetic model introduced by Randall and Wilkins, in which a single trap is described by two parameters, the activation energy E and the frequency factor s [22]. The model is expressed by

$$I(T-\Delta T) = n_0\, s \exp\left(\frac{E}{kT}\right) \exp\left(\frac{s}{\beta}\right) \int_{T_1}^{T_2} \exp\left(\frac{E}{kT'}\right) dT' \qquad (2)$$

where n is the initial concentration of filled traps, and k stands for the Boltzmann constant. For our measurements, the thermal lag ΔT between the sample and the heating element was 2-3 K, and the constant heating rate β was 0.15 K/s. The fitted TL spectra are also shown in Figure 3.6.

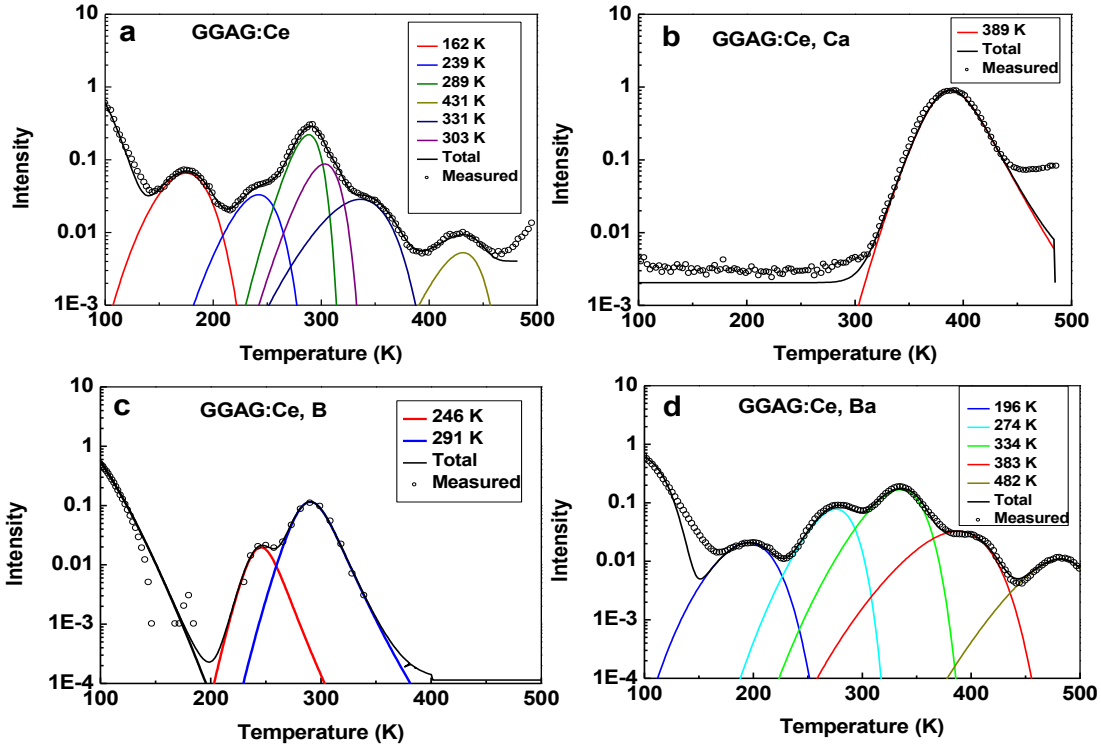

Figure 3.6. The fitted TL spectra for GGAG:Ce crystals with different co-dopants. Solid circle is experimental data, solid line is fitted to data using the equation (2).

The calculated trap parameters given by the curve fitting are listed in Table 3.2. The error of the thermal depths is approximately 10%. In order to

know the effect of lifetime of traps on afterglow, the lifetime of the traps was calculated by Arrhenius formula (eq. 3),

$$t = \frac{\exp\left(\frac{E}{kT}\right)}{s} \tag{3}$$

where s and E were calculated from the TL fitting curve. The calculated lifetime of the traps at room temperature (T = 298 K) is also shown in table II. Between 300 K and 500 K, the TL spectra and the calculated trap parameters of Ce-only doped GGAG agreed well with results reported by Mihóková [23]. In our study, the spectrum below 300 K was also measured.

Table 3.2 Summary of calculated traps parameters of GGAG:Ce crystal with different co-dopants.

Sample	Tmax (K)	n_0	E	ln s (s^{-1})	t 298K (s)
GGAG:Ce	162	21.66	0.420	28.944	3.60E-06
	239	9.721	0.525	26.352	2.90E-03
	289	43.06	0.619	24.542	7.00E-01
	303	20.67	0.809	26.460	1.71E+02
	331	12.21	0.883	27.634	9.52E+02
	431	1.583	1.136	25.780	1.19E+07
GGAG:Ce, Ca	389	305.8	0.962	21.341	1.12E+07
GGAG:Ce, B	246	3.900	0.663	25.953	9.46E-01
	291	26.84	0.788	26.054	1.13E+02
GGAG:Ce, Ba	196	7.432	0.539	28.172	8.17E-04
	274	21.62	0.685	25.443	3.72E+01
	334	55.11	0.894	30.039	1.32E+02
	383	15.14	1.027	27.090	4.55E+05
	482	4.317	1.173	27.623	8.00E+07

Afterglow

The traps responsible for TL peaks around room temperature may affect the afterglow signal of the materials. Here they can be the traps associated with the TL peaks around 300 K and 330 K in Ce-only doped crystal with the lifetime around 170 s and 950 s respectively, the traps around 290 K in B codoping with the lifetime of 113 s and the traps around 330 K in Ba codoping with the lifetime of 132 s (cf. Table 3.2). However, there was no room temperature traps in the Ca codoped crystal thus very low afterglow were expected. This was verified by the afterglow time profiles of different codopants measured at room temperature shown in Figure 3.7. Before the cut-off of the X-ray, the intensity was the same for all samples, which is the steady state luminescence intensity. After the cut-off of the X-ray, significant reduction of afterglow was observed for Ca codoped GGAG:Ce compared to other samples. About 100 seconds after the cut-off, afterglow was around 5.8% of the steady state luminescence for the Ca codoped sample, while the value is reduced to 58%, 18% and 36%, for the Ce-only doped, the B and Ba codoped samples respectively. The results strongly suggested that Ca codoping reduced afterglow, which is consistent with the less room temperature traps observed in TL spectra of Ca sample.

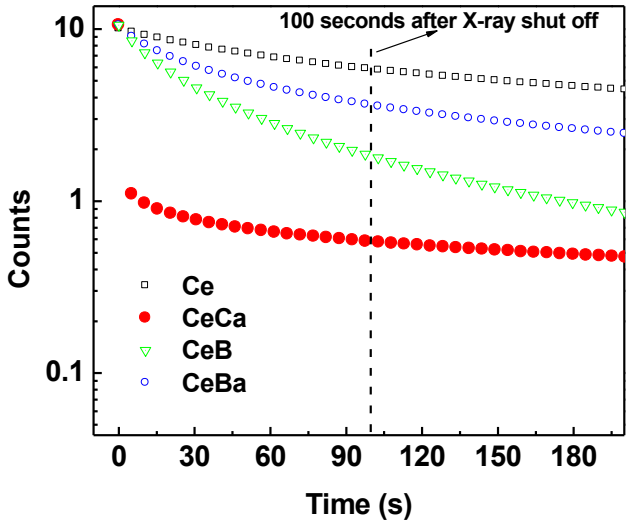

Figure 3.7. The afterglow time profiles of different codopants measured at room temperature.

Conclusion

The scintillation and optical properties of GAGG:Ce crystals can be modified by incorporating different codopant ions. The main results can be summarized as following.

1) Ca codoping decreases the absorbance intensity at 345 nm and the RL intensity, while B and Ba codoping increase them.

2) Ca codoping introduces an F^+ luminescence center with an excitation peak at 350 nm and emission peak at 400 nm. The PL decay time of this luminescence center is around 3.5 ns, which is independent of temperature, although its luminescence intensity, including excitation and emission intensity, decreases linearly as temperature increases.

3) Codoping affects the profile of temperature dependent PL decay time for the

Ce luminescence center, which consequently changes the quenching temperature and activation energy. The quenching for the Ce center occurs around RT, and the emission rapidly decreases above RT.

4) TL measurements show that Ca codoping significantly suppresses the charge trap population in GGAG:Ce crystals under RT. This decrease in traps below RT accounts for the strong suppression of afterglow.

References for Chapter 3

[1] C. Melcher, (2005). “Perspectives on the future development of new scintillators.” Nucl. Instrum. Methods Phys. Res. Sect. A. 537: 6-14.

[2] M. Nikl, (2006). “Scintillation detectors for x-rays.” Meas. Sci. Technol. 17: R37.

[3] O. B. Drury, et al., (2009). “Garnet scintillator-based devices for gamma-ray spectroscopy,” IEEE Nuclear Science Symposium Conference Record (NSS/MIC), pp. 1585-1587.

[4] M. Moszyński, et al., (1994). “Properties of the YAG:Ce scintillator.” Nucl. Instrum. Methods Phys. Res. Sect. A. 345: 461-467.

[5] M. Balcerzyk, et al., (2000). “Future hosts for fast and high light output cerium-doped scintillator.” J. Lumin. 87: 963-966.

[6] V. Baryshevsky, et al., (1993). “Spectroscopy and scintillation properties of cerium doped $YAlO_3$ single crystals.” J. Phys. Condens. Matter 5: 7893.

[7] C. R. Ronda, (2007). “Luminescence: from theory to applications.” John Wiley & Sons.

[8] J. A. Mares, et al., (2004) “Scintillation response of Ce-doped or intrinsic scintillating crystals in the range up to 1MeV.” Radiat. Meas. 38: 353-357.

[9] K. Kamada, et al., (2011). “Composition engineering in cerium-doped (Lu, $Gd)_3(Ga,Al)_5O_{12}$ single-crystal scintillators. Cryst. Growth Des. 11: 4484-4490.

[10] K. Kamada, et al., (2011). “Scintillator-oriented combinatorial search in Ce-doped $(Y,Gd)_3(Ga,Al)_5O_{12}$ multicomponent garnet compounds.” J. Phys. D: Appl. Phys. 44: 505104.

[11] K. Kamada, et al., (2012). “2 inch diameter single crystal growth and scintillation properties of Ce: $Gd_3Al_2Ga_3O_{12}$.” J. Cryst. Growth 352: 88-90.

[12] K. Kamada, et al., (2012). “Crystal growth and scintillation properties of Ce doped single crystals.” IEEE Trans. Nucl. Sci. 59: 2112-2115.

[13] M. Koschan, et al., (2012). “A comparison of the effect of Ca^{2+} codoping in cerium doped GSO with that of LSO and YSO.” J. Cryst. Growth 352: 133-136.

[14] H. E. Rothfuss, et al., (2009). “The effect of codoping on shallow traps in

YSO:Ce scintillators." IEEE Trans. Nucl. Sci. 56: 958-961.

[15] K. Yang, et al., (2011). "Effect of Ca co-doping on the luminescence centers in LSO:Ce single crystals." IEEE Trans. Nucl. Sci. 58:1394-1399.

[16] J. G. Kang, et al., (2008). "Preparation and luminescence characterization of GGAG:Ce^{3+},B^{3+} for a white light-emitting diode." Mater. Res. Bull. 43:1982-1988.

[17] S. B. Donnald, et al., (2013). "The Effect of B and Ca Co-Doping on Factors Which Affect the Energy Resolution of $Gd_3Ga_3Al_2O_{12}$:Ce." IEEE Trans. Nuc. Sci. 60(5): 4002-4006.

[18] M. Tyagi, et al., (2013). "Effect of codoping on scintillation and optical properties of a Ce-doped $Gd_3Ga_3Al_2O_{12}$ scintillator." J. Phys. D, Appl. Phys. 46(47): 475302.

[19] Y. Zorenko, et al., (2011). "Luminescence centers in $Y_3Al_5O_{12}$:La single crystals." Journal of Physics: Conference Series. IOP Publishing, pp. 012028.

[20] B. D. Bartolo, B., (2010). "Optical interactions in solids." World Scientific.

[21] J. M. Ogiegło, et al., (2013). "Luminescence and Luminescence Quenching in $Gd_3(Ga,Al)_5O_{12}$ Scintillators Doped with Ce^{3+}." J. Phys, Chem. A 117: 2479-2484.

[22] J. Randall, et al., (1945). "Phosphorescence and electron traps. I. The study of trap distributions." Proc. Royal Soc. Lond. Math. Phys. Sci. 184: 365-389.

[23] E. Mihóková, et al., (2013) "Deep trapping states in cerium doped (Lu, Y, $Gd)_3(Ga, Al)_5O_{12}$ single crystal scintillators." Radiat. Meas. 56: 98-101.

Chapter 4 RELATIONSHIP BETWEEN CA^{2+} CONCENTRATION AND THE PROPERTIES OF $GD_3GA_3AL_2O_{12}$:CE SCINTILLATORS

A version of this chapter by Fang Meng was accepted and published by a peer-reviewed journal. The full citation is as following: F. Meng, M. Koschan, Y. Wu and C. L. Melcher, "*Relationship between Ca^{2+} Concentration and the Properties of codoped $Gd_3Ga_3Al_2O_{12}$:Ce Scintillators", Nuclear Instruments and Methods in Physics Research Section A* 797 (2015) 138-143.

This chapter is the reformatted version of the original work submitted to the referenced journal. No additional changes to the content of the original article were done other than formatting to conform to the dissertation format.

Abstract

Codoping is a method of current interest for modifying the properties of scintillators. The study reported here explores the effect of codoping on cerium doped $Gd_3Ga_3Al_2O_{12}$ (GGAG:Ce) crystals with various concentrations of Ca. These single crystals were grown via the Czochralski technique with Ce concentrations fixed at 0.2 at% and Ca concentrations ranging from 0.1 at% to 0.4 at% in the initial melt. The relationship between dopant concentration and light yield, rise time, and scintillation and photoluminescence decay times was determined. In addition, the absorbance, photoluminescence, radioluminescence, afterglow and thermoluminescence dependence on the dopant concentration are presented. In some of the Ca codoped crystals, an additional luminescence center was observed with an excitation wavelength of 350 nm and an emission wavelength of 400 nm and a photoluminescence decay time of ~ 3.5 ns.

Introduction

Oxide garnet materials such as $Y_3Al_5O_{12}$ (YAG) and $Lu_3Al_5O_{12}$ (LuAG) are well known materials with good optical transparency that are easily doped and useful as laser host and scintillators. The light yield of Ce^{3+} activated YAG and LuAG has been reported at ~ 25,000 [1] and ~ 20,000 [2] photons/MeV, respectively, which are far below the theoretical value of ~ 60,000 photons/MeV calculated by the Bartram-Lempicki equation [3]. Many attempts have been made to find new potential scintillators with high density, high light yield, fast decay time and high stopping power via both experimental and theoretical research. Recently, Kamada, et al. have done extensive combinatorial band gap engineering for multicomponent garnet compounds and found that Ce doped $Gd_3Ga_3Al_2O_{12}$ (GGAG) crystals have promising scintillation properties. These crystals have a high density (6.5 g/cm^3), good scintillation light yield (45,000 photons/MeV), and fast decay time (90 ns) [4, 5]. This light yield is higher than those typically reported for LSO, but the decay time is unfortunately longer. Given that, improving the scintillation properties of GGAG is clearly of interest.

Over the last decade, it has been found that the performance of several scintillators could be affected by codoping. In particular, codoping by divalent alkali earth ions, such as Ca^{2+} and Mg^{2+}, embedded at a trivalent cation site, has been repeatedly employed to improve the scintillation performance of some inorganic scintillator materials. The introduction of divalent codopants could change the point defect structure in single crystal materials by changing the

charge compensation mechanisms and/or affecting the concentration of vacancies. Improvements of the scintillation performance for LSO:Ce, Ca [7], YSO:Ce, Ca [8] and LYSO:Ce, Mg [9] have been achieved by codoping with divalent ions at the trivalent cation sites.

Recently, our group extended the idea of codoping to Ce doped GGAG crystals, and reported the effect of Ca, B, and Ba codoping on energy resolution, scintillation kinetics and optical properties of Ce-doped GGAG scintillators [10-12]. B and Ba codoping increased the light yield and improved the energy resolution, whereas Ca codoping shortened the scintillation decay time via eliminating many of the shallow electron traps, and decreased the light yield. Later, Kamada et al. [13] studied the Ca/Mg codoped GGAG:Ce crystals grown by micro-pulling down method and reported that both the decay time and light yield decreased as the increase of Ca/Mg concentration from 0.0 to 0.1 at%. Here, we investigate Ca codoped GGAG:Ce crystals grown by Czochralski (CZ) technique with a wide Ca concentration up to 0.4 at%, aiming to explore the relationship between Ca concentration and the optical/scintillation properties.

Experimental methods

Crystal growth

GGAG:Ce boules were grown from the melt by the Czochralski (CZ) technique in inductively heated iridium crucibles. The Gd_2O_3, Ga_2O_3, Al_2O_3, CeO_2 and CaO as raw materials were at least 99.99% pure. Crystal growth was

initialized on seed crystals and was controlled automatically by using the derivative of the crystal weight as the process variable. All melts were doped with 0.2 atomic % Ce and codoped with 0.0-0.4 atomic % Ca with respect to the rare earth; the exact compositions are given in Table 4.1. All concentrations given are those of the initial starting melt; the concentration in the finished crystal would differ due to segregation at the solid-liquid interface during growth. The flowing atmosphere was nitrogen mixed with a small amount of oxygen. The boule dimensions were ~ 80 mm tall and ~ 32 mm diameter. Two sample sizes were used in these experiments: unpolished 5 mm cubes and polished wafers of approximately 1 mm thick. The wafers were used for the absorbance measurement and the cubes were for all other measurements. All samples were cut from the same point in the boule in order to get consistent Ce concentration. Color differences accompanied the differences in Ca concentration, as shown in Figure 4.1. The sample with 0.4% Ca is a rust color, whereas the samples with lower Ca concentration are yellow-green.

Table 4.1 List of crystal compositions.

Composition	At % Ce (in the melt)	At % Ca (in the melt)
GGAG:Ce	0.2	0.0
GGAG:Ce, Ca	0.2	0.1
GGAG:Ce, Ca	0.2	0.2
GGAG:Ce, Ca	0.2	0.4

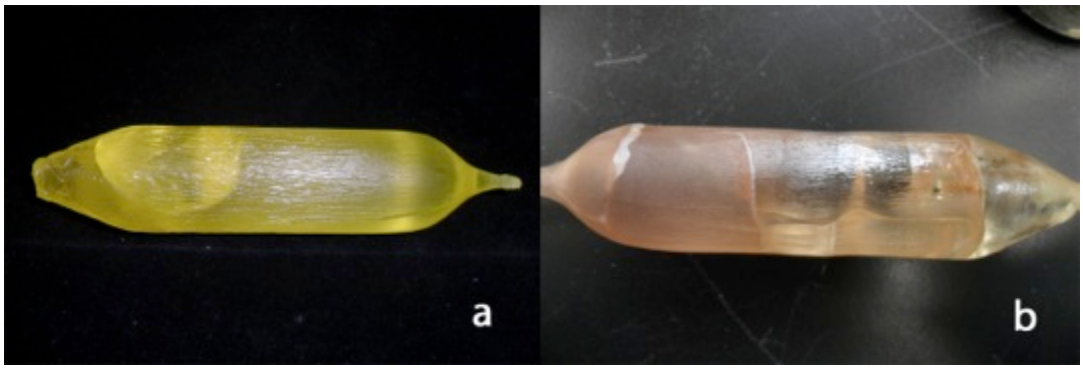

Figure 4.1. A GGAG:Ce crystal codoped with (a) 0.1 at % Ca and (b) 0.4 at % Ca.

Characterization

Absorbance and transmission were measured with a Varian Cary 5000 UV–VIS–NIR spectrophotometer in the 200–800 nm range. Emission and excitation were acquired with a HORIBA Jobin Yvon Fluorolog-3 Spectrofluorometer with a 450 W continuous Xenon lamp as the excitation source. The X-ray excited luminescence spectra were obtained at room temperature under the X-ray radiation at 35 kV and 0.1 mA using an ACTON SP-2155 monochromator.

Photoluminescence (PL) decay was measured on the same spectrofluorometer using a time-correlated single photon counting module, where Nano LEDs were used as the excitation source. The emission monochromator was set at 1 ns bandpass to select the emission light of a specific wavelength. The duration of the light pulse from the Nano LEDs was 0.6 ns.

The scintillation decay time and rise time profiles were measured using the Bollinger-Thomas time-correlated single photon technique and a ^{137}Cs

gamma-ray source. The instrumental response was less than 1 ns and was not deconvolved from the much slower rise and decay profiles. To determine the light yield, energy spectra were measured with a 10 μCi ^{137}Cs gamma-ray source. Cubes of 5 mm sides were placed directly on the window of a Hamamatsu R2059 PMT with optical couplant, and a hemispherical Spectralon reflector was used to enhance the light collection. The signal went through a Canberra model 2005 pre-amplifier, an Ortec 672 shaping amplifier (shaping time = 3 μs), a Tukan 8k multi-channel analyzer, and finally to a personal computer.

For thermoluminescence (TL) glow curve measurements, the sample was mounted within an Advanced Research Systems cryostat (model DE202AE). The sample chamber was evacuated to 20 mTorr and the sample was then heated to 600 K in order to empty charge carrier traps. The sample was then cooled to 9 K and irradiated with X-ray tube (35 keV, 0.1mA) through a beryllium window for approximately 15 min. Subsequently, the sample was returned to 600 K at a rate of 9.0 K/min. A Hamamatsu H3177 PMT was used to measure the luminescence emitted by the sample as a function of temperature.

All afterglow measurements were done at room temperature. The crystals were coupled to a Hamamatsu R2059 photomultiplier tube with a Dow Corning Q2-3067 optical couplant, and covered with a Tetratex TX3104 PTFE membrane. The crystals were then irradiated with X-ray tube (35 keV, 0.1 mA) for 15 min, after which a Uniblitz XRS6S2P1-040 shutter was used to cut off the X-ray beam and the luminescence emitted was subsequently recorded as a function of time.

Results and discussion

Absorption and photoluminescence

Figure 4.2 shows the absorbance and PL spectra of GGAG:Ce with various Ca codopant concentrations. Higher Ca concentrations result in greater absorbance in the 200-350 nm range, as shown in Figure 4.2a. This phenomenon was previously observed in Ca/Mg codoped GGAG:Ce [13] and Mg codoped LuAG:Ce scintillators [14-16] and was attributed to the enhancement of Ce^{4+} charge transfer (CT) absorption. The peak at 440 nm due to Ce^{3+} 4f-$5d_1$ transition decreases in intensity as Ca concentration decreases, indicating a reduction in the Ce^{3+} concentration. In particular, the crystal with rust color shows essentially no Ce^{3+} absorbance around 440 nm in Figure 4.2a. Such significant changes of absorbance around 440 nm are unique in Ca codoped GGAG, as suggested by our previous study [12], and are unlikely caused by the minor variation of Ce concentration from sample to sample. A reasonable explanation is that replacing the trivalent site by divalent calcium in the GGAG lattice promotes a change in the charge state of Ce ion from Ce^{3+} to Ce^{4+} in order to achieve charge neutrality. Therefore, as Ca concentration increases the conversion from Ce^{3+} to Ce^{4+} also increases, and the intensity of Ce^{3+} absorbance at 440 nm decreases. In our case, the absence of the absorption at 440 nm in the sample with 0.4% Ca indicates that most of Ce^{3+} has been converted to Ce^{4+}, and hence the color changes from yellow-green to rust. Detailed mechanism was presented in our previous work [17]. The PL spectra are shown in Figure 4.2b, in which the

excitation peaks around 345 nm and 440 nm are due to the Ce 4f-$5d_2$ and 4f-$5d_1$ transitions and the emission peak around 550 nm is due to the Ce 5d-4f transition [18]. The absorbance around 310 nm and 275 nm are ascribed to the Gd^{3+} 4f-4f absorption transition [19]. The absorbance intensity at 345 nm decreases as the increase of Ca concentration, which is due to the increase of Ce^{4+} charge transfer. The similar phenomenon about higher energy absorption in the PL spectra was also reported in some silicates [20,21].

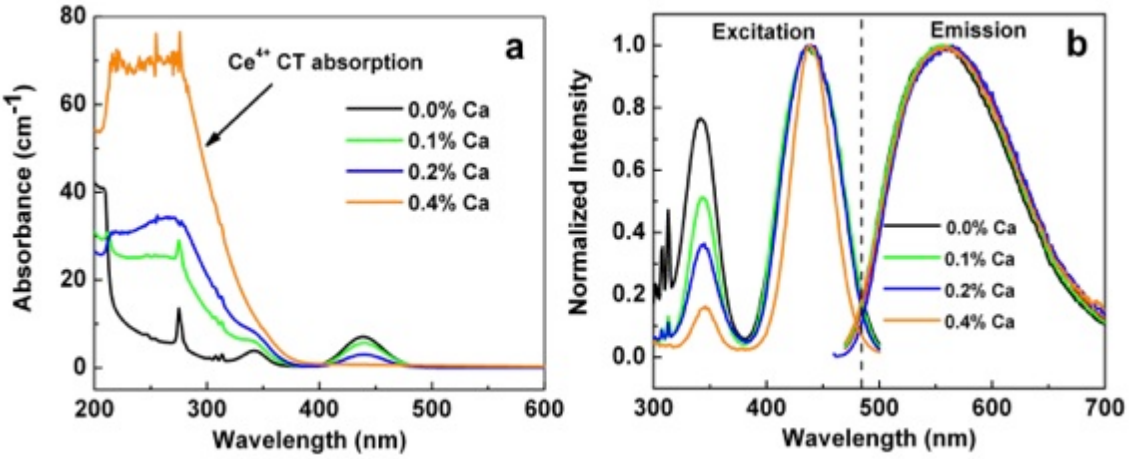

Figure 4.2. (a) Absorbance and (b) PL spectra of GGAG:Ce samples with different Ca concentrations (excitation was measured for emission at 550 nm and emission was measured for excitation at 440 nm).

In addition, GGAG:Ce codoped with 0.1% and 0.2% Ca appear to have an additional luminescence center with an emission wavelength around 400 nm (3.1 eV) for excitation at 345 nm (4f-$5d_2$ transfer wavelength), as shown in Figure 4.3a. The corresponding excitation spectra were measured for emission at 400 nm and the excitation peak was located at 350 nm. The PL decay time of the additional luminescence center is ~ 3.5 ns obtained by fitting with a single

exponential decay model, shown in Figure 4.3b. This emission energy and fast PL decay of the additional luminescence center were ascribed to an F^+ center related to the oxygen vacancy.

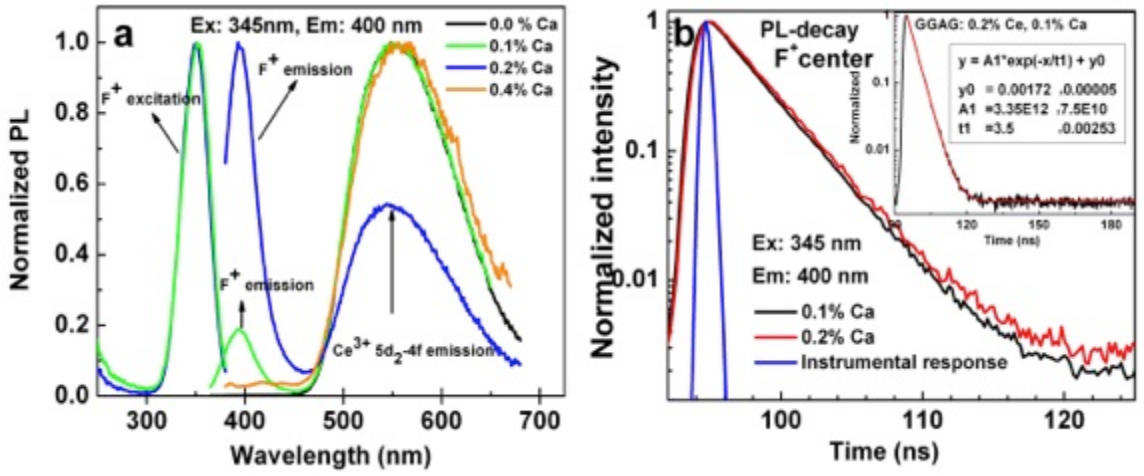

Figure 4.3. (a) PL spectra showing an 'additional' luminescence center in some Ca-doped GGAG:Ce crystals and (b) PL decay of the 'additional' luminescence in GGAG:Ce with 0.1% Ca and 0.2% Ca. The insert shows the fitting curve of PL decay using a single exponential model and the PL decay time of ~3.5 ns was obtained.

The introduction of divalent Ca into a trivalent site leads to a local excess charge with potential to result in or interact with oxygen vacancies [22], which may in turn one electron and become F^+ center, or two electrons and become F center. An F^+ center has been previously reported in YAG [23-25] and LuAG [26] crystals, with an excitation peak around 360 nm and emission peak around 400 nm, whereas an F center was also reported in YAG crystals [23, 25] with an excitation peak at 240 nm and emission peak at 460 nm. The PL decay time of the new luminescence center is in the same order of magnitude as that of the F^+ center found in YAG [23] and LuAG [26] crystals, further supporting the idea that

the new center here is primarily an F^+ center. Since this F^+ center is related to oxygen vacancy, a series annealing study at different atmospheres of the F^+ center was investigated in our previous work [17].

Radioluminescence, light yield and decay time

Figure 4.4 shows the RL spectra of GGAG:Ce crystals with various Ca concentrations. The additional PL emission peak at 400 nm appears in both the 0.1% and 0.2% Ca samples, while it does not show up in the RL spectra in neither of the samples. This may be due to the different excitation source, and further investigation is in progress to study the difference observed between the PL and RL spectra. Although the peak position around 550 nm due to Ce^{3+} emission is not affected by the Ca codopant concentration, the addition of more Ca reduces the intensities of the RL peaks. This is consistent with the energy spectra results shown in Figure 4.5. In other words, Ca reduces the light yield of GGAG.

Figure 4.6 shows the scintillation decay of GGAG:Ce crystals with various Ca concentration as well as the instrumental response. The peak at 370 ns is believed to be an experimental artifact. The scintillation kinetics can be characterized by two exponential decay components. The fast component can be ascribed to the de-excitation of the 5d state to the 4f state. The slower component can be attributed to energy transfer from Gd^{3+} to Ce^{3+} as reported in other Gd based scintillators [27, 28]. The fast component of scintillation decay

becomes shorter with increasing Ca concentration, as seen in Figure 4.6. The rise time was fitted by single exponential component. The relationship between the fast component of decay time, the light yield and rise time for Ca doped crystals is illustrated in Figure 4.7. The decay constant and light yield both decreases monotonically with increasing Ca concentration up to 0.4 at%, which follows the same trend observed by Kamada et al. [13] in the low Ca concentration range (0.0-0.1 at%). The rise time is also shortened in Ca codoped samples, as seen in Figure 4.7b, but the highest Ca concentration does not give the shortest rise time. Figure 4.8 shows the PL decay spectra for various Ca concentrations measured under the excitation at 345 nm and the emission at 550 nm. Due to the unavailability of a 445 nm LED, we could not measure the decay time by exciting the $5d_1$ level of Ce^{3+} directly. Therefore we used excitation of $5d_2$ level with a 345 nm LED. The PL decay time for 0.2% Ca slightly decreases compared to those with 0.0% and 0.1% Ca. It is apparent that the PL decay of the sample with 0.4% Ca is fundamentally different from the samples with lower Ca concentrations, in terms of a steep decrease at the beginning of decay and lower signal-to-noise ratio (SNR). This steep initial decay is believed to be the instrumental response. The lower SNR is probably due to the lack of Ce^{3+} in the 0.4% Ca codoped sample, considering Ce^{4+} is the primary valence state whereas Ce^{3+} dominates the samples with lower Ca concentrations [17].

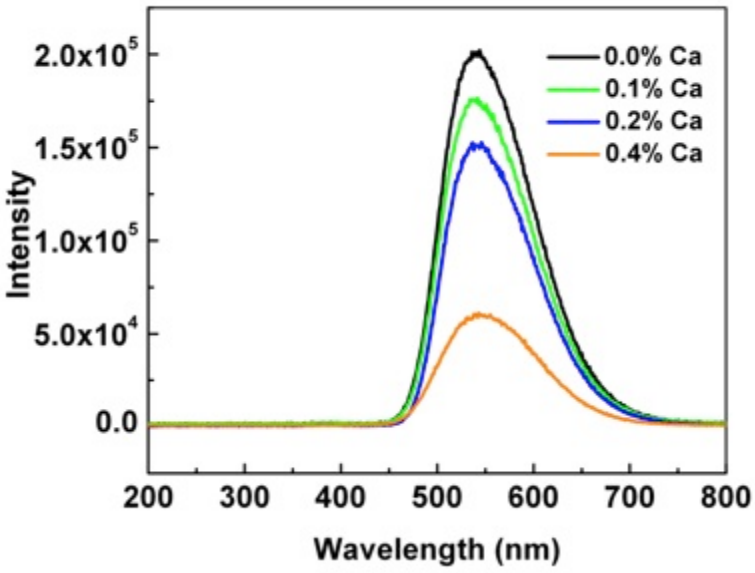

Figure 4.4. RL spectra of GGAG:Ce crystals with various Ca concentrations irradiated by a X-ray tube (35 keV, 0.1mA).

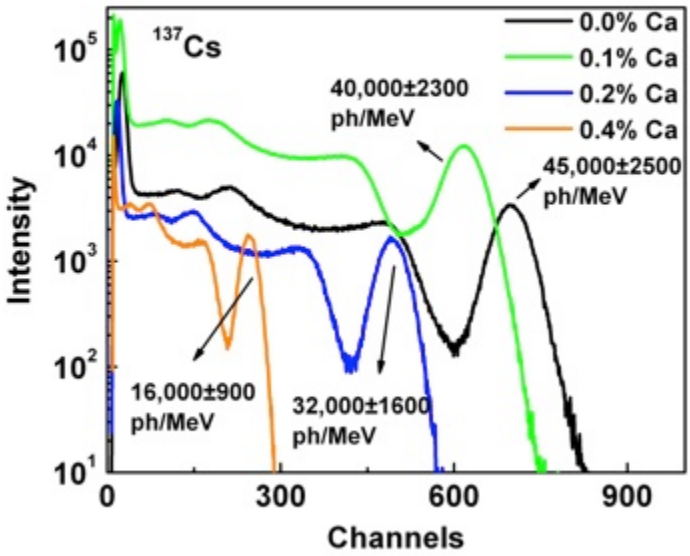

Figure 4.5. Energy spectra of GGAG:Ce crystals with various Ca concentrations, excited by a ^{137}Cs source (662 keV).

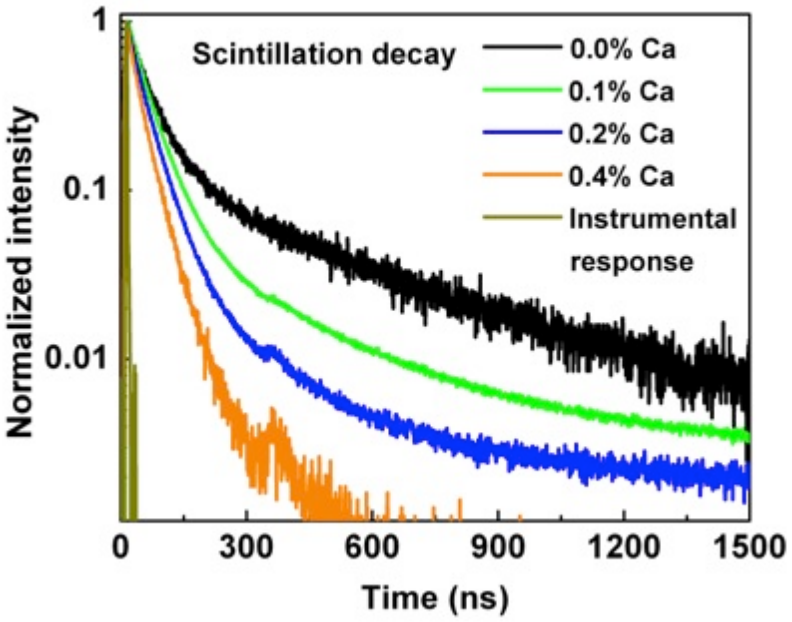

Figure 4.6. Scintillation decay of GGAG:Ce crystals with various Ca concentrations, excited by a ^{137}Cs source (662 keV).

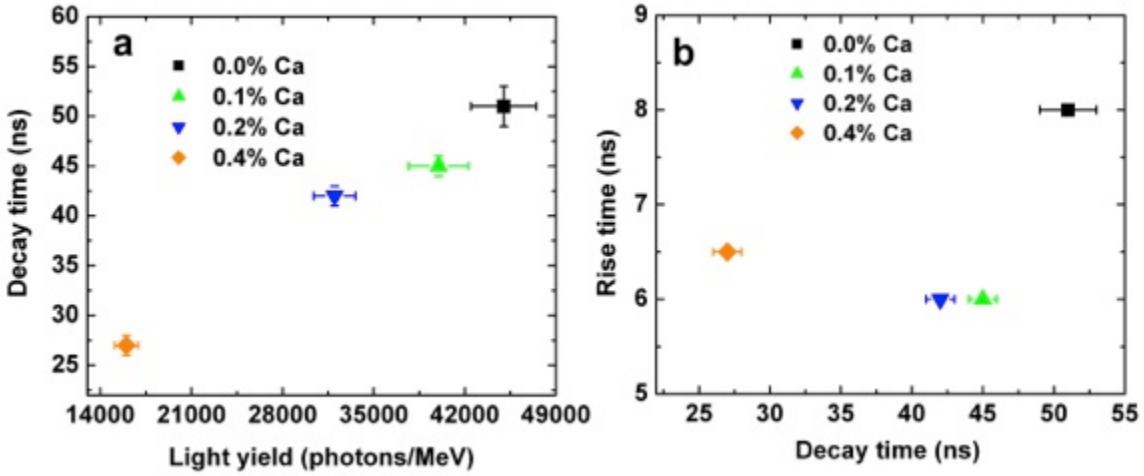

Figure 4.7. (a) Decay time vs. absolute light yield and (b) rise time vs. scintillation decay time for different Ca concentrations.

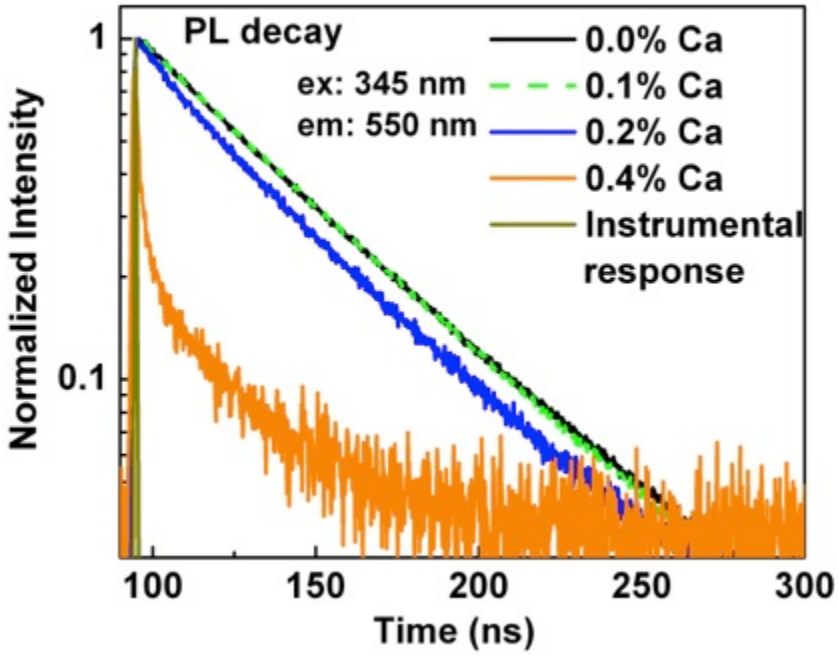

Figure 4.8. PL decay spectra of GGAG:Ce crystals with various Ca concentrations, measured under the excitation at 345 nm and the emission at 550 nm.

Thermoluminescence and afterglow

TL glow curve was measured to study the influence of Ca concentration on traps. Figure 4.9 shows the TL glow curve corrected by luminescence thermal quenching. The example of thermal quenching can be found in our previous study on codoping [11]. The size and weight of the samples for the TL measurements were made approximately the same in order to compare the TL intensity directly. For Ce only sample, the glow curve in low temperature (< 350 K) shows similar shape and peak positions to those reported by Brylew [29]. For the Ca codoped samples, it can be observed that the TL intensity in low

temperature (< 350 K) region is reduced compared to the Ce only sample. In particular, no shallow traps were observed in the crystal with 0.4 at% Ca. This is possibly due to a) the elimination of the shallow traps by Ca codoping, b) the decrease of Ce^{3+} luminescence intensity by Ca codoping if Ce^{3+} luminescence is involved in this TL signal, or the effect of both. However, a new deeper trap dominates at high temperature (> 350 K) in the crystals with 0.1 and 0.2 at% Ca.

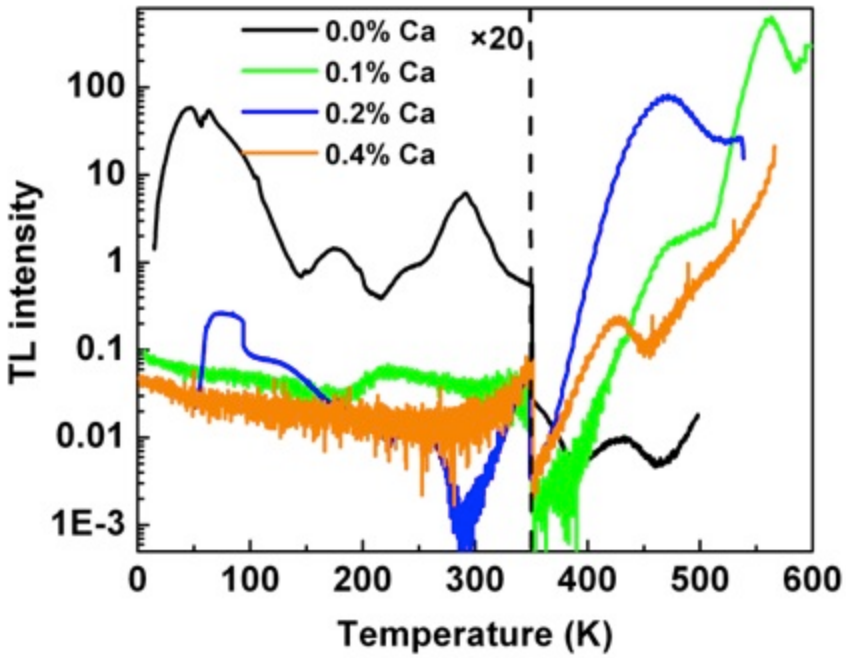

Figure 4.9. TL spectra measured for GGAG:Ce with various Ca concentrations. The TL intensity is magnified by 20 times below 350 K. All curves are corrected for luminescence thermal quenching.

The X-ray induced afterglow curves for all four compositions are shown in Figure 4.10. Within a few seconds after X-ray cut off, there is at least one order of magnitude reduction in the intensity for the Ca codoped samples compared to

the steady state luminescence, in contrast to less than 10% reduction for the Ca-free sample. The afterglow level of the Ca-free sample does not drop by one order of magnitude until 6000 s. For Ca codoped samples, the weakest afterglow was observed in 0.1% and 0.4% Ca samples. The relative values of afterglow intensity at 100 s after X-ray cut off are listed in Table 4.2. To conclude, the afterglow of GGAG was improved by Ca codoping.

The effect of Ca codoping on the light yield and decay time follows the similar trend as observed in the GGAG:Ce,Ca crystals grown by micro pulling down method [13]. The shortened decay time had been successfully explained by a fast radiative de-excitation model related to Ce^{4+} in the Ca doped LYSO [9] and the Mg codoped LuAG crystals [14]. We applied the similar model to our recent study [18] and established a correlation between the stable Ce^{4+} fraction and Ca^{2+} codoping concentration. A Ce^{4+} emission model [14,15] was given through a Ce^{3+} state by capturing an electron from the conduction band, radiative de-excitation of Ce^{3+}, and a return to the initial state by capturing a hole from a nearby hole trap or the valence band. Therefore, Ce^{4+} gives the faster emission in comparison to Ce^{3+}. Since Ca^{2+} in the GGAG lattice promotes the transition from Ce^{3+} to Ce^{4+} [17], the decay time can be reduced by Ca^{2+} codoping. The deterioration of the light yield after Ca^{2+} codoping in GGAG:Ce is attributed to the negative consequence of narrowed E_{cd} (energy gap between conduction band and $5d_1$) for Ce^{4+} and the formation of deep traps [18].

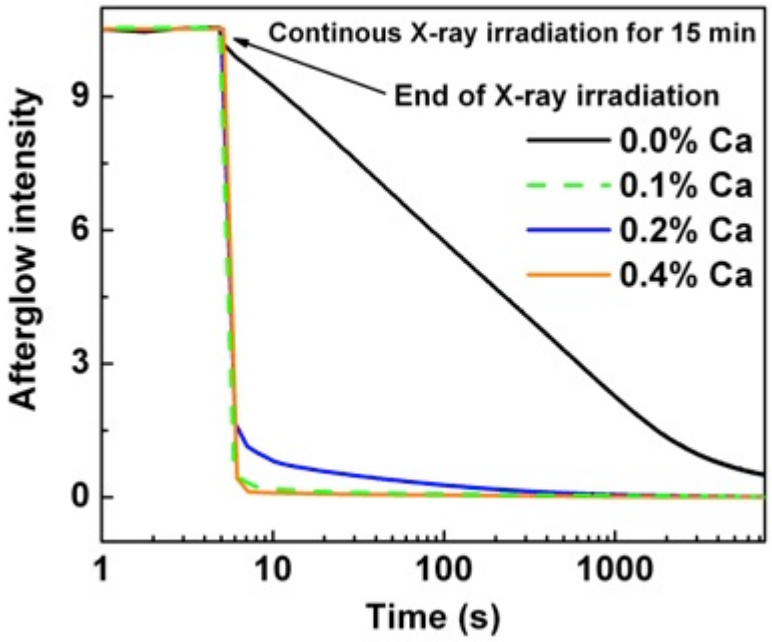

Figure 4.10. Afterglow profiles of GGAG:Ce with various Ca concentrations after continuous X-ray irradiation for 15 min.

Table 4.2. Scintillation properties of GGAG: Ce, Ca crystals.

C (Ca)	LY	ER	S-DT (ratio)	t_{rise}	Afterglow @100 s
0.0%	45000	7.6%	51 (49%)	8	~ 56.3%
0.1%	40000	8.3%	45 (75%)	6	~ 0.71%
0.2%	32000	9.3%	41 (74%)	6	~ 2.66%
0.4%	16000	10.8%	27 (59%)	6.5	~ 0.45%

C (Ca): Ca concentration
LY: light yield (photons/MeV)
ER: energy resolution
S-DT: fast component of scintillation decay time (ns)
t_{rise}: rise time (ns)
Afterglow @ 100 s: relative afterglow intensity at 100 s

Conclusion

The Ca codoped GGAG:0.2% Ce single crystals were grown by the CZ method and their optical, luminescence and scintillation properties were characterized. Ca promotes the transition of Ce valence state from Ce^{3+} to Ce^{4+} in GGAG:Ce crystals and hence the absorbance intensity of Ce^{3+} at 440 nm decreases while the Ce^{4+} charge transfer absorption increases. Since Ce^{4+} is the primary valence state in the sample with 0.4% Ca, it shows a distinct color from those at lower codoping levels. Although the light yield and energy resolution are deteriorated after Ca codoping, the decay time, rise time, shallow traps level and afterglow are remarkably improved. The sample codoped with 0.1% Ca shows shorter decay time (~ 45 ns), shorter rise time (~ 6 ns), lower afterglow intensity (0.71% at 100 s after X-ray cut off) and slightly reduced light yield (~ 40,000 photons/MeV) compared to those of the Ca free sample. Based on the above results, Ca codoped GGAG is a promising candidate of scintillator for applications which require fast timing resolution such as PET, even TOF-PET.

References for chapter 4

[1] C. Dujardin, et al., (2010). “LuAG:Ce fibers for high energy calorimetry.” J. Appl. Phys., 108: 013510.

[2] M. Nikl, et al., (2015). “The role of cerium variation charge state in the luminescence and scintillation mechanism in complex oxide scintillation scintillators: The effect of air annealing.” J. Lumin. DOI: 10.1016/j.jlumin.2015.01.008.

[3] A. M. Srivastava, et al., (2007) Luminescence: Theory and Applications, Wiley-VCH, Weinheim, Germany, chapter 5.

[4] K. Kamada, et. al., (2011). "Composition engineering in cerium-doped (Lu, $Gd)_3(Ga,Al)_5O_{12}$ single-crystal scintillators." Cryst. Growth Des. 11(10): 4484-4490.

[5] K. Kamada, et al., (2011). "Scintillator-oriented combinatorial search in Ce-doped $(Y,Gd)_3(Ga,Al)_5O_{12}$ multicomponent garnet compounds." J. Phys. D: Appl. Phys. 44(50): 505104.

[6] J. A. Mares, et al., (2008). “Scintillation response comparison among Ce-doped aluminum garnets, perovskites and orthosilicates.” IEEE Trans. Nucl. Sci. 55:1142-1147.

[7] M. A. Spurrier, et al., (2008). "Effects of co-doping on the scintillation properties of LSO:Ce." IEEE Trans. Nucl. Sci. 55(3): 1178-1182.

[8] H. E. Rothfuss, et al., (2009). "The effect of codoping on shallow traps in YSO: Ce scintillators." IEEE Trans. Nucl. Sci. 2009, 56(3): 958-961.

[9] S. Blahuta, et al., (2013). “Evidence and Consequences of Ce in LYSO:Ce, Ca and LYSO:Ce,Mg Single Crystals for Medical Imaging Applications." IEEE. Trans. Nucl. Sci. 60(4): 3134−3141.

[10] S. B. Donnald, et al., (2013). "The Effect of B and Ca Co-Doping on Factors Which Affect the Energy Resolution of $Gd_3Ga_3Al_2O_{12}$:Ce." IEEE Trans. Nuc. Sci. 60(5): 4002-4006.

[11] M. Tyagi, et al., (2013). "Effect of codoping on scintillation and optical properties of a Ce-doped $Gd_3Ga_3Al_2O_{12}$ scintillator." J. Phys. D, Appl. Phys. 46(47): 475302.

[12] M. Tyagi, et al., (2014). "Effect of Co-Doping on the Scintillation Kinetics of

Ce Doped." IEEE Trans. Nuc. Sci. 60(1): 297-300.

[13] K. Kamada, et al., (2015). “Alkali earth co-doping effects on luminescence and scintillation properties of Ce doped $Gd_3Al_2Ga_3O_{12}$ scintillator.” Opt. Mater. 41: 63-66.

[14] S. Liu, et al., (2014). "Effect of Mg^{2+} co-doping on the scintillation performance of LuAG: Ce ceramics." Phys. Status Solidi RRL 8(1): 105-109.

[15] M. Nikl, et al., (2014). "Defect engineering in Ce-Doped aluminum garnet single crystal scintillators." Cryst. Growh Des. 14(9): 4827-4833.

[16] K. Kamada, et al., (2015). “Co-doping effect on luminescence and scintillation properties of Ce doped $Lu_3Al_5O_{12}$ scintillators.” Nucl. Instr. Meth. Phys. Res. 782: 9-12.

[17] F. Meng, et al., (2015). "Effect of annealing atmosphere on the cerium valence state and F^+ luminescence center in Ca-codoped GGAG: Ce single crystals." Phys. Status Solidi B, 292: 1394-1401.

[18] Y. Wu, et al., (2014). "Role of Ce^{4+} in the Scintillation Mechanism of Codoped $Gd_3Ga_3Al_2O_{12}$:Ce." Phys. Rew. Appl. 2(4): 044009.

[19] J. M. Ogiegło, et al., (2013). "Luminescence and Luminescence Quenching in $Gd_3(Ga,Al)_5O_{12}$ Scintillators Doped with Ce^{3+}." J. Phys. Chem. A. 117(12): 2479-2484.

[20] K. Yang, et al., (2009). “Effect of Ca codoping on charge traps in LSO:Ce crystals.: IEEE Trans. Nucl. Sci. 56: 2960-2965.

[21] H. Rothfuss, et al., (2009). “Effect of Ca^{2+} Codoping on shallow traps in YSO:Ce crystals.” IEEE Trans. Nucl. Sci. 56: 958-961.

[22] S. R. Rotman, et al., (1992). "Defect-property correlations in garnet crystals. VI. The electrical conductivity, defect structure, and optical properties of luminescent calcium and cerium-doped yttrium aluminum garnet." J. Appl. Phys. 1992, 71(3): 1209-1214.

[23] Y. Zorenko, et al., (2011). "Luminescence centers in Y3Al5O12: La single crystals." In: Journal of Physics: Conference Series (IOP publishing), 289(1): 012028.

[24] M. Springis, et al., (1991). “Polarization of luminescence of color centers in YAG crystals.” J. Phys. Condens. Matter, 3: 5457-5461.

[25] A. Pujats, et al., (2011). “The F type centers in YAG crystals.” Radiat. Eff. Defect S. 155: 65-69.

[26] V. Babin, et al., (2011). “Luminescence of F^+ type centers in undoped $Lu_3Al_5O_{12}$ single crystals.” Phys. Status Solidi B, 248: 239-242.

[27] H. Suzuki, et al., (1994). “Engergy transfer mechanism in $Gd_2(SiO_4)O$:Ce scintillators.” IEEE Trans. Nucl. Sci. 41: 681-688.

[28] M. Kucera, et al., (2013). “Gd^{3+} to Ce^{3+} energy transfer in multi-component GdLuAG and GdYAG garnet scintillators.” Phys. Status Solidi RRL, 8: 571-574.

[29] K. Brylew, et al., (2014). “Studies of low temperature thermoluminescence of GGAG:Ce and LuAG:Pr scintillator crystals using the Tmax-Tstop method.” J. Lumin. 154: 452-457.

Chapter 5 EFFECT OF ANNEALING ATMOSPHERE ON THE CERIUM VALENCE STATE AND F^+ LUMINESCENCE CENTER IN CA CODOPED GGAG:CE SINGLE CRYSTALS

A version of this chapter by Fang Meng was accepted and published by a peer-reviewed journal. The full citation is as following: F. Meng, Y, Wu, M. Koschan, C. L. Melcher and P. Cohen, "*Effect of annealing atmosphere on the cerium valence state and F+ luminescence center in Ca codoped GGAG:Ce single crystals", Physica Status Solidi B 252 (2015) 1394-1401.*

This chapter is the reformatted version of the original work submitted to the referenced journal. No additional changes to the content of the original article were done other than formatting to conform to the dissertation format.

Abstract

GGAG:Ce crystals with various Ca concentrations were grown by the Czochralski technique. The introduction of Ca^{2+} ions into a trivalent site results in a change in the Ce valence state as well as an additional F^{+} luminescence center. The changes of Ce valence state could be affected by various annealing atmospheres and were investigated via measuring the Ce^{3+} absorbance and observing the color change of the sample. Photoluminescence spectra and photoluminescence decay were used to reveal the occurrence of F^{+} center related to the oxygen vacancies during the annealing. A redox mechanism and a charge compensation process are proposed to explain the change in Ce state charge and F^{+} center during the annealing.

Introduction

Cerium doped $Gd_3Ga_xAl_{5-x}O_{12}$ scintillator crystals have been proposed for various applications, including radiation monitoring and medical imaging, due to their favorable crystal structure and scintillation properties [1]. They belong to the garnet structural family with a cubic unit cell and Ia3d space group [2]. The optical and scintillation properties are related to another garnet scintillator compound $Gd_3Ga_3Al_2O_{12}$:Ce (GGAG) crystal derived from the composition $(Lu,Gd)_3(Ga,Al)_5O_{12}$ [3]. GGAG:Ce has good light output (46,000 photons/MeV), fast decay time (~92 ns) and high stopping power, which is due to its high density (6.5 g/cm^3) and effective atomic number (54), [4].

In the past few years, codoping with divalent alkali earth ions such as Ca^{2+} and Mg^{2+} has been used to improve the performance of some Ce doped inorganic scintillators [5-7]. On one hand, the introduction of divalent ions can change the point defect structure of single crystal materials by lowering the concentration of the charge traps, and thus enhancing the energy migration in scintillators such as LSO:Ce, Ca [5], YSO:Ce, Ca [6], LYSO:Ce, Ca and LYSO:Ce, Mg [7]. On the other hand, the introduction of divalent ions could change the Ce or Pr valence state by the charge compensation mechanism. For example, the optical properties of YAG:Pr were affected by introducing Mg^{2+} into the host, which led to the conversion of Pr^{3+} to Pr^{4+} [8], and turned the green YAG:Pr scintillators into a brown YAG:Pr:Mg. In the case of YAG:Ce, codoping with a critical amount of Ca^{2+} caused the full conversion of Ce^{3+} to Ce^{4+}, but no

color change was reported [9].

Recently, we reported the scintillation properties of GGAG:Ce codoped with Ca^{2+} [10-12]. Ca^{2+} codoping eliminates many of the shallow electron traps and shortens the scintillation decay time, possibly improving its suitability for some applications. The detailed mechanism for the decay time improvement was discussed later [13]. However, the detailed mechanism that eliminates the traps has not been identified.

In this work, we investigate the effect of Ca^{2+} codoping on the Ce valence state as well as point defect structures in GGAG:Ce. The Ce valence state was explored via optical absorbance measurements and visual observations of color change. The relationship between Ce valence state and annealing atmosphere was also studies by the absorbance spectra. In addition, the occurrence of F^+/F centers related to oxygen vacancies was investigated for the first time in the GGAG:Ce.

Experimental procedure

Crystal growth

Four GGAG boules were grown from the melt by the Czochralski (CZ) technique in inductively heated iridium crucibles. These boules were nominally 32 mm in diameter and 180 mm long and were grown in a growth atmosphere composed of a fraction of a percent of oxygen in bulk nitrogen. All melts were doped with 0.2 at% Ce and codoped with 0.0-0.4 at% Ca with respect to the rare earth. Composition calculations were based on the assumption that all dopants

substituted for Gd. All concentrations given are those of the initial starting melt; the concentrations of Ce and Ga in the grown crystal may differ due to segregation at the solid-liquid interface during growth. Table 5.1 lists all crystal compositions. Two sample sizes were used in these experiments, unpolished 5 × 5 × 5 mm^3 cubes and ~1mm thick polished wafers. All samples were cut from the same point in the boule in order to get consistent Ce concentration. Figure 5.1 shows the GGAG:Ce cubes with various Ca concentration.

Table 5.1 List of crystal compositions.

Composition	At % Ce (in the melt)	At % Ca
GGAG:Ce	0.2	0.0
GGAG:Ce, Ca	0.2	0.1
GGAG:Ce, Ca	0.2	0.2
GGAG:Ce, Ca	0.2	0.4

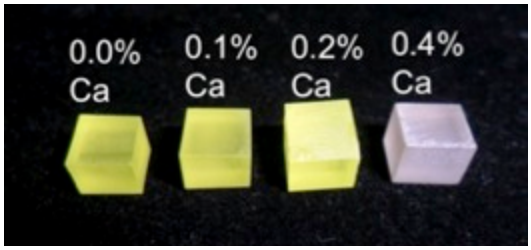

Figure 5.1. Photos of GGAG:Ce cubes with various Ca concentrations. The sample with the highest Ca concentration is a rust color, while the samples with lower Ca concentration are yellow.

Annealing treatment

The samples described in Table 1 were annealed at 1100 °C for 5 h in both an oxidizing (air) and reducing (2% H_2 in bulk N_2) atmosphere. This

temperature was selected in order to avoid the decomposition of crystals (evaporation of Ga) that may occur at higher temperatures [14]. A tube furnace (CM model number: 1730-12-HT) was used with a ramp rate of 200 °C/h. The gas flow rate of the reducing atmosphere was ~4.5 L/min.

Characterization

Absorbance was measured with a Varian Cary 5000 UV-VIS-NIR spectrophotometer. Emission and excitation spectra were acquired with a HORIBA Jobin Yvon Fluorolog-3 Spectrofluorometer using a 450 W continuous Xenon lamp as the excitation source. The data were corrected for the spectral response of the instrument.

Photoluminescence (PL) decay time was measured on the same spectrofluorometer using a Time-Correlated-Single-Photon-Counting module. HORIBA Jobin Yvon Nano LEDs (pulsed light emitting diodes) were used as the excitation source. The emission mono-chromator was set at 0.6 nm bandpass to select the emission light of a specific wavelength. The duration of the light pulse from the Nano LEDs was 1 ns. All data were fit with a single exponential decay model.

For thermoluminescence (TL) glow curve measurements, the sample was mounted within an Advanced Research Systems cryostat (model DE202AE). The pressure was reduced to 20 mTorr and the sample was then heated to 600 K in order to empty the traps. The sample was then cooled to 5 K and irradiated via an X-ray tube (35 kV, 0.1 mA) through a beryllium window for approximately 15

minutes. Subsequently, the sample was brought back to 600 K at a rate of 0.15 K/s. A Hamamatsu H3177 PMT was used to measure the luminescence emitted by the sample as a function of temperature.

Results and discussion

Evidence of changes in Ce valence state

Absorption of as-grown samples

Absorbance measurements were used to reveal changes in the Ce^{3+}:Ce^{4+} ratio. Figure 5.2 show the absorbance spectra of GGAG:Ce with various Ca codopant concentrations. Higher Ca concentrations result in greater absorbance in the 200-350 nm region. This phenomenon was previously observed in Mg codoped LuAG ceramics [15] and single crystals [16], and was attributed to the enhancement of Ce^{4+} charge transfer (CT) absorption. It has been reported by Blahuta [7] and Chewpraditkul [17] that Ce^{4+} CT absorption result in a similar absorbance in some silicates. The peak at 440 nm (the Ce^{3+} 4f-5d1 transition) decreases in intensity as Ca concentration increases, indicating a reduction in the Ce^{3+} concentration. In particular, the rust color crystal with 0.4% Ca shows essentially no Ce^{3+} absorbance at 440 nm. Such significant changes of absorbance around 440 nm are unique in Ca codoped GGAG, as suggested by our previous study [12], and are unlikely caused by the minor variation of Ce concentration from sample to sample. A possible explanation is described in the following reaction using standard Kröger-Vink notation:

$$Me^{\times}_{Me} + Ce^{\times}_{Me} \xrightarrow{CaO} Ca'_{Me} + Ce^{\bullet}_{Me} \quad (Me=Gd, Ga, Al) \qquad (1)$$

Reaction (1) indicates that occupying Gd^{3+}, Al^{3+} or Ga^{3+} sites by Ca^{2+} in the GGAG lattice may lead to a change in the charge state of the Ce ion from Ce^{3+} to Ce^{4+} in order to achieve charge neutrality. Therefore, as the Ca concentration increases the conversion from Ce^{3+} to Ce^{4+} also increases, and the intensity of Ce^{3+} absorbance at 440 nm decreases. When the amount of Ca arrives at a critical level, i.e. 0.4% Ca in this case, most of the Ce^{3+} in the sample has been converted to Ce^{4+}. This explains why no Ce^{3+} absorption at 440 nm is observed and the color change from yellow to rust in the sample with 0.4% Ca.

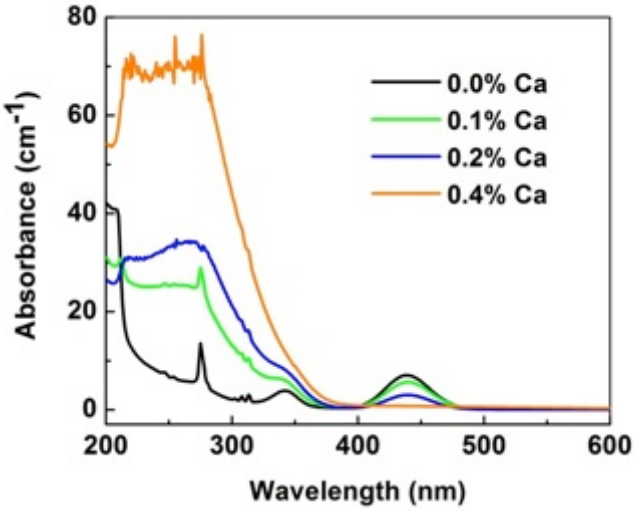

Figure 5.2. Absorbance spectra of GGAG:Ce samples with different Ca concentrations.

Absorption of annealed samples

The color of the samples may also be changed via annealing, and this reveals a relationship between the annealing atmosphere and the Ce valence

state. The samples with lower Ca concentrations were visually unchanged in color after annealing. However the sample codoped with 0.4% Ca turned yellow, the same color as the samples with lower Ca concentrations, after annealed in a reducing atmosphere (2% H_2 in bulk N_2), while it had a strong rust color as-grown and after annealed in air, as shown in Figure 5.3. This is a reversible change; it reverted to rust after re-annealing in air and back to yellow after re-annealing in a reducing atmosphere. The similar reversible color changes have been reported by Pawlak in Mg codoped YAG:Pr crystals annealed in both oxidizing and reducing atmospheres due to the Pr^{3+}:Pr^{4+} conversion [8].

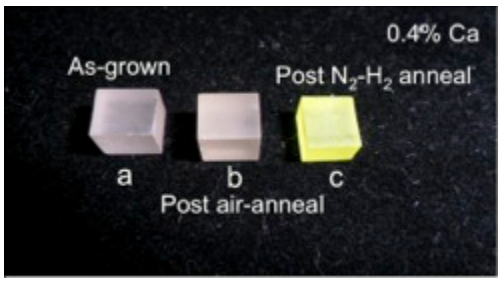

Figure 5.3. Color changes of GGAG:Ce crystals codoped with 0.4 at% Ca: the as-grown (sample a), the post air-anneal (sample b), and the post N_2-H_2 anneal (sample c).

Absorbance measurements reveal a relationship between annealing atmosphere and Ce^{3+} emission that is also correlated with reversible color changes in highly codoped samples. The Ce valence state change is clearly revealed in the absorbance spectra of the sample with 0.4 at% Ca, as shown in Figure 5.4. For these measurements, two similar polished wafers with approximately equal absorbance were chosen. One sample was only annealed

once in air while the other was annealed multiple times, in the following sequence of atmospheres: N_2-H_2, air and N_2-H_2. While the as-grown and post air-annealed samples show no absorbance at the Ce^{3+} 4f-$5d_1$ transition, which would be seen around 440 nm, the sample annealed in a reducing atmosphere clearly shows Ce^{3+} absorbance at that wavelength. The reason for the intensity difference of Ce^{3+} absorbance is not clear.

In the above section we proposed a mechanism whereby Ca^{2+} occupancy of trivalent cation sites results in oxidation of Ce^{3+} to Ce^{4+}. Here we propose an additional mechanism to explain the relationship between cerium valence state and annealing atmosphere [15]:

$$2CaO+Me_2O_3 \rightarrow 2\left(Ca'_{Me}\right)+V_O^{\bullet\bullet} \quad (Me=Gd, Ga, Al) \tag{2}$$

$$V_O^{\bullet\bullet}+2Ce_{Me}^{\times}+\frac{1}{2}O_2 \rightleftarrows O_O^{\times}+2Ce_{Me}^{\bullet} \tag{3}$$

Since these crystals were grown in a low oxygen environment, the likelihood of oxygen vacancies is high. Reaction (2) indicates a possible mechanism by which locating Ca^{2+} at trivalent sites in the GGAG lattice could lead to the potential for forming ($Ca'_{Me} – V_O^{\bullet\bullet}$ - Ca'_{Me}) complexes via Columbic compensation of oxygen vacancies. Reaction (1), in the above section, shows a pathway for the creation of some Ce^{4+} with divalent codoping. Here, reaction (3) shows a possible mechanism for the elimination of oxygen vacancies and oxidation of more Ce^{3+} to Ce^{4+} when the sample is annealed in an oxidizing atmosphere, leading to a condition in which the bulk of the existing Ce^{3+} ions are oxidized to Ce^{4+}. This oxidized Ce^{4+} should then reduce to Ce^{3+} when annealed

in the reducing atmosphere, observable by reappearance of the Ce^{3+} absorbance peak. A similar phenomenon has been observed in Ca codoped YAG:Ce crystals. It was reported that the as-grown and air-annealed samples show no absorbance peak at 460 nm because most of the Ce was in the Ce^{4+} state. After annealing in a reducing atmosphere (CO with 1% CO_2), the absorbance peak at 460 nm appeared, indicating that the Ce^{4+} reverted to Ce^{3+} [9].

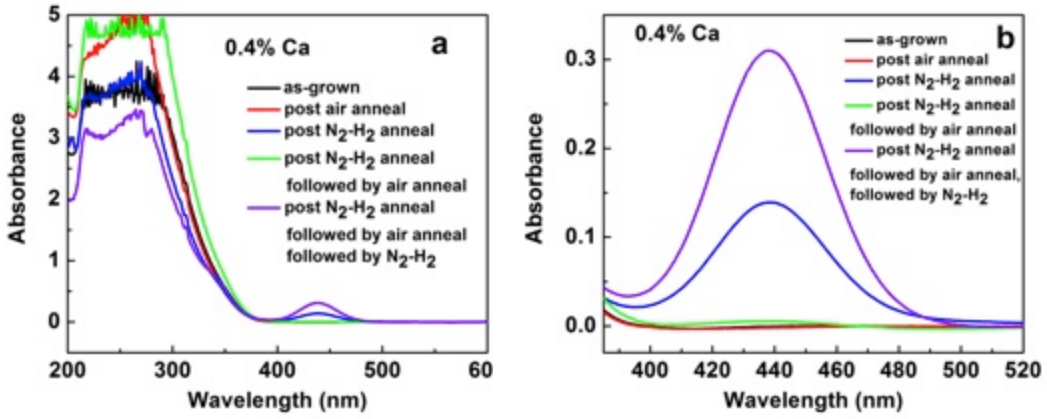

Figure 5.4. The absorbance spectra of GGAG:Ce with 0.4% Ca under different annealing atmospheres. Part b shows an enlargement of the absorbance region between 385 and 520 nm.

In order to verify that this mechanism works in samples with lower Ca codoping levels within 0.0%-0.2% region, we selected two polished wafers from each compo-sition, one annealed in an oxidizing (air) atmosphere and the other in a reducing (2% H_2 in bulk N_2) atmosphere, and measured the absorbance in the 390-500 nm range. The crystals with lower Ca concentrations did not visibly change color after annealing in either atmosphere. The changes in the

absorbance ($\mu_{after} - \mu_{before}$) with annealing are shown in Figure 5.5. After annealing in air, the intensity of the Ce^{3+} 4f-$5d_1$ transition at 440 nm did not change in the sample with 0.4% Ca because there was not much Ce^{3+} in the as-grown sample to convert. However, it decreased significantly for the sample with 0.2% Ca, indicating oxidization of Ce^{3+} to Ce^{4+}. Although no noticeable change was observed in the sample with 0.1% Ca, it was not clear whether any change in valence state had occurred. On the other hand, after annealing in a reducing atmosphere, the conversion from Ce^{4+} to Ce^{3+} had clearly occurred in all Ca samples, evidenced by the increase of the 440 nm Ce^{3+} absorbance. For the purpose of comparison, a sample with no Ca was annealed in both atmospheres and the changes in the absorbance were also plotted in Figure 5.5. There was no change in intensity at the 440 nm Ce^{3+} absorbance for the Ca-free sample, indicating the valence state change only occurred as a direct result of Ca^{2+} codoping.

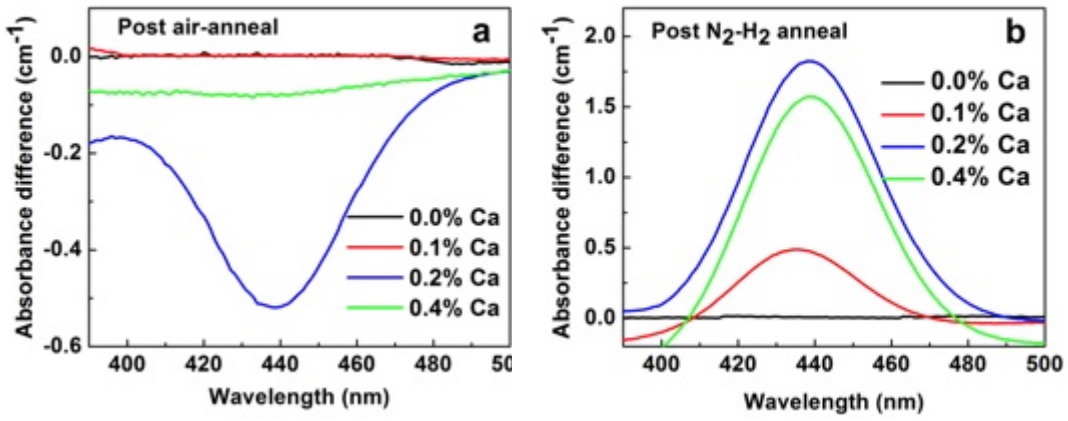

Figure 5.5. The change ($\mu_{after} - \mu_{before}$) in the absorption of GAGG:Ce crystals with different Ca concentrations after annealing in (a) air and (b) N_2-H_2.

Evidence of F^+ center

Photoluminescence of F^+ center

GGAG is known to have PL excitation peaks at 345 nm and 440 nm and an emission peak at 550 nm due to the Ce^{3+} 5d-4f radiative transition. However, an additional luminescence center with an excitation wavelength of 350 nm and an emission at 400 nm was found in the as-grown Ca codoped samples. This center appears to result from an F^+ center related to the oxygen vacancies shown in reaction (2). The introduction of divalent Ca into a trivalent site leads to a local excess charge with the potential to result in or interact with oxygen vacancies [9], which may in turn trap electrons and become F^+ or F center, as in reactions (4) and (5):

$$V_O^{\bullet\bullet} + e \rightarrow V_O^{\bullet} \quad (F^+) \tag{4}$$

$$V_O^{\bullet} + e \rightarrow V_O \quad (F) \tag{5}$$

An F^+ center has previously been reported, with an excitation peak at 360 nm and emission peak at 400 nm, in YAG crystals; an F center with an excitation peak at 240 nm and emission peak at 460 nm was also reported [18-23]. The location of the F^+ center in the YAG crystal is similar to that of the new additional center found in our GGAG, further supporting the idea that this is primarily an F^+ center.

Since the F^+ center is related to oxygen vacancy, we ran a series annealing tests to understand the relationship be-tween F^+ center and annealing atmosphere. Figures 5.6 and 5.7 show the photoluminescence spectra of

GGAG:Ce crystals with 0.1% and 0.2% Ca after annealing in different atmospheres. In Figure 5.6a, the excitation spectra were measured at an emission wavelength of 550 nm (the Ce 5d-4f transition), and the emission spectra were measured at an excitation wavelength of 350 nm (the Ce 4f-$5d_2$ transition). In particular, an F^+ center with an excitation peak at 350 nm and emission peak at 400 nm was observed in the as-grown sample. The enlarged region of F^+ emission (circle mark) in Figure 5.6a is shown in Figure 5.6b, in which the emission spectra were measured at an excitation wavelength of 350 nm. From Figure 5.6b, the F^+ center disappears after annealing in air, while it still exists after annealing in a reducing atmosphere.

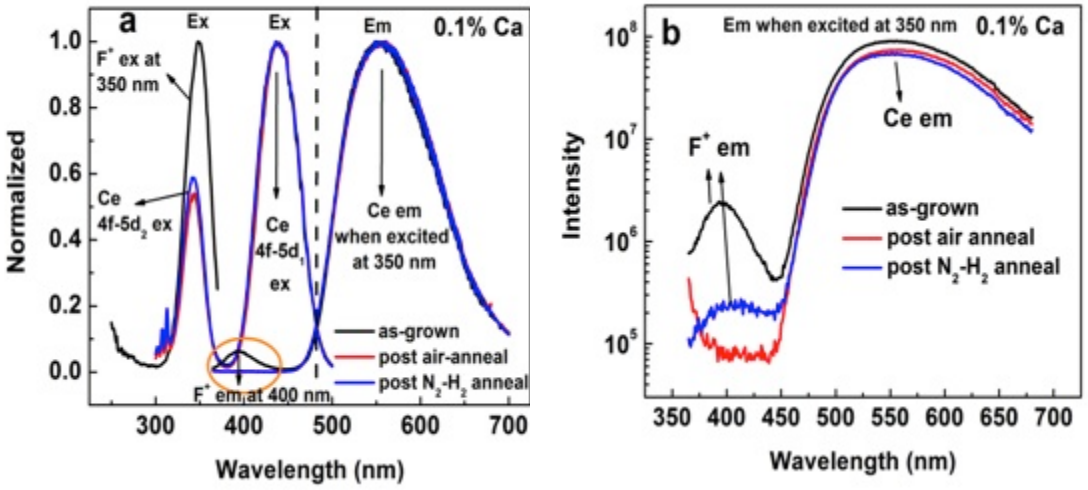

Figure 5.6. (a) the photoluminescence spectra of GGAG: 0.2% Ce with 0.1% Ca both as-grown and annealed in different atmospheres; (b) enlarged region of F+ emission. Dashed line separates the excitation and emission spectra. Note the additional luminescence located at excitation 350 nm and emission 400 nm.

The similar phenomenon was observed in the samples with 0.2% Ca, as shown in Figure 5.7, where the excitation spectra were measured at an emission wavelength of 400 nm. This is because when Ca samples with F^+ center are annealed in an oxidizing atmosphere, oxygen vacancies ($V_O^{\bullet\bullet}$) will be suppressed as shown in reaction (3). Since an F^+ center is an oxygen vacancy that has trapped an electron, eliminating the oxygen vacancy also eliminates the F^+ center, and therefore eliminates its accompanying emission. On the other hand, annealing in a reducing atmosphere has the opposite effect, and may produce an F^+ center where one did not previously exist.

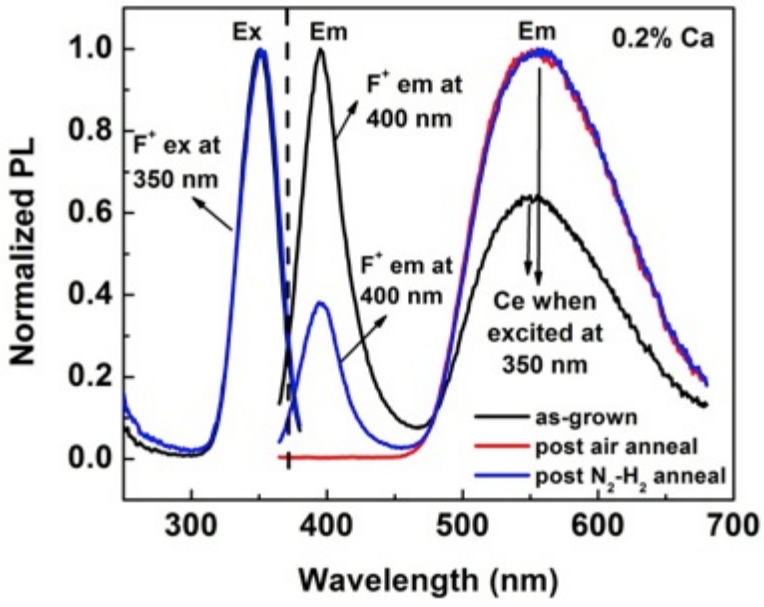

Figure 5.7. The photoluminescence spectra of GGAG: 0.2% Ce with 0.2% Ca both as-grown and annealed in different atmospheres; Note the additional luminescence center located at excitation 350 nm and emission 400 nm. Dashed line separates the excitation and emission spectra.

The sample with the highest (0.4%) Ca concentration behaved differently from the samples with lower concen-trations. The PL spectra of this sample following annealing in different atmospheres are shown in Figure 5.8a. An en-largement ofthe F+ center excitation and emission region is shown in Figure 5.8b. The F+ center persists even after an-nealing in an oxidizing atmosphere, while it is considerably enhanced after annealing in a reducing atmosphere. There is also a noticeable shift in the location of this F^+ center in the 0.4% Ca codoped sample compared to the other samples, from excitation wavelength at 350 nm and emission wavelength at 400 nm to excitation wavelength at 380 nm and emission wavelength at 430 nm, in both the as-grown and the air-annealed samples. When annealed in a reducing atmosphere, this shift disappeared, and the excitation/emission wavelengths were observed at the same location as in the other Ca samples. This shift may be the result of the different primary Ce valence state (Ce^{4+}) in the sample with 0.4% Ca. Considering that 1) different accidental impurities (e.g., Ce, Si, Fe, etc.) may occupy Al^{3+} sites in YAG or LuAG crystal [24]; 2) the EPR signal from F^+ center located close to Si^{2+}_{Al} was detected in YAG:Si crystal [25]; and 3) GGAG and YAG have the similar garnet structure; the F^+ center in GGAG may be possibly located close to Ce^{3+}_{Al} or Ce^{4+}_{Al} site, thus can be easily affected by the Ce valence state. In addition, the cerium may be nearly completely in Ce^{4+} form in the as grown sample with 0.4% Ca [13] and therefore cannot be further oxidized by air annealing. The Ce^{4+} can however be partially reduced by annealing in a reducing atmosphere, causing the

emission of F^+ center to be similar to the samples with lower Ca concentrations (primary Ce^{3+} form).

TL measurements were done to investigate the relationship between the annealing atmosphere and the traps related to oxygen vacancies. Figure 5.9 shows the TL spectra of the samples with different Ca concentrations in different annealing atmospheres. With 0.1% Ca addition (Figure 5.9a), the air-annealed sample showed low TL intensity with no noticeable peaks around 210 K and 450 K, in contrast to the as-grown sample. For the samples with 0.2% Ca (Figure 5.9b), peaks around 90 K and 520 K were diminished after air annealing. This was likely due to the decrease of oxygen vacancies. However, after annealing in a reducing atmosphere, higher TL intensity was observed throughout the temperature range, especially below 450 K, in the lower Ca samples (0.1% and 0.2%), indicating more oxygen vacancies were created. The similar phenomenon was also observed in LYSO crystals [26]. By correlating the suppression of the traps below room temperature in TL spectra with the absence of F^+ center in PL spectra for the samples with lower Ca concentrations after air annealing, one can conclude that the F^+ center is likely associated with the shallow traps below room temperature.

The TL measurements for the sample with 0.4% Ca are shown in Figure 5.9c. No shallow traps were observed in the as-grown sample, thus neither in the air-annealed sample. However, shallow traps appeared after annealing in a reducing atmosphere, which was consistent with the formation of a noticeable F^+

center in PL spectra as shown in Figure 5.8b. Contrary to the previous conclusion from the samples with low Ca concentrationss, a faint F^+ center (Figure 5.8b) can still be observed in the as-grown and air-annealed samples with 0.4% Ca, despite the absence of shallow traps (Figure 5.9c). Considering the different primary Ce valence state (Ce^{4+}) in the sample with 0.4% Ca from the other samples (Ce^{3+}), it is reasonable to think that the F^+ center can be affected by Ce valence state. Further investigations are necessary to better understand the relationship between the F^+ center and Ce valence state in Ca codoped GGAG crystals.

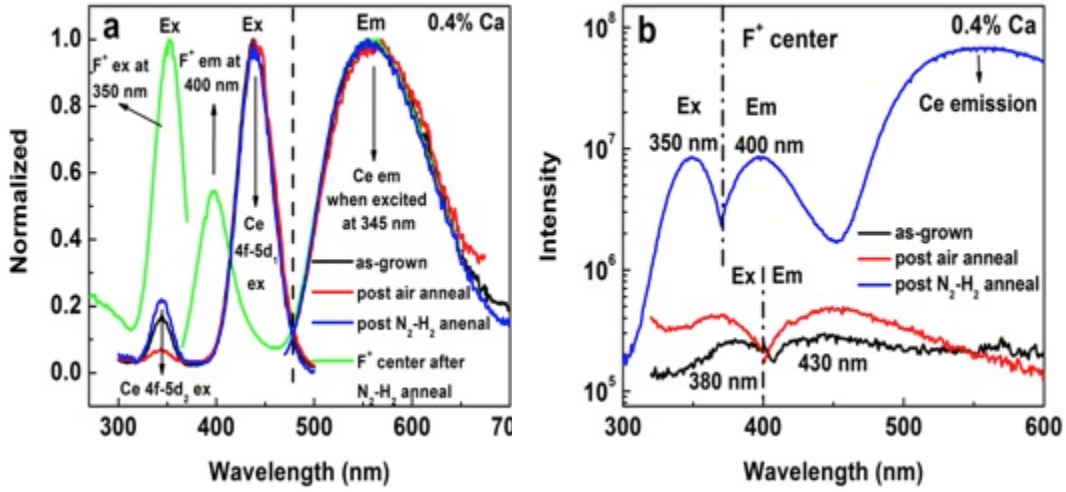

Figure 5.8. (a) The photoluminescence spectra of GGAG: 0.2% Ce with 0.4% Ca both as-grown and annealed in different atmospheres; (b) enlarged regions of F+ luminescence. Dashed line separates the excitation and emission spectra.

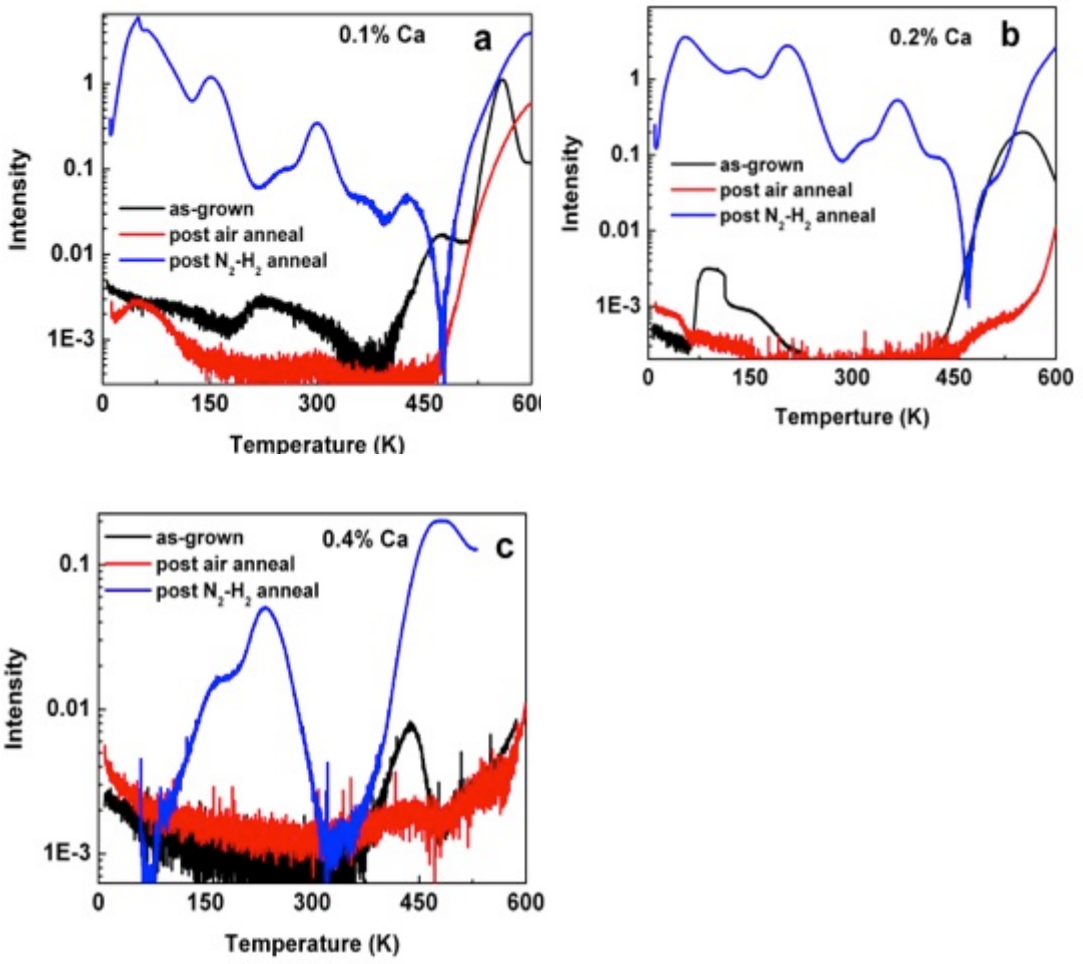

Figure 5.9. Thermoluminescence spectra of GGAG with (a) 0.1 at%, (b) 0.2 at% and (c) 0.4 at% Ca under different annealing atmospheres.

Photoluminescence decay of F^+ center

The PL decay time (measured at 350 nm excitation and 400 nm emission) of all Ca samples under both annealing atmospheres was measured to confirm the occurrence of the F^+ center. Figure 5.10 shows the PL decay spectra of F^+ center in the GGAG:Ce crystals with 0.1%, 0.2% and 0.4% Ca after annealing in different atmospheres, as well as the instrumental response. Considering the

pulse width of the Nano LEDs is comparable to the decay time of the F^+ center in Figure 5.10, especially to those of the as-grown and post air-annealed samples in Figure 5.10c, it is necessary to eliminate the instrumental response from the decay profile by deconvolution. The insets show examples of fitting the deconvolved PL decay curves in the as-grown samples using a single exponential model. All fitted data are shown in Table 5.2. The PL decay time of the F^+ center was ~3.5 ns obtained in the as-grown crystals with 0.1% and 0.2% Ca. Similar energy levels and PL decay time in the same order of magnitude were previously reported in F^+ center found in YAG crystal [18, 23]. No PL decay signal was detected for the F^+ center in samples with 0.1% and 0.2% Ca after air annealing, indicating no F^+ luminescence center appeared in these samples, which was consistent with the steady-state PL results. A PL decay time of around 1.2 ns was obtained under excitation at 380 nm and emission at 430 nm for the as-grown and air-annealed samples with 0.4% Ca, which was slightly faster than that of the other low Ca samples (~3.5 ns) under excitation at 350 nm and emission at 400 nm. After annealing in a reducing atmosphere, the PL decay time became comparable to the other samples. Different energy locations and PL decay time of the F^+ center were observed in the Ca codoped samples with different Ce valence state, which are in different colors. Further studies need to be done to understand the relationship between the location of the F^+ center and the Ce valence state of crystals.

Table 5.2 Photoluminescence decay (lifetime) of F^+ center in GGAG:Ce crystals with various Ca concentrations (a: Ex: 350 nm, Em: 400 nm; b: Ex: 380 nm, Em: 400 nm)

Sample	PL decay time (ns)		
	0.1% Ca	0.2% Ca	0.4% Ca
As-grown	3.5[a]	3.5[a]	1.2[b]
Air-annealed	n/a	n/a	1.2[b]
N_2-H_2 annealed	3.3[a]	3.5[a]	3.6[a]

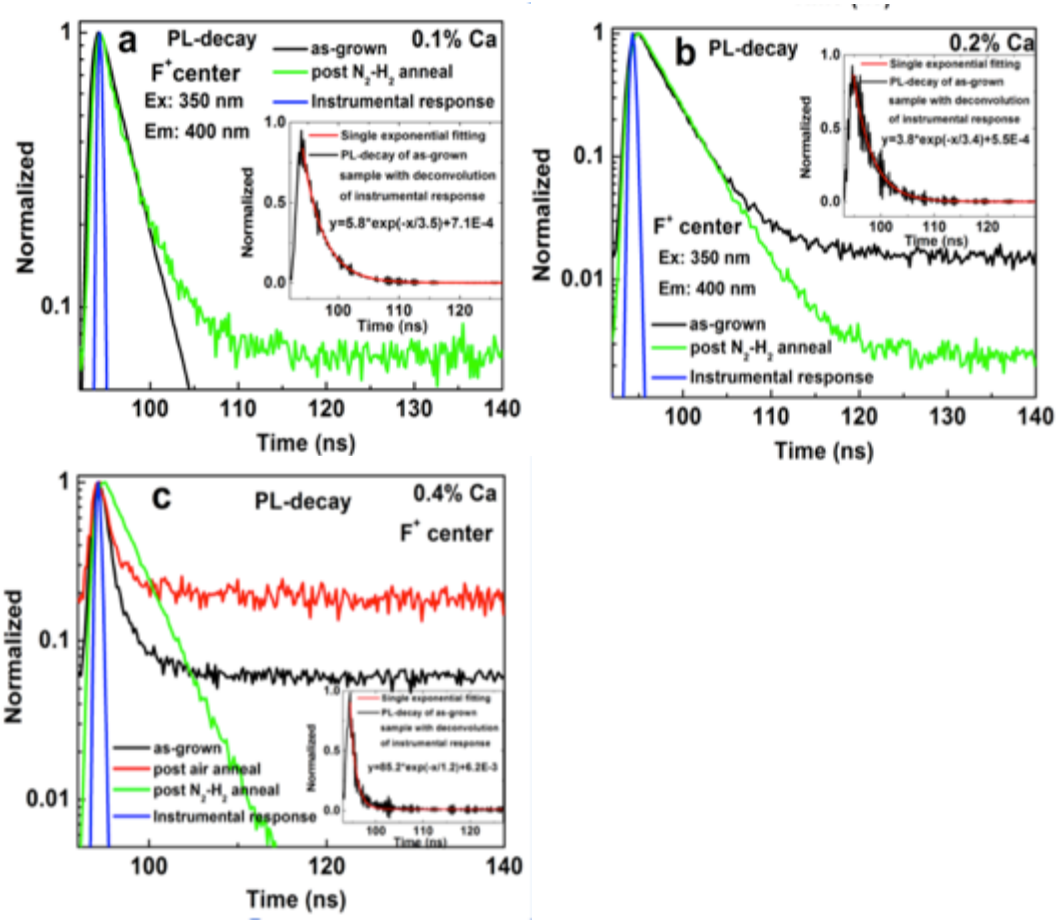

Figure 5.10. PL decay spectra of the 'additional' luminescence center (F+ center) in GGAG:Ce crystals with (a) 0.1% Ca, (b) 0.2% Ca and (c) 0.4% Ca in different annealing atmospheres. The insert shows the fitting curve of PL decay using a single exponential model.

Conclusion

GGAG:Ce crystals with various Ca concentrations were grown by the CZ technique; the introduction of Ca^{2+} ions into a trivalent site results in a change in the Ce^{3+}:Ce^{4+} ratio as well as an additional F^{+} luminescence center. The changes of Ce valence state could be affected in the more highly codoped samples by various annealing atmospheres and as indicated by changes in the Ce^{3+} absorbance band around 440 nm as well as the color changes. The sample with the highest Ca concentration and more Ce^{4+} is rust color, while the samples with lower Ca concentration and more Ce^{3+} are yellow color. A reversible Ce valence state change correlated with color change was also observed in the GGAG:Ce crystals with the highest Ca concentration under various annealing atmospheres. An F^{+} luminescence center was observed at an excitation wavelength of 350 nm and an emission wavelength 400 nm with PL lifetime at ~3.5 ns in the Ca codoped samples and was affected by annealing atmospheres. In the samples with lower Ca concentrations, annealing in an oxidizing atmosphere (air) helped to reduce or eliminate the oxygen vacancies, diminishing the F^{+} center. In the crystal with the highest Ca concentration, the F^{+} center appears after annealing in a reducing atmosphere (2% H_2 in bulk N_2) presumably due to the increase of oxygen vacancies.

References for Chapter 5

[1] K. Kamada, K., et al., (2012). "Crystal growth and scintillation properties of Ce doped single crystals." IEEE Trans. Nucl. Sci. 59(5): 2112-2115.

[2] L. Seijo and Z. Barandiarán, (2013). "Host effects on the optically active 4f and 5d levels of Ce^{3+} in garnets." Phys. Chem. Chem. Phys. 15(4): 19221.

[3] K. Kamada, et al., (2011). "Composition engineering in cerium-doped $(Lu,Gd)_3(Ga,Al)_5O_{12}$ single-crystal scintillators." Cryst. Growth Des. 11(10): 4484-4490.

[4] K. Kamada, et al., (2012). "2inch diameter single crystal growth and scintillation properties of $Ce:Gd_3Al_2Ga_3O_{12}$." J. Cryst. Growth 352(1): 88-90.

[5] M. A. Spurrier, et al., (2008). "Effects of co-doping on the scintillation properties of LSO:Ce." IEEE Trans. Nucl. Sci. 55(3): 1178-1182.

[6] H. E. Rothfuss, et al., (2009). "The effect of codoping on shallow traps in YSO:Ce scintillators." IEEE Trans. Nucl. Sci. 2009, 56(3): 958-961.

[7] S. Blahuta, et al., (2013). “Evidence and Consequences of Ce in LYSO:Ce, Ca and LYSO:Ce,Mg Single Crystals for Medical Imaging Applications." IEEE. Trans. Nucl. Sci. 60(4): 3134−3141.

[8] D. Pawlak, et al., (1998). "Spectroscopic and crystallographic studies of YAG: Pr^{4+} single crystals." J. Alloys Compd. 275: 361-364.

[9] S. R. Rotman, et al., (1992). "Defect-property correlations in garnet crystals. VI. The electrical conductivity, defect structure, and optical properties of luminescent calcium and cerium-doped yttrium aluminum garnet." J. Appl. Phys. 1992, 71(3): 1209-1214.

[10] S. B. Donnald, et al., (2013). "The Effect of B and Ca Co-Doping on Factors Which Affect the Energy Resolution of $Gd_3Al_2Ga_3O_{12}$:Ce." IEEE Trans. Nuc. Sci. 60(5): 4002-4006.

[11] M. Tyagi, et al., (2014). "Effect of Co-Doping on the Scintillation Kinetics of Ce Doped." IEEE Trans. Nuc. Sci. 60(1):297-300

[12] M. Tyagi, et al., (2013). "Effect of codoping on scintillation and optical properties of a Ce-doped $Gd_3Ga_3Al_2O_{12}$ scintillator." J. Phys. D, Appl. Phys. 46(47): 475302.

[13] Y. Wu, et al., (2014). "Role of Ce^{4+} in the Scintillation Mechanism of

Codoped $Gd_3Al_2Ga_3O_{12}$:Ce." Phys. Rew. Appl. 2(4): 044009.

[14] F. Meng, et al., (2014). "A novel method to create an intrinsic reflective layer on a $Gd_3Al_2Ga_3O_{12}$:Ce scintillation crystal." Nucl. Instr. Meth. Phys. Res. 2014, 763, 591-595.

[15] S. Liu, et al., (2014). "Effect of Mg^{2+} co-doping on the scintillation performance of LuAG:Ce ceramics." Phys. Status Solidi RRL 8(1): 105-109.

[16] M. Nikl, et al., (2014). "Defect engineering in Ce-Doped aluminum garnet single crystal scintillators." Cryst. Growh Des. 14(9): 4827-4833.

[17] W. Chewpraditkul, et al., (2013). "Comparison of absorption, luminescence and scintillation characteristics in $Lu_{1.95}Y_{0.05}SiO_5$:Ce,Ca and Y_2SiO_5:Ce scintillators." Opt. Mater. 35(9): 1679:1684.

[18] Y. Zorenko, et al., (2011). "Luminescence centers in $Y_3Al_5O_{12}$:La single crystals." In: Journal of Physics: Conference Series (IOP publishing), 289(1): 012028.

[19] Y. Zorenko, et al., “Luminescence of F^+ and F centers in Al_2O_3 -Y_2O_3 oxide compounds” Materials Science and Engineering: Conference Series, (IOP publishing), 15: 012060.

[20] Y. Zorenko, et al., (2004). "Luminescence of F^+ and F centers in $YAlO_3$." Opt. Spectrosc. 96(4): 532-537.

[21] A. Pujats and M. Springis, (2001). "The F-type centres in YAG crystals." Radiat. Eff. Defects Solids 155(1-4): 65-69.

[22] M. Springis, et al, (1991). "Polarization of luminescence of colour centres in YAG crystals." J. Phys.: Condens. Matter 3(28): 5457.

[23] V. I. Graveris and I. A. Krumin’sh, (1983). “Thermo-activation Spectroscopy of Defects in Ion Crystals” (Zinante, Riga), pp. 145.

[24] V. Babin, et al., (2011). "Luminescence of F^+ type centers in undoped $Lu_3Al_5O_{12}$ single crystals." Phys. Status Solidi B 248(1): 239-242.

[25] D. F. Peters, et al., (2007). "High quantum efficiency YbAG-crystals." J. Lumin. 125(1): 238-247.

[26] S. Blahuta, et al., (2011). "Defects identification and effects of annealing on $Lu_{2(1-x)}Y_{2x}SiO_5$ (LYSO) single crystals for scintillation application." J., Mater. 4(7):

1224-1237.

Chapter 6 A NOVEL METHOD TO CREATE AN INTRINSIC REFLECTIVE LAYER ON A $GD_3GA_3AL_2O_{12}$:CE SCINTILLATION CRYSTAL

A version of this chapter by Fang Meng was accepted and published by a peer-reviewed journal. The full citation is as following: F. Meng, M. Koschan, M. Tyagi, C. L. Melcher and P. Cohen, "*A Novel Method to Create an Intrinsic Reflective layer on a $Gd_3Ga_3Al_2O_{12}$:Ce Scintillation Crystal", Nuclear Instruments and Methods in Physics Research A 763 (2014): 591-595.*

This chapter is the reformatted version of the original work submitted to the referenced journal. No additional changes to the content of the original article were done other than formatting to conform to the dissertation format.

Abstract

An innovative method to produce a reflective layer on a scintillation detector element was devised in order to provide an alternative approach to the traditional method of applying extrinsic reflectors. It is known that many inorganic oxides can decompose into suboxides when heated in an oxygen-deficient atmosphere. After heat treating a $Gd_3Ga_3Al_2O_{12}$ (GGAG) crystal in a reducing atmosphere for several hours we observed that a white surface layer was formed, which was found to have good reflective properties. The resulting reflective layer is robust and firmly attached to the crystal; X-ray diffraction analysis showed that the white reflective layer is primarily composed of $GdAlO_3$. The reflectivity of this reflective layer can reach 92% and the thickness increases with the cumulative soaking time. The performance of the reflective layer in terms

of maximizing photon collection was compared to the performance of Teflon tape.

Introduction

Cerium (Ce) doped scintillators are scientifically and economically important materials used to detect high-energy photons and particles in various applications, including medical imaging, high-energy physics, geological exploration, and homeland security. These scintillators are packaged together with a photosensor, such as a photomultiplier tube, in detector assemblies. A detector assembly may contain an array composed of many smaller scintillator elements, often referred to as pixels. In most cases, it is desirable to optically isolate the pixels from each other in order to maximize the scintillation light that reaches the photodetector and to prevent the light interference from the adjacent pixels [1], for example see Figure 6.1. The common solution is to separate the pixels with a reflective material, such as Teflon [2] or barium sulfate [3]. The effect of applying reflectors on scintillators as well as the choice of the reflector materials has been intensively investigated [3-5]. However, they were all externally applied reflectors.

In this paper, we report a technique to create an intrinsic reflective layer on a Ce doped $Gd_3Al_2Ga_3O_{12}$ (GGAG) [6] single crystal. It is known that many of inorganic oxides can decompose into suboxides when heated in an oxygen-deficient atmosphere [7,8]. After heat treating a GGAG crystal in reducing

atmosphere, we observed that the suboxides of gallium evaporate from the surface of the crystal and leave a white surface layer behind, which serves well as an intrinsic reflector [9]. We evaluated the composition and reflectivity of the white layer, and investigated the effect of soaking time on layer thickness as well as the reflector performance in terms of maximizing photon collection, namely maximizing the scintillation light that reaches the photodetector.

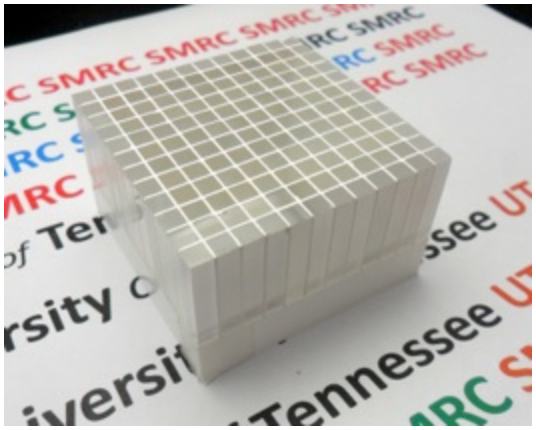

Figure 6.1. Array of scintillator pixels with a white reflective material filling the spaces between the pixels in order to maximize light collection.

Experimental methods

The GGAG crystals were grown by Czochralski method, as previously reported [10-11]. Cubic GGAG crystals, approximately 10 mm x 10 mm x 10 mm were heated at 3.3 °C /min to 1300°C in bulk N_2 with 2% H_2 in a tube furnace and held at that temperature and atmosphere for 5-10 h before cooling to room temperature at the same rate. During this high temperature treatment, a stable white reflective layer formed on the surface of the crystal (see Figure 6.2c). This

layer was securely bonded to the underlying crystal, although it could be removed with common polishing techniques.

While heat treating in a reducing atmosphere is useful for forming the reflective layer, it unfortunately reduces the light yield. Therefore, a subsequent heat treatment was done for 10 h at the same temperature in an air atmosphere in order to restore the light yield to the previous value. A detailed explanation of this process can be found in our previous work [11]. It should be noted that this additional heat treatment did no harm to the reflective layer.

Light yield (LY) measurements were conducted on a test set using a Hamamatsu R877 photomultiplier tube (PMT) and a 10 μCi ^{137}Cs source; no optical couplant was used. LY value is on a scale where BGO reference crystal is set to 100. Four crystals of approximately the same size were cut from the same boule, and an initial LY measurement was done with a hemispherical reflector to establish that all had equivalent starting LY. One sample was kept in the as-grown state; three were then subjected to heat treatment in a reducing atmosphere to form the white layer. The white layer was removed with polishing paper from all six sides of one sample, as shown in Figure 6.2b, and from one side of another sample, as shown in 2c. The sample shown in Figure 6.2d has also had the white layer removed from all 6 sides; it was then wrapped with at least 5 layers of Teflon tape. A second LY measurement revealed that the heat treatment in the reducing atmosphere had significantly reduced the LY and a second anneal was done in an air atmosphere to restore it to the original value

so that all samples again had equivalent LY. In these measurements with the reflective dome, the measured LY indicates the total quantity of photons emitted from the sample.

The performance of the intrinsic reflective layer relative to externally applied Teflon tape was evaluated by measuring the LY of the crystals without the previously used reflective dome. In this case, the relative LY is an indicator of the relative ability of the intrinsic reflector and the Teflon tape to redirect photons into the PMT.

Pieces of the as-grown GGAG crystals were crushed and ground into powder with a ball mill for X-ray diffraction (XRD) measurements with a Bruker Axs powder diffractometer Model D2 Phaser. On the other hand, the reflective layer was measured with a Philips X'Pert diffractometer while the layer was still attached to the crystal, since the layer was too thin to be removed without introducing impurities in the cutting and grinding process. Furthermore, A LEO Gemini 1525 Field Emission Scanning Electron Microscope (SEM) equipped with Energy-Dispersive Spectrometer (EDS) was used to verify the composition of reflective layer.

Additional heat cycles were subsequently done in order to study film thickness vs. time and the effect on detector performance. A crystal cube was heat treated at 1300 °C in N_2 +2% H_2 in four cycles. The soaking time for each cycle was 10, 15, 10 and 15 h, thus the cumulative soaking time was 10, 25, 35 and 50 h. After each heating cycle, the reflective layer on the top surface was

removed with polishing paper (see Figure 6.2c), and the thickness of the layer was measured by viewing its cross-section with a KEYENCE VHX-1000E Digital Microscope. In addition, reflectivity measurement of reflective layer was carried out using an integrating sphere attachment on Shimadzu spectrophotometer Model 3100.

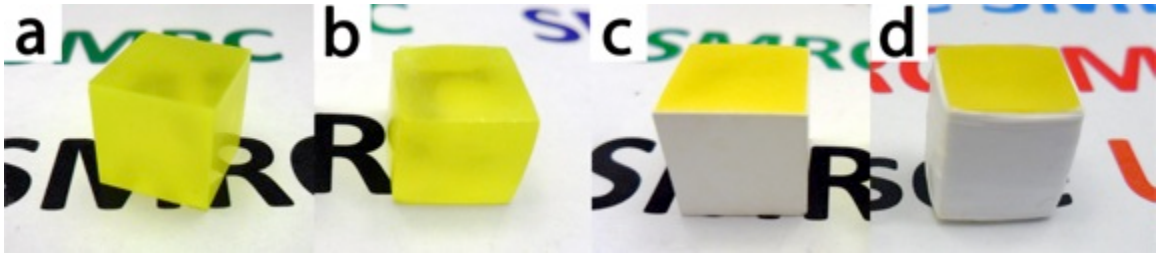

Figure 6.2. a) as grown GGAG crystal, b) annealed crystal with intrinsic reflective layer removed, c) annealed crystal with reflective layer on five surfaces (top layer was removed), and d) crystal b wrapped with Teflon tape on five surfaces.

Results and discussion

XRD analysis of as-grown GGAG crystal and reflective layer

The phase purity and composition of the as grown crystal as well as the reflective layer were measured by XRD and EDS, respectively. As shown in Figure 6.3a, the diffraction pattern of the as-grown GGAG crystal was in good agreement with GGAG reference pattern in Pearson's Crystal Data (No. 1627563). The diffraction pattern (Figure 6.3b) of the reflective layer strongly suggested that the white layer was mostly $GdAlO_3$, because it matched very well the diffraction pattern of $GdAlO_3$ (No. 1818268). The EDS analysis of the

reflective layer showed Gd, Al and O peaks but no Ga peaks (Figure 6.4). The absence of Ga in the reflective layer could be explained by the reaction described by Brandle [7], namely the decomposition of gallium sesquioxide (Ga_2O_3) to the suboxide (Ga_2O) occurred when heating at high temperature and a reducing atmosphere. The Ga_2O formed by decomposition has a much higher vapor pressure than the garnet does, causing it to vaporize from the garnet surface. Due to the lack of O_2, the decomposition of the sesquioxide and the vaporization of the suboxide can proceed continuously, leaving only Gd, Al and O at the surface of the crystal [9]. We believe the remaining materials at the surface form mixed oxides of Gd and Al, which was identified as mostly $GdAlO_3$ seen as the white layer. In our experiment, the self-reflecting layer was not formed before the temperature reaches 1300 °C in reduced atmosphere.

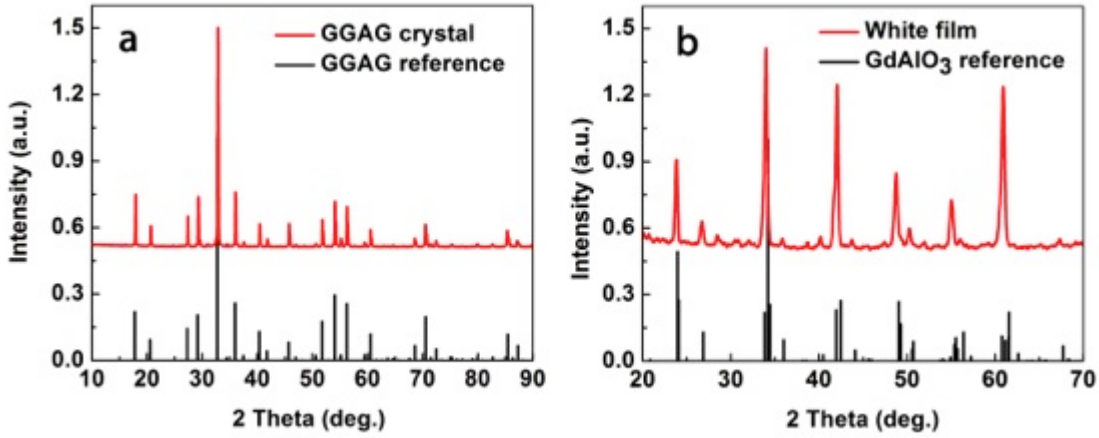

Figure 6.3. XRD of (a) as-grown GGAG crystal and (b) self-reflecting film (b) compared to a GGAG reference (No. 1627563 from Pearson's Crystal Data) and a $GdAlO_3$ reference file (No. 1818268 from Pearson's Crystal Data) respectively.

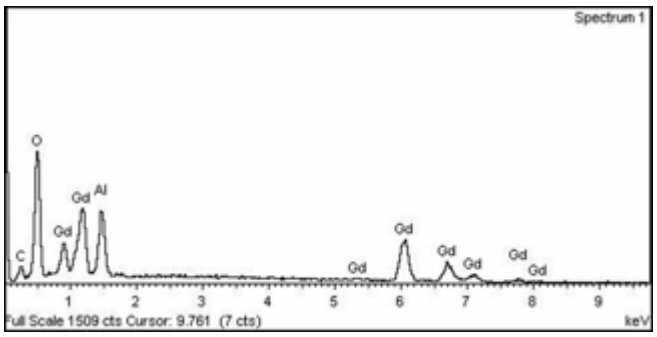

Figure 6.4. EDS spectra of the self-reflecting film.

Reflectivity of the reflective layer

Figure 6.5 shows reflectivity of a 350 μm reflective layer and the radioluminescence of GGAG crystals as a function of wavelength. The peak emission wavelength of Ce doped GGAG crystal due to the 4f-5d transition is 540 nm [6], which is indicated by the dash line in the plot. At 540 nm, the reflectivity of the reflective layer was 92%, which is enough to be used as reflector.

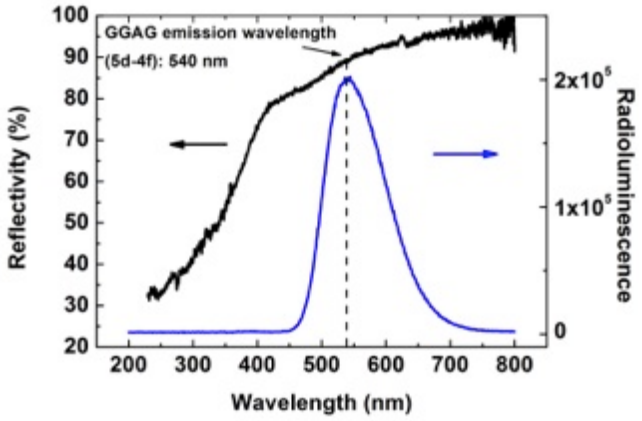

Figure 6.5. Reflectivity (black solid line) of the reflective layer and the radioluminescence (blue solid line) of GGAG crystals as a function of wavelength. The dashed line indicates the 540 nm emission of GGAG crystal.

Thickness of the reflective layer

The thickness dependence of the reflective layer on cumulative soaking time is plotted in Figure 6.6. The average thickness of the self-reflecting film increased monotonically with the increase of cumulative soaking time, and was ~ 1 mm thick after 50 h of heating treatment, as shown in Figure 6.7.

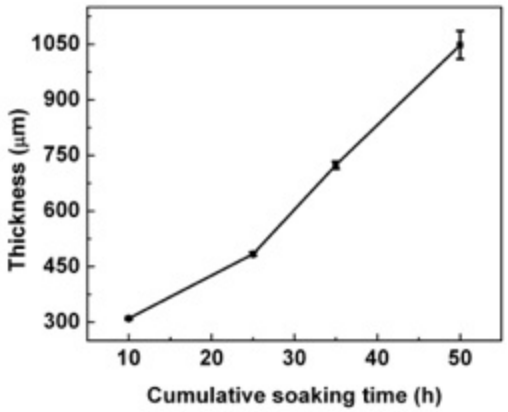

Figure 6.6. Change of thickness of the self-reflecting film as the cumulative soaking time increases.

Reflector performance of the reflective layer

The performance of the reflective layer was studied by measuring the relative LY as a function of the layer thickness. Different thicknesses of the reflective layer were obtained by multiple heating cycles. The relative LY of GGAG crystal covered with reflective layer without dome increased from 184 to 221 channels as the layer thickness increased from 205 to 1048 μm (5 to 50 h cumulative soaking time), as shown in Figure 6.8. As expected, the reflector performance improved as the film thickness increased up to 1 mm.

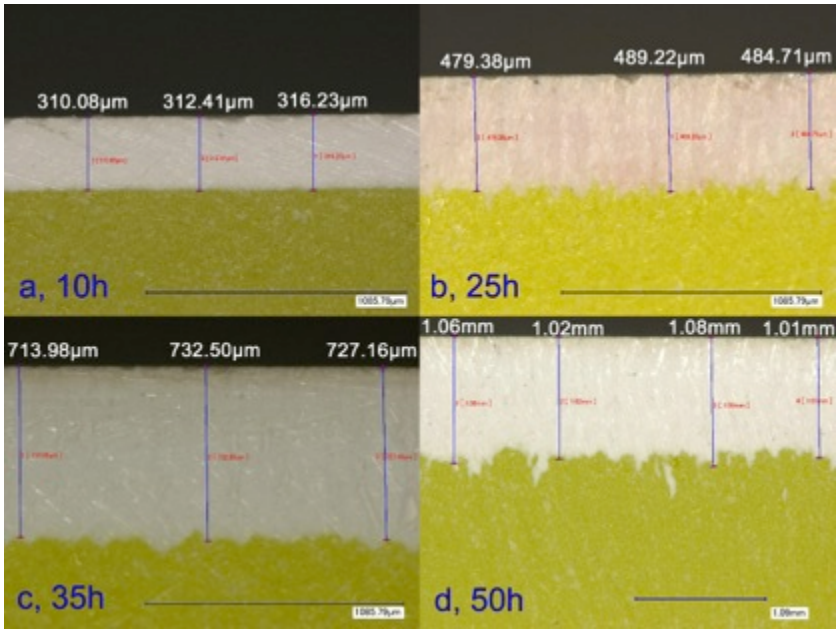

Figure 6.7. From a-d, the average thicknesses of the white self-reflecting film are 313 ± 3, 484 ± 5, 724 ± 10 and 1048 ± 38 μm with respect to cumulative soaking time of 10, 25, 35 and 50 h. (Note that the horizontal scale of Figure 4.7d is a factor of twice larger compared to that of Figure 4.7a-c.)

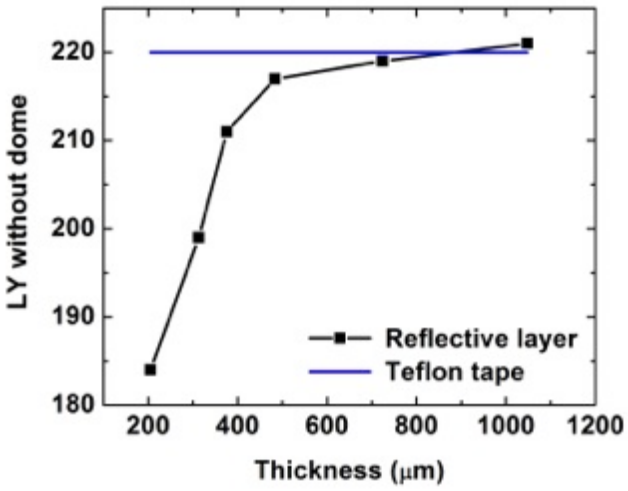

Figure 6.8. The LY of the GGAG crystal shown in Figure 4.2c as a function of the thickness of the reflective layer on a scale where a BGO reference crystal is set to 100. The horizontal line shows the light yield of a comparable crystal wrapped in several layers of Teflon tape.

In order to compare the reflector performance of the reflective layer and the Teflon tape, we measured the relative LY of the four types of samples described earlier. The results are presented in Table 6.1. The LY measured with dome are very close for all samples as assumed earlier. Therefore, the LY measured without the dome indicated directly the performance of the reflective layer. The LY without dome are very similar for the sample a and b (both are bare GGAG crystals). This is expected since both samples had no reflector coating to collect the photons. The LY for sample c and d (both covered with reflector) without dome increased compared to those of sample a and b. Figure 6.9 shows the energy spectra of LY without the dome for sample a, sample c (covered with the reflective layer of 1048 μm), sample d and the BGO reference. The reflective layer and external Teflon tape have a similar ability to reflect photons into a PMT when the reflective layer is sufficiently thick, as indicated by LY of sample c and d. It should be noted here that the LY achieved by sample c increased monotonically as the film thickness increased; see Figure 6.8.

Table 6.1 The LY measurements of GGAG crystals under different conditions as shown in Fig. 2. The value is on a scale where BGO reference crystal is set to 100.

Relative LY	Sample a	Sample b	Sample c	Sample d
With dome	275	273	274	275
Without dome	109	107	182-221	218

a) As-grown GGAG
b) GGAG with intrinsic reflective layer removed
c) GGAG with reflective layer on five surfaces (values include multiple measurements with increasing cumulative soak times, see Figure 4.8)
d) GGAG wrapped with Teflon tape on five surfaces

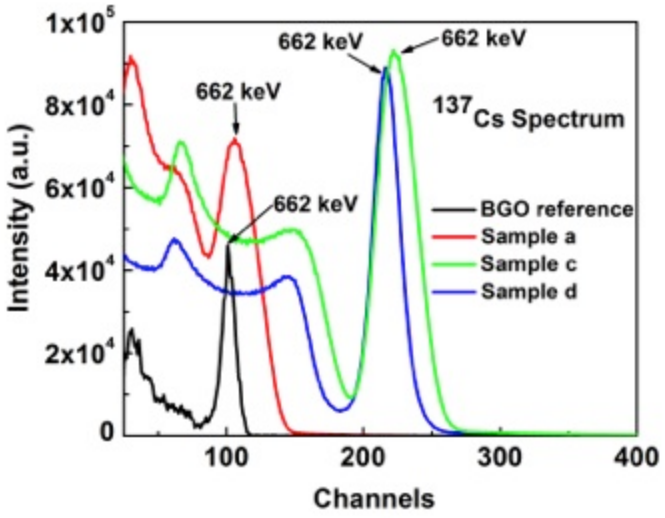

Figure 6.9. LY energy spectra of sample a (as-grown GGAG crystal), sample c (GGAG crystal covered with thick reflective layer) and sample d (GGAG crystal wrapped with Teflon tape) using a ^{137}Cs source.

Conclusion

The essence of this paper is that a reflective layer can be readily formed on the surface of a crystal, eliminating or minimizing the need for external reflectors. We have demonstrated the effectiveness of this in GGAG, and have found that soak times at high temperature can be used to control the thickness of the reflective layer. This idea may also be extended to other scintillator materials that exhibit the tendency to decompose, leaving a "white" or otherwise reflective layer on the surface.

References for Chapter 6

[1] P. Lecoq, et al., (2006). “Inorganic Scintillators for Detector Systems.” Springer-Verlag Berlin Heidelberg. 251.

[2] D. Hoffman, et al., “Scintillator array having a reflector with integrated air gaps.” US patents: 20040174952 A1.

[3] J.S. Huber, et al., (2001). “A LSO Scintillator Array for a PET Detector Module with Depth of Interaction Measurement.” IEEE Trans. Nucl. Sci. 48: 684-688.

[4] E. Auffray, et al., (2011). “A Comprehensive & Systematic Study of Coincidence Time Resolution and Light Yield Using Scintillators of Different Size, Wrapping and Doping.” IEEE Nuclear Science Symposium Conference Record, N4-6, 64-71.

[5] H. Sato, et al., (2012). “Evaluation and Development for Positron Emission Mammography based on Pr:LuAG Scintillator Crystals.” IEEE Nuclear Science Symposium and Medical Imaging Conference Record (NSS/MIC), 3537-3539.

[6] K. Kamada, et. al., (2011). "Composition engineering in cerium-doped (Lu, $Gd)_3(Ga,Al)_5O_{12}$ single-crystal scintillators." Cryst. Growth Des. 11(10): 4484-4490.

[7] C. D. Brandle, et al., (1972). “The Elimination of Defects in Czochralski Grown Rare-Earth Gallium Garnets.” J. Cryst. Growth 12: 195-200.

[8] A. Golubovi, et al., (2001). “The growth of sapphire single crystals.” J. Serb. Chem. Soc. 66(6): 411-418.

[9] S. B. Donnald, et al., (2013). "The Effect of B and Ca Co-Doping on Factors Which Affect the Energy Resolution of $Gd_3Ga_3Al_2O_{12}$: Ce." IEEE Trans. Nuc. Sci. 60(5): 4002-4006.

[10] M. Tyagi, et al., (2014). "Effect of Co-Doping on the Scintillation Kinetics of Ce Doped." IEEE Trans. Nuc. Sci. 60(1): 297-300.

[11] M. Tyagi, et al., (2013). "Effect of codoping on scintillation and optical properties of a Ce-doped $Gd_3Ga_3Al_2O12$ scintillator." J. Phys. D, Appl. Phys. 46(47): 475302.

Chapter 7 SUMMARY AND CONCLUSION

I. Codopant screening technique for GGAG:Ce

In order to fast screen the proper codopant candidates for GGAG:Ce from a wide range of materials, a cost-effective method was developed to predict the performance of codoped crystals before growing the crystals. Specifically, the radioluminescence (RL) intensity and photoluminescence (PL) decay of the pellets were used to predict the light yield (LY) and scintillation decay of the single crystals. This method was applied to GGAG:Ce pellets codoped with B, Ca, Ba Mg, Sr, Zr, Fe, Bi, Zn, Ag, Nb, Cu, K and Na. B and Ba were selected for crystal growth due to their increased RL intensity, and Ca was selected due to its reduced PL decay time, compared to the uncodoped pellets. Chapter 2 demonstrated this method using Ca, B, and Ba codoping as an example, and reported their improved scintillation properties. In the GGAG:Ce crystals, B and Ba codoping help to improve the LY from ~ 47,000 to ~ 53,000 ph/MeV, which is consistent with the increased RL intensity in the pellets. Ca codoping reduces the scintillation decay time from 51 to 43 ns, which is in agreement with the shortened PL decay time in Ca codoped pellets. The results from pellets and crystals are sufficiently similar for one to use pellets as an inexpensive and quick way to evaluate the compositions prior to undertaking the time and expense involved in the single crystal growth. This idea may also be extended to other scintillator materials whose scintillation properties could be improved by codoping.

II. The effect of codoping on the luminescence centers and charge traps in GGAG:Ce crystals

Besides the scintillation properties (LY and decay time), the optical properties (luminescence centers) and charge traps were also studied for the GGAG:Ce crystals codoped with Ca, B and Ba.

Ca codoping decreases the absorbance intensity at 345 nm and the RL intensity, while B and Ba codoping increase them. An F^+ luminescence center was introduced with an excitation peak at 350 nm and emission peak at 400 nm only by Ca codoping. The PL decay time of this luminescence center is around 3.5 ns, which is independent of temperature. Codoping affects the profile of temperature dependent PL decay time for the Ce luminescence center, which consequently changes the quenching temperature and activation energy. The quenching for the Ce center occurs around RT, and the emission rapidly decreases above RT.

Ca codoping significantly suppresses the charge trap population in GGAG:Ce crystals under RT, suggested by the TL measurements. This decrease in traps below RT accounts for the strong suppression of afterglow.

III. The effect of Ca codoping concentration on GGAG:Ce crystals

A series of experiments was designed to explore the effect of Ca codoping concentration on GGAG. GGAG:0.2 at% Ce crystals codoped 0.0-0.4 at% Ca

were grown by CZ technique. The relationship between Ca concentration and the optical/scintillation properties is explored. The Ce valence state and F^+ center are first studied by annealing in the Ca codoped crystals. The findings are summarized below.

1) Both the LY and decay time of Ca codoped samples decrease as Ca concentration increases from 0.0 to 0.4% as shown in Figure 7.1 and Figure 7.2. The detailed LY and decay time values are shown in Figure 7.3 and Table 7.1. Although the LY and energy resolution are deteriorated by Ca codoping, the decay time, rise time, shallow traps level and afterglow are remarkably improved. Therefore, Ca codoped GGAG:Ce crystals are promising candidates of scintillators for applications requiring fast timing resolution such as PET, even TOF-PET.

2) Ca promotes the transition of Ce valence state from Ce^{3+} to Ce^{4+} in GGAG:Ce crystals and hence the absorbance intensity of Ce^{3+} at 440 nm decreases while the Ce^{4+} charge transfer absorption increases. Since Ce^{4+} is the primary valence state in the sample with 0.4% Ca, it shows a distinct color from those at lower codoping levels. The sample with the 0.4% Ca and more Ce^{4+} is rust color, while the samples with 0.0-0.2% Ca and more Ce^{3+} are yellow color. In the sample with 0.4% Ca, the Ce valence state can be affected by various annealing atmospheres, as indicated by changes in color and in the Ce^{3+} absorbance band around 440 nm. Moreover, this valence state change can be reversed by annealing.

3) An F^+ center is observed in all Ca codoped samples, and can be affected by annealing atmospheres. In the samples with lower Ca concentrations (0.0-0.2 at%), annealing in an oxidizing atmosphere (air) helps to reduce or eliminate the oxygen vacancies, diminishing the F^+ center. In the crystal with the highest Ca concentration (0.4 at%), the F^+ center appears after annealing in a reducing atmosphere (2% H_2 in bulk N_2), presumably due to the increase of oxygen vacancies.

4) A Ce^{4+} emission model is applied to understand the improvement of the scintillation decay time. A redox mechanism and a charge compensation process are proposed to explain the change in Ce valence state and F^+ center during annealing.

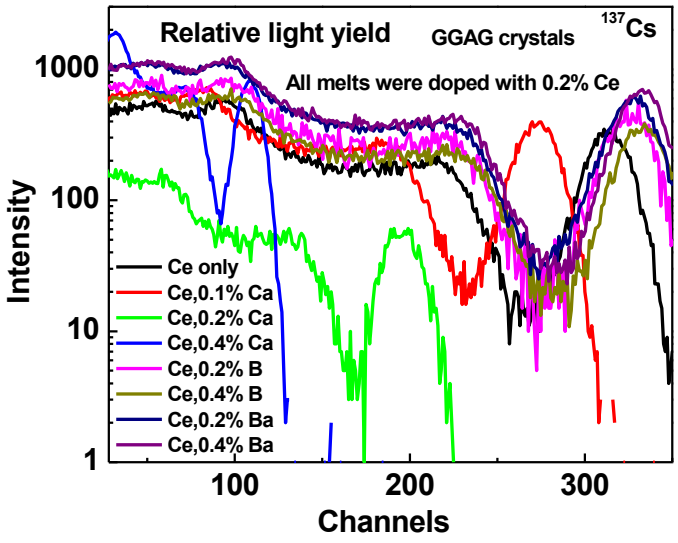

Figure 7.1. The relative light yield of different GGAG compositions.

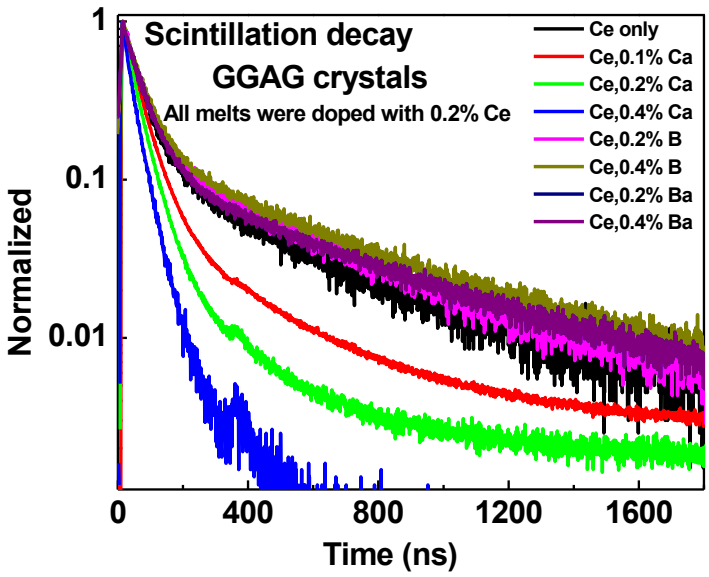

Figure 7.2. The scintillation decay curve of different GGAG compositions.

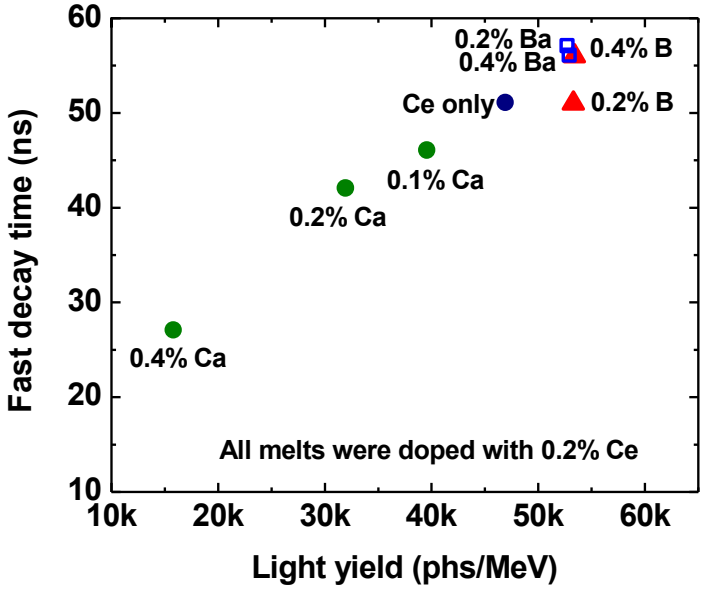

Figure 7.3. The relationship between light yield and fast decay component relative of different GGAG compositions.

Table 7.1 Summary of light yield and decay time of GGAG:Ce scintillators

Composition	Light yield (phs/MeV)	Scintillation decay time (ns)/ ratio
GGAG:0.2% Ce	47,000	51 (73%), 381 (27%)
GGAG:0.2% Ce, 0.1% Ca	39,600	46 (75%), 234 (25%)
GGAG:0.2% Ce, 0.2% Ca	32,000	42 (74%), 144 (26%)
GGAG:0.2% Ce, 0.4% Ca	15,870	27 (59%), 51(41%)
GGAG:0.2% Ce, 0.2% B	53,300	51 (69%), 388 (31%)
GGAG:0.2% Ce, 0.4% B	53,400	56 (66%), 464 (34%)
GGAG:0.2% Ce, 0.2% Ba	52,800	57 (59%), 468 (41%)
GGAG:0.2% Ce, 0.4% Ba	53,000	56 (59%), 438 (41%)

IV. An innovative intrinsic reflective layer for scintillation detectors

An innovative method to produce a reflective layer on a scintillation detector element was devised in order to provide an alternative approach to the traditional method of applying extrinsic reflectors. It is known that many inorganic oxides can decompose into suboxides when heated in an oxygen-deficient atmosphere. After heat treating a GGAG crystal in a reducing atmosphere for several hours, a white surface layer is formed. The resulting reflective layer is robust and firmly attached to the crystal. X-ray diffraction analysis shows that the white reflective layer is primarily composed of $GdAlO_3$. The reflectivity of this reflective layer can reach 92%. The performance of the reflective layer in terms of maximizing photon collection is improved as the thickness of layer increases and comparable to the performance of Teflon tape. This idea may also be

extended to other scintillator materials that exhibit the tendency to decompose, leaving a "white" or otherwise reflective layer on the surface.

APPENDICES

Appendix A

General characterization techniques for scintillation materials

X-ray diffraction

X-ray crystallography is a tool to identify the atomic and molecular structure of a crystal. The crystalline atoms diffract the beam of incident X-ray into many specific directions [1, 2]. By measuring the angles and intensities of these diffracted beams, a crystallographer can produce a three-dimensional picture of the density of electrons within the crystal, from which the arrangement of the atoms in the crystal can be determined, as well as their chemical bonds, and various other information [1]. The theory is according to Bragg's law [2]:

$$2dsin\theta = n\lambda \quad (1)$$

Here *d* is the spacing between the diffracting planes, *θ* is the incident angle, *n* is any integer, and λ is the wavelength of the beam. These specific directions appear as spots (peaks) on the diffraction pattern called reflections [2]. In this work, the X-ray diffraction measurements are performed on finely powdered single crystal and sintered pellet samples using a Bruker Axs D2 Phaser instrument.

Absorbance/transmittance

Absorbance is the fraction of radiation absorbed by a sample at a specified wavelength [3]. Absorbance spectrum of the scintillator is related to the activator; typically it indicates the information of the copant (e.g. Ce^{3+} ion) in the

scintillation host. Transmittance is the fraction of incident light (electromagnetic radiation) at a specified wavelength that passes through a sample [3]. In this work, absorbance/transmission were measured with a Varian Cary 5000 UV–VIS– NIR spectrophotometer in the 200–800 nm range.

Photoluminescence and photoluminescence decay

Photoluminescence (PL) is light emission from any form of matter after the absorption of photons (electromagnetic radiation) [4], typically a much smaller energy around 3-6 eV. In the Ce doped scintillator, the electrons are stimulated from the 4f ground state to 5d excited state after absorbing the external energy. Then the electrons de-excited and emit the photons. PL measurement provides the information about the dopant energy level positions. The time-resolved single photon counting is a method that the sample is excited with a light pulse and then the PL decay is measured with respect to time. PL decay usually reflects the lifetime of electrons in the emission process. Figure A.1 shows a typical excitation and emission process [5]. In this work, emission and excitation spectra are acquired by a HORIBA Jobin Yvon Fluorolog-3 Spectrofluorometer with a 450 W continuous Xenon lamp as the excitation source. PL decay is measured on the same spectrofluorometer with nano LEDs (pulsed light emitting diodes) as the excitation source.

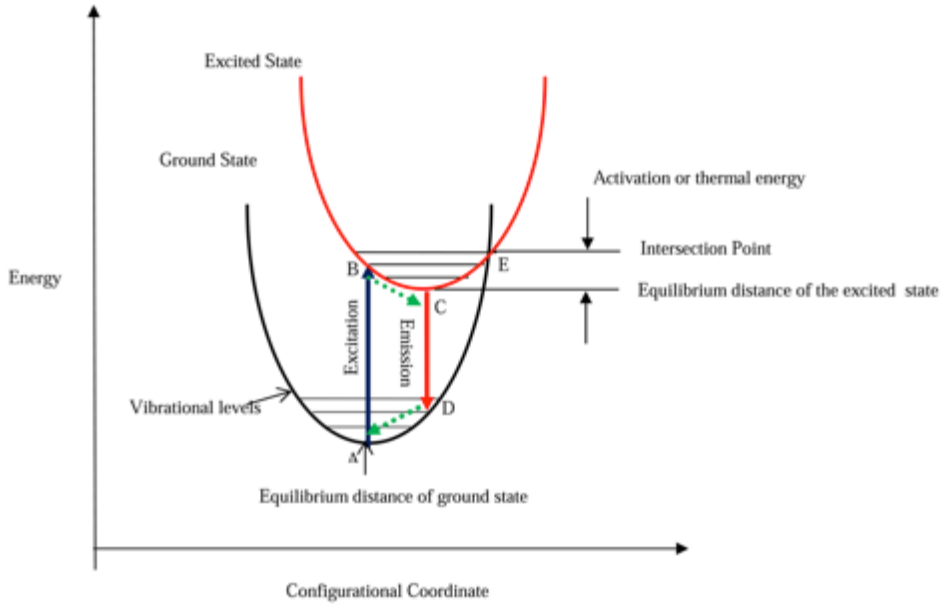

Figure A.1. An excitation and emission processes [5].

Radioluminescence

Radioluminescence (RL) is the phenomenon by which light is produced in a material by interacting with x-ray [6]. RL occurs when an incoming radiation particle collides with an atom or molecule in the scintillator, exciting an orbital electron to a higher energy level. The electron then returns to its ground energy level by emitting the extra energy as a photon of light [6]. The RL spectrum represents the wavelength distribution of the scintillation light arising from incident ionizing radiation [6]. Ideally, the wavelength of the emitted light will match well with current photomultiplier technology. In this work, the RL spectra were obtained at room temperature under the X-ray radiation at 35 kV and 0.1 mA using an ACTON SP-2155 monochromator.

Light yield

Light yield (LY) affects both the efficiency and the resolution of the detector. The efficiency is the ratio of the detected particles to the total number of particles impinging upon the detector; the energy resolution is the ratio of the full width at half maximum of a given energy peak to the peak position, usually expressed in % [7]. The LY is a strong function of the type of incident particle or photon and of its energy [7], which therefore strongly influences the type of scintillation material to be used for a particular application. Generally, the total LY of a scintillator can be described using [7, 8]:

$$Y_{ph} = \frac{10^6 SQ}{\beta E_g}\ photons/MeV \qquad (2)$$

where Y_{ph} is the number of photons emitted by the scintillator per unit of energy absorbed (usually photons/MeV). $\beta \cdot E_g$ is the mean energy necessary for the formation of one thermalized electron-hole pair in a material with a band gap E_g. β is a constant that appears approximately 2.5. S describes the efficiency of energy transfer to the luminescence center, and Q is the quantum yield of the intracenter luminescence. In ideal situation, the transfer efficiency S and the quantum efficiency Q of the activator ion are 100%.

In this work, the absolute LY was measured using a 10 μCi ^{137}Cs gamma-ray source, a Hamamatsu R2059 PMT with a known quantum efficiency, a 3 μs shaping time, and a hemispherical Spectralon reflector to enhance the light collection.

Scintillation decay

The scintillation decay time is a measure of how quickly scintillation light is emitted from a scintillator after a radiation interaction. The decay time is defined as the amount of time it takes for the initial light intensity to reach 1/e of its initial intensity [7]. A faster decay time will allow for better timing performance and allow for more radiation interactions to be measured within a given time window [7]. Generally, Ce^{3+} and Pr^{3+} are used as dopants because of the fast 5d-4f transition, allowing a fast decay component of 15-60 ns in both Ce^{3+} and Pr^{3+} doped materials which are approximately twice as fast as Eu^{2+} doped material.

In this dissertation, the scintillation decay time profiles are measured using the Bollinger-Thomas time-correlated single photon technique [9]. This technique employs two photomultiplier tubes (PMTs) and a ^{137}Cs gamma-ray source. The first PMT is used as a start PMT and it is placed near the test scintillator, allowing it to create a time stamp for the beginning of the scintillation event. Its signal is fed into a constant fraction discriminator (CFD) set with a low trigger threshold. The second PMT is used as a stop PMT and is partially covered by an iris in order to reduce the number of incident photons from the scintillator. Its signal is also fed into a CFD with a threshold setting that is optimized in order to trigger on a single photon. If the number of detected single photoelectrons is small compared to the number of start triggers (approximately 5% or less), the time difference between the start and stop triggers is then statistically dependent upon the scintillation decay time [9].

Thermoluminescence

Thermoluminescence (TL) measurements can act as a useful tool for understanding the trap structure of a scintillator. During the charge migration phase of crystal relaxation, many of the electrons may embed in shallow traps after an x-ray source was used to excite the scintillator. The charge carriers need to acquire enough thermal energy to escape the trap and recombine at the luminescence center [10]. TL measurements use this property by cooling a test scintillator to temperatures as low as 5 K and then intentionally filling the charge traps using an x-ray source. At this low temperature, the trapped charge carriers have a very small probability of escape and will remain trapped indefinitely. During the measurement, the sample is then slowly heated in order to release the charge traps, and the resulting light output from the scintillator is monitored [10]. The TL intensity spectra can be written [11] as:

$$I(T - \Delta T) = n_0 \, s \exp\left(\frac{E}{kT}\right) \exp\left(\frac{s}{\beta}\right) \int_{T_1}^{T_2} \exp\left(\frac{E}{kT'}\right) dT' \qquad (4)$$

where ΔT is the thermal lag between the sample and the heating element (ΔT = 2~3 K), E is the energy of traps need to escape from the traps, β is the constant heating rate, n_0 is the initial concentration of filled traps, s is the frequency factor and κ is the Boltzman constant. In our experiment, the sample was mounted within an Advanced Research Systems cryostat (model DE202AE). The sample chamber was evacuated to 20 mTorr before the sample was heated to 600 K in order to empty charge carrier traps. The sample was then cooled to 9 K and irradiated with x-rays through a beryllium window for approximately 15 min.

Subsequently, the sample was brought back to 600 K at a rate of 0.15 K/s. A Hamamatsu H3177 PMT was used to measure the luminescence emitted by the sample as a function of temperature.

Afterglow

Afterglow is the scintillation light that is given off after several milliseconds or seconds. It is caused by impurities and defects that create traps or metastable states with long lifetime [12]. Typically, BGO, GSO(Ce), $PbWO_4$, and $CdWO_4$ tend to have small afterglow ~0.005% after 3 ms. The doped alkali halides like NaI(Tl) and CsI(Tl) can be quite high, ~ 0.1-5% after 3 ms [13]. Generally speaking, those traps shown in TL spectra around room temperature are the origin of afterglow in a scintillator. The lifetime of the traps at room temperature was calculated by Arrhenius formula [14]:

$$t = \frac{\exp\left(\frac{E}{kT}\right)}{s} \tag{4}$$

where s and E were calculated from the TL fitting curve. In our afterglow measurements process, the charge carrier traps were first emptied by heating the crystals for 10 min at 600 K. After cooling to room temperature, the crystals were coupled to a Hamamatsu R3177 photomultiplier tube with a Dow Corning Q2-3067 optical couplant, and covered with a Tetratex TX3104 PTFE membrane. The crystals were then irradiated with x-rays for 15 min. The luminescence emitted was then measured as a function of time.

References for Appendix A

[1] K. Prathap, (2014). “X-Ray Diffraction and Characterization of Crystalline Materials.” Proceedings of The Intl. Conf. on Information, Engineering, Management and Security, 320-324.

[2] J. Kacher, et al., (2009). "Bragg's Law diffraction simulations for electron backscatter diffraction analysis." Ultramicroscopy 109 (9):1148-1156.

[3] O. Stenzel, (2005). “The physics of thin film optical spectra: an introduction.” Vol. 44. Springer Science & Business Media.

[4] P. J. Dean, (1966). “Luminescence of inorganic solids.” Ed. Paul Goldberg. Vol. 54. New York: Academic Press.

[5] A. H. Khalid and K. Kontis. (2008). "Thermographic phosphors for high temperature measurements: principles, current state of the art and recent applications." Sensors 8(9):5673-5744.

[6] K. V. R. Murthy, and H. S. (2014) Virk. "Luminescence Phenomena: An Introduction." Defect and Diffusion Forum. 347: 1-34.

[7] G. F. Knoll, (2010). “In Radiation Detection and Measurement” Wiley: New York, fourth edition, pp. 238.

[8] P. Dorenbos, (2002). “Light output and energy resolution of Ce^{3+} doped scintillators.” Nucl. Instr. Meth. Phys. Res. A. 486(1): 208-213.

[9] L. Bollinger and G. Thomas, (1961). “Measurement of the time dependence of scintillation intensity by a delayed coincidence method.” Review of Scientific Instruments 32: 1044–1050.

[10] M. J. Aitken, (1985). “Thermoluminescence dating.” Academic press.

[11] J. G. Kang, et al., (2008). “Preparation and luminescence characterization of GGAG:Ce^{3+}, B^{3+} for a white light-emitting diode.” Mater. Res. Bull. 43: 1982-1988.

[12] T. Yanagida, et al., (2014). “Development of X-ray-induced afterglow characterization system.” Appl. Phys. Express 7(6): 062401.

[13] M. Chen. "Scintillation and Light Sensitive Detectors-I."

[14] K. J. Laidler. (1984). "The development of the Arrhenius equation." J. Chem.

Educ. 61 (6):494-499.

Appendix B

Publication and presentation

Peer-reviewed journals

1. **F. Meng,** Yuntao Wu, M. Koschan, C. L. Melcher, P. Cohen, "Effect of annealing atmosphere on the cerium valence state and F^+ luminescence center in Ca codoped GGAG:Ce single crystals." Physics state solid (b), vol. 252, pp. 1394-1401, 2015.
2. **F. Meng,** M. Koschan, C. L. Melcher, P. Cohen, "Sintered pellets: a simple and cost effective method to predict the performance of GGAG:Ce single crystals." Material Science and Engineering B, vol. 193, pp. 20-26, 2014.
3. **F. Meng**, M. Koschan, M. Tyagi, C. L. Melcher, P. Cohen, "A innovative method to create an intrinsic reflective layer on a $Gd_3Ga_3Al_2O_{12}$:Ce scintillation crystals", Nuclear Instruments and Methods in Physics Research Section A, vol. 763, pp. 591-595, 2014.
4. **F. Meng,** M. Koschan, Yuntao Wu, C. L. Melcher, "Relationship of Ca^{2+} concentration and the properties of codoped $Gd_3Ga_3Al_2O_{12}$:Ce Scintillators", Nuclear Instruments and Methods in Physics Research Section A, vol. 797, pp. 138-143, 2015.
5. **F. Meng**, M. Koschan, Hua Wei, Yuntao Wu, C. L. Melcher, "Effect of codoping on the luminescence centers and charge traps in GGAG:Ce crystals", being submitted to Journal of Luminescence.
6. Y. Wu, **F. Meng**, Q. Li, M. Koschan, C. L. Melcher, "Role of Ce^{4+} in the Scintillation Mechanism of Codoped $Gd_3Ga_3Al_2O_{12}$:Ce", Physical Review Applied, 2 (4), pp. 044009, 2014.
7. M. Tyagi, **F. Meng**, M. Koschan, A. K. Singh, C. L. Melcher, S. C. Gadkari, "Effect of Co-doping on the Radiation Hardness of $Gd_3Ga_3Al_2O_{12}$:Ce Scintilaltors", IEEE Transaction on Nuclear Science, vol. 62, pp. 336-339, 2015.

8. M. Tyagi, **F. Meng**, M. Koschan, S. B. Donnald, H. E. Rothfuss, C. L. Melcher, " Effect of codoping on scintillation and optical properties of of a Ce-doped $Gd_3Ga_3Al_2O_{12}$ scintillator", Journal of Physics D, vol. 46, pp. 475302, 2013.
9. Y. Wu, G. Ren, **F. Meng**, X, Chen, D. Ding, H. Li, S. Pan, C. L. Melcher, " Scintillation characteristics of indium doped cesium iodide single crystal", IEEE transaction on nuclear science, vol. 62, pp. 571-576, 2015.
10. Y. Wu, G. Ren**, F. Meng**, X. Chen, D. Ding, H. Li, "Effects of Bi^{3+} codooping on the optical and scintillation properties of CsI: Tl single crystals, Physica status solidi (a), vol. 211, pp. 2586-2591, 2014.
11. Y. Wu, G. Ren, **F. Meng**, X. Chen, D. Ding, H. Li, S. Pan, "Ultralow-concentration Sm codoping in CsI:Tl scintillator: A case of little things can make a big difference." Optical Materials, vol. 38, pp. 297-300, 2014.
12. Y. Wu, Z. Luo, H. Jiang, **F. Meng**, M, Koschan, C. L. Mlecher, "Single crystal and optical ceramic multicomponent garnet scintillators: A comparison study", Nuclear Instruments and Methods in Physics Research Section A, vol. 780, pp. 45-50, 2015.
13. H. Wei, M. Zhuravleva, **F. Meng**, C. L. Melcher, "Temperature dependence spectroscopic study of Ce-doped Cs_3LaCl_6 and Cs_3LaBr_6 scintillators", Journal of luminescence, vol. 160, pp.64-70, 2015.
14. H. Wei, L. Stand, M. Zhuravleva, **F. Meng**, V. Martin, C. L. Melcher, "Two new cerium-doped mixed-anion elpasolite scintillators: $Cs_2NaYBr_3I_3$ and $Cs_2NaLaBr_3I_3$." Optical Materials, vol. 38, pp. 154-160, 2014.
15. S. B. Donnald, M. Tyagi, H. E. Rothfuss, **F. Meng**, J. P. Hayward, M. Merry, C. L. Melcher, "The effect of B^{3+} and Ca^{2+} Co-Doping on Factors which Affect the Energy Resolution of $Gd_3Ga_3Al_2O_{12}$", IEEE Transactions on Nuclear Science, vol. 60, pp. 4002-4006, 2013.
16. S. B. Donnald, M. Tyagi, H. E. Rothfuss, J. P. Hayward, M. Koschan, M. Zhuravleva, **F. Meng**, C. L. Melcher, "Sample to Sample Variation in Single Crystal YAP:Ce Non-proportionality, vol. 61, pp. 332-338, 2014.

Conference proceeding papers

1. **F. Meng**, M. Koschan, S. B. Donnald, Yuntao Wu, C. L. Melcher, "Suppression of YAG phase formation in YAP:Ce pellets", Nuclear Science Symposium and Medical Imaging Conference (NSS/MIC), 2014 IEEE.
2. **F. Meng**, M. Koschan, Y. Wu, C. L. Melcher, P. Cohen, "Relationship between Ca^{2+} concentration and the properties of codoped GGAG:Ce scintillators", Nuclear Science Symposium and Medical Imaging Conference (NSS/MIC), 2014 IEEE.
3. M. Tyagi, **F. Meng**, K. Darby, M. Koschan, C. L. Melcher, "Effect of cation size at Gd and Al site on Ce energy levels in $Gd_3(GaAl)_5O_{12}$ sintered pellets", American Institute of Physics Conference Series, vol. 1512, pp. 870-871, 2013.

Peer-reviewed Conference Presentations

1 "The relationship between Ca^{2+} concentration and the properties of codoped GGAG:Ce scintillators", Nuclear Science Symposium and Medical Imaging Conference (NSS/MIC), 2014 IEEE, Seattle, Washington (**oral**).

2 "A novel method to create an Intrinsic reflective layer on a $Gd_3Ga_3Al_2O_{12}$:Ce scintillation crystal", Nuclear Science Symposium and Medical Imaging Conference (NSS/MIC), 2014 IEEE, Seattle, Washington (**poster**).

3 "Effect of annealing atmosphere on the cerium valence state in Ca codoped GGAG:Ce single crystals", Nuclear Science Symposium and Medical Imaging Conference (NSS/MIC), 2014 IEEE, Seattle, Washington (**poster**).

4 "Suppression of YAG phase formation in YAP:Ce pellets", Nuclear Science Symposium and Medical Imaging Conference (NSS/MIC),2014 IEEE, Seattle, Washington (**poster**).

5 "Investigation the effect of co-dopants in GGAG crystals by making GGAG:Ce pellets with different co-dopants", 2014 Symposium on Radiation Measurements and Applications (SORMA XV), Ann arbor, Michigan (**poster**).

6 "The effect of co-doping on the luminescence centers and charge traps in

GGAG:Ce crystals", 2014 Symposium on Radiation Measurements and Applications (SORMA XV), Ann arbor, Michigan (**poster**).

7 "Understanding the Improvement by Codoping in RE_2SiO_5:Ce (RE=Lu, Y) Single Crystal Scintillators: Insights from Experiments and Theory", 13th International Conference on Inorganic Scintillators and their Applications, 2015 SCINT, Berkeley, California (**oral, co-author**).

8 "The role of Ce^{4+} in the Scintillation Mechanism of Codoped $Gd_3Ga_3Al_2O_{12}$:Ce", Nuclear Science Symposium and Medical Imaging Conference (NSS/MIC), 2014 IEEE, Seattle, Washington (**oral, co-author)**.

9 **"**Effect of co-doping on the radiation hardness of $Gd_3Ga_3Al_2O_{12}$:Ce Scintillators", Nuclear Science Symposium and Medical Imaging Conference (NSS/MIC), 2014 IEEE, Seattle, Washington (**poster, co-author)**.

10 "Effect of cation size at Gd and Al site on Ce energy levels in $Gd_3(GaAl)_5O_{12}$ sintered pellets", Proceedings of the 57th DAE Solid State Physics Symposium 2012, Mumbai, India (**poster, co-author**).

11 "Cerium-doped Mixed Elpasolite Scintillators: $Cs_2NaYBr_3I_3$ and $Cs_2NaLaBr_3I_3$", 2014 Symposium on Radiation Measurements and Applications (SORMA XV), Ann arbor, Michigan (**poster, co-author**).

12 "Engineering the proportionality of YAP: Scintillators", 2014 The University and Industry Technical Interchange (UITI) (**poster, co-author**).

VITA

Fang Meng (蒙 芳) was born on December 16, 1986 in Jingzhou, China. She enrolled in Hefei University of Technology in 2004, and graduated with a bachelor degree in Microelectronics in June of 2008. She continued her study at Huazhong University of Science and Technology from September of 2008, and received her master degree in Microelectronics and Solid State Electronics in March of 2011. She attended the University of Tennessee at Knoxville since August of 2011. Currently she is a graduate research assistant and pursuing her Ph.D. degree in the Department of Materials Science and Engineering and Scintillator Materials Research Center.